Doctoral Thesis

ELECTROSTATIC TRANSPORT CHARACTERISTIC OF NOM AND IONS AT THE SURFACE OF NEGATIVELY CHARGED MEMBRANES

Hojung Rho

Department of Urban and Environmental Engineering
(Environmental Science and Engineering)

Graduate School of UNIST

2019

ELECTROSTATIC TRANSPORT CHARACTERISTIC OF NOM AND IONS AT THE SURFACE OF NEGATIVELY CHARGED MEMBRANES

Hojung Rho

Department of Urban and Environmental Engineering
(Environmental Science and Engineering)

Graduate School of UNIST

Electrostatic transport characteristic of NOM and ions at the surface of negatively charged membranes

A thesis/dissertation
submitted to the Graduate School of UNIST
in partial fulfillment of the
requirements for the degree of
Doctor of Philosophy of Science

Hojung Rho

7. 18. 2019 of submission

Approved by

Advisor
Jaeweon Cho

Electrostatic transport characteristic of NOM and ions at the surface of negatively charged membranes

Hojung Rho

This certifies that the thesis/dissertation of Hojung Rho is approved.

7. 18. 2019 of submission

signature

Advisor: Jaeweon Cho

signature

Young-Nam Kwon: Thesis Committee Member #1

signature

Kyunghwa Cho: Thesis Committee Member #2

signature

Hokyung Shon: Thesis Committee Member #3

signature

Kangmin Chon: Thesis Committee Member #4;

ABSTRACT

We characterized the surface charge properties of negatively charged nanofiltration (NF) membranes and a reverse osmosis (RO) membrane by potentiometric titrations and electrophoresis to predict the electrostatic transport at the membrane surfaces affecting their salt rejection, fouling propensities and cleaning behavior. This study focused on 1) the validation of a potentiometric titration method based on the quantification of ionized functional groups (termed as functionality) to estimate the surface charge properties of nanofiltration (NF) membranes, 2) the determination of intrinsic pK_a and PZC values of virgin and fouled NF membranes with three organic matters that have different charge (positive, negative or neutral) and to investigate their reversibility using chemical cleaning (HCl, NaOH, NaCl, and deionized (DI) water), 3) the investigation of the fouling behavior and the effects of desorbing agents (i.e., DI water, acid, base, and salt solutions) on the fouled RO membrane through membrane autopsies and various analytical techniques.

The surface charge properties (i.e., functionality and zeta (ζ) potential) of two NF membranes were characterized by potentiometric titrations and electrophoresis to predict the electrostatic transport at the membrane surfaces affecting their salt rejection and fouling propensities. The ζ potential was not suitable for evaluating the rejection of Na^+ (NE20 membrane =21–25%; NE70 membrane =65–70%) and Cl^- ions (NE20 membrane =19–22%; NE70 membrane=60–63%), and the fouling propensities of organic materials in the NF membranes due to its inherent measurement inaccuracies (Δ ζ potential $=-1.8 \times$(Δ amount of desorbed organic foulants) +45.9, R^2 =0.07). The functionality accurately predicted both the rejection of NaCl and the fouling propensities of the organic materials, as the charge densities of the membranes determined by the functionality measurements (only TFC membranes are applicable) truly reflected the acid dissociation constants of the carboxylic and amine functional groups and the points of zero charge values. These results indicate that potentiometric titrations may provide valuable insights into the electrostatic transport at the membrane surface influencing salt rejection and fouling mechanisms of the NF membranes.

In addition, the electrical surface properties (pK_a and PZC) of virgin and fouled NF membranes were determined using potentiometric titration with regard to the reversibility of the membranes (i.e., salt rejection and permeate flux). The lower PZC value observed for fouled with m-phenylenediamine (MPD) membrane compared to virgin NF membrane can be explained by the adsorption of positively charged foulants on the negatively charged membrane surface. In addition, the higher PZC value was observed for fouled with coumarin-3-carboxylic acid (CCA) membrane based on the adsorption of negatively charged foulants on the negatively charged membrane surface. Moreover, no significant changes in PZC values were observed for fouled with D-(+)-glucose (DG) membrane. This is due to the adsorption of neutral foulants on the negatively charged membrane surface. These observations

indicate that the PZC measurements may offer significant insights into the differences in PZC values in terms of properties of membrane foulants based on the ionization degree of the surface functional groups.

Finally, the fouling and cleaning behaviors of reverse osmosis (RO) membranes in a lab–scale ultrapure water (UPW) production system were investigated via membrane autopsies and characterization of dissolved organic matter (DOM) and membrane foulants. Most of the DOM were effectively removed by the MFC filter, with the exception of the peak at 150 Da. The RO membranes were effective in reducing conductivity, DOM, total nitrogen (TN), and ultraviolet A ($UVA_{254\ nm}$) concentration; the polishing stage using IER filter resulted in ultra-trace levels of all these parameters required for semiconductor manufacturing (> 18.2 MΩ). The quantity of the desorbed RO membrane foulants, in terms of dissolved organic carbon (DOC), varied considerably depending on the type of desorbing agents: 0.1 N NaCl (65.12 mgC m^2) > 0.1 N NaOH (46.14 mgC m^2) > deionized water (25.39 mgC m^2) > 0.1 N HCl (15.95 mgC m^2). High cleaning efficiency of the salt solution (0.1 N NaCl) was attributed to the efficient desorption of hydrophilic DOM foulants from the RO membrane surfaces. These results demonstrate that salt cleaning may provide a promising option to recover the performance of the RO membranes fouled primarily by hydrophilic DOM fractions.

This research begins with defining the differences between “exist” and “being”. Let’s think about a car on a track. If the car is accelerated steadily and the velocity of the car reaches infinity, the car will disappear. It implies that the car will not exist at that time but in reality, it is on the track. Thus, it seems that only something that humans can see (is visible) is denoted to “exist”. Additionally, “exist” is a completely temporal concept. If time ever reached infinite, everything that exists would disappear. In contrast, it could be considered that “being” is completely irrelevant to time, implying that something humans cannot see can be denoted as “being”.

The relation between the system and its environment can be presented using the concept of “exist” and “being”. While a system is considered as being, its environment exists around the system, and constantly affects the movement and the reactions of the system. Consequently, the system gets its own characteristics defined by the interactions between the system and environment. In other words, the characteristics of the system change is significantly depending on its environment. Therefore, studying the interactions between the system and its environment is key for a wholistic understanding of the system.

Environment at the surface is one of the most important aspects in water treatment (e.g., membrane process, advanced oxidation process, biological process etc.). Surface chemistry involves basic research to develop solutions, as numerous studies on surface chemistry and environments at the surface have been conducted over the past few decades. As previously mentioned, the concept of the

system and its environment, however, is necessary to investigate the interaction between them to understand the characteristics of surface chemistry. Therefore, the objective of this study is to thoroughly investigate the characteristics of surface chemistry depending on the changes in the environment. It is believed that by transforming surface chemistry which is invisible into visible is the true vision for surface chemistry research.

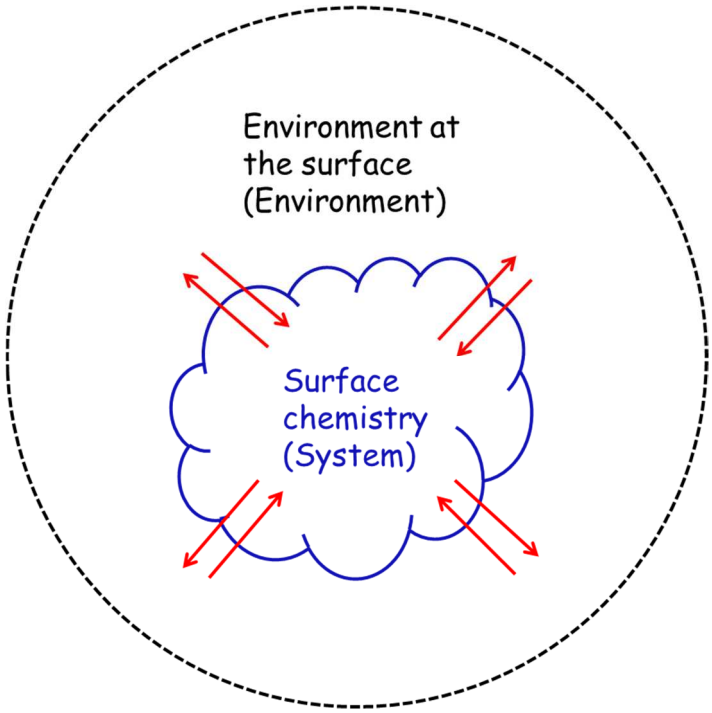

Fig. 1-1. Schematic concept of the relation between system and environment

ACKNOWLEDGEMENTS

I would first like to express my sincere appreciation to my advisor, Dr. Jaeweon Cho, for his advice, support, guidance, and above all his consistent encouragement. His brightness, generosity, and kindness encourage me to concentrate on my research. I really enjoyed having discussion with him about membrane and NOM. I am also honored to have been his student. I deeply would like to thank Dr. Young-nam Kwon, Dr. Kyonghwa Cho, Dr. Hokyong Shon (University of Technology Sydney), and Dr. Kangmin Chon (Kangwon National University) for serving on this committee, their valuable comments and sharing their expertise. I thank my colleague, Dr. Jongkwan Park for his support and kindness. I deeply appreciate his contribution and advice to my research. I am also impressed by his kindness. I would not have endured without his encouragement. I would like to thank Dr. Byung-Moon Jun for his advice about UNIST (Ulsan National Institute of Science and Technology) life. I greatly acknowledge all faculty members and graduate students in Department of Urban and Environmental Engineering at UNIST. I also thank Dr. Kyung-hyuk Lee (Korea Water Resources Corporation, K-water) for his guidance and comments about my career.

I would like to share my happiness with my parents; they have always trusted my ability and encouraged me. I also would like to share my happiness with my girlfriend, MJ; she encouraged and trust me with her kind words and supported me emotionally. I really appreciate God's guidance, blessing, and His being around me with me all the times.

Contents

List of Figures

List of Tables

1. Introduction

1.1 Motivation for research

The technology of polymeric membrane has been developed for water purification, sea water desalination and recently for energy production and storage. Despite several practical applications, membrane fouling is the most common issue affecting the performance of the membrane. Therefore, membrane fouling has been studied to identify the mechanism of fouling and solute rejection, which can be used to predict the performance of membrane processes. Current technology is challenging to identify the mechanisms, since silt density index (SDI), and modified fouling index (MFI), one of widely used for predicting membrane fouling only considers the physicochemical property of solution and operating condition of the membrane process. Moreover, the mechanism of solute rejection has not been completely explained by the size exclusion theory. Large differences between the conventional indices and the performance of full-scaled membrane process were observed.

The membrane fouling and solute rejection are strongly influenced by the interaction between solute and membrane surface (e.g., electrostatic repulsion, hydrophobicity interaction, and roughness of membrane surface). Therefore, determination of the transport phenomena at the membrane surface, based on the interaction between solutes and membrane surface, is required for the future technology of membrane process.

1.2 Background and consideration

1.2.1 NOM Characterization

NOM characteristics - including size (average molecular weight [MW] and MW distribution), structure (aromatic (or hydrophobic) versus aliphatic (or hydrophilic)), and functionality (charge density in terms of carboxylic and phenolic acidity) - are factors influencing membrane process because of interactions between NOM and membranes, such as size exclusion, hydrophobic interaction, and electrostatic repulsion [1-3]. NOM characteristics are also important factors since these are closely related to disinfection by-products (DBPs) formation potential (DBPFP) [4-6], taste and odor, and bacterial regrowth and biofilm formation in the distribution systems [7-8]. Therefore, various NOM characterization tools, including isolation of colloidal NOM [9], measurement of biodegradable dissolved organic carbon (BDOC), and assimilable organic carbon (AOC) content [10], and DBP reactivity

analysis [6, 9], have been developed to gain a better understanding of the nature of NOM.

1.2.2 Specific UV Absorbance and its Applicability

A specific UVA (SUVA = UVA_{254}/DOC) is a simple and reliable index, with generally higher SUVA value for an aromatic (or hydrophobic) structure and lower value for an aliphatic (or hydrophilic) structure. The aromatic structure of NOM absorbs more UV light than the aliphatic structure, whereas DOC measures the total concentration of carbon in NOM [11-12]. SUVA for fulvic acid was higher than that for NOM contained in natural bulk waters [13]. Ozonated water generally exhibits a lower SUVA than the corresponding raw water due to the breakdown of aromatic structure by ozone [11]. SUVA depends not only on the origin of the NOM (i.e., specific for a given water), but also on seasonal changes and temperature variations [14-15]. Furthermore, SUVA for NOM of the same source water may be significantly influenced by the water chemistry, such as pH, ionic strength, and Ca^{2+} concentration. Therefore, the applicability of a SUVA should be carefully investigated when using SUVA as a measure of aromatic (or hydrophobic) character.

1.2.3 NOM Molecular Weight (MW)

NOM molecular weight (MW) influences NOM removal by membrane since size (steric) exclusion is one of the NOM-removal mechanisms of membrane filtration. The MW of NOM can be determined experimentally by ultrafiltration (UF) membrane fractionation and high-performance size-exclusion chromatography (HPSEC) methods. The UF membrane fractionation method is conducted with regenerated cellulose membranes with different molecular weight cutoff (MWCO) and a stirred-cell dead-end filtration unit to obtain a MW fraction between two nominal MWCO values [1, 2, 16]. The UF method of MW fractionation is not significantly influenced by pH variation because the surface of the membranes used in the method is uncharged. YM-series membranes with an uncharged surface were used in MW fractionation [16]. However, it is better to perform UF experiments without significant changes in pH, since NOM size is influenced by pH variation (i.e., NOM size decreases with decreasing pH owing to molecular compaction [17-18]. In addition, concentration polarization (CP) near the membrane surface is another important limitation in the UF method. In case of high or low CP, a permeation coefficient model was used to calculate the removal percentage [19].

MW distribution, weight- and number-average MW (M_W and M_n), and polydispersity ($=M_w/M_n$) were analyzed and calculated by HPSEC method, using a modified silica column and sodium polystyrene sulfonates (PSS) [20]. Colligate (only depending on the number of molecules present and not based on their chemical nature) and most of the mechanical properties correlate with M_n, and solution viscosities correlate with M_w. Using the HPSEC method, z-average MW (M_z) is also calculated, which is correlated with viscoelastic properties (i.e., a large value of M_z implies a significant number of long chain molecules that are more prone to chain entanglements). The HPSEC method is useful when determining MW of NOM from different water source with different chemistries (i.e., pH and ionic strength) since the eluent (mobile phase) used in the method is often a buffered solution with high ionic strength. Various detection techniques can be used in the HPSEC method, such as UVA, DOC, and fluorescence. Each of these detection techniques exhibit different MW for the same NOM, because each technique has different detection mechanisms. Rigorous investigations on the HPSEC method were performed with different detection techniques and compared with each other [21]. MW values of fulvic acids from the HPSEC method were smaller than those from the UF method [1, 20], suggesting that the UF method provided higher DOC removal than the actual value due to concentration polarization.

1.2.4 NOM Structure

NOM structure is also an key factor in membrane filtration because hydrophobic interaction affects NOM-membrane interactions. NOM isolation by XAD-8 and XAD-4 resins was used to obtain hydrophobic NOM (XAD-8 adsorbable), transphilic NOM (XAD-4 adsorbable), and hydrophilic NOM (neither XAD-8 nor XAD-4 adsorbable) [22-24]. Another NOM fraction defined as *colloidal* NOM (the NOM fraction with MW larger than 3500 g/mole) exists [9]. Detailed descriptions on colloidal NOM will be presented later in this chapter. Hydrophobic and transphilic NOM components contain acids and neutral salts, while hydrophilic NOM components contain mostly neutral salts and bases. Hydrophobic acids include strong acids, including fulvic and humic acids, and weak acids such as alkyl monocarboxylic and dicarboxylic acids [23]. Hydrophilic NOM is comprised of acids (hydroxy, sugar, and sulfonic acids), neutral compounds (polysaccharide, low MW alkyl alcohols, and amides), and bases (low MW alkyl amines and amino acids). Hydrophilic acids are fractions adsorbed on XAD-4 resin, and both hydrophilic neutral compounds and bases are collected in

the effluent of XAD-8/4 resins (but not XAD-8 or XAD-4 adsorbable). These different organic matters have different size, hydrophobicity, and functionality, resulting in different hydrophobic and electrostatic interactions between NOM and the membrane surface. One of the main limitations of this fractionation method is that each NOM fraction (isolated from XAD-8 (hydrophobic NOM), XAD-4 (transphilic NOM), collected in effluent of XAD-8/4 (hydrophilic NOM)) contains high salt concentration (NOM fractions adsorbed on XAD-8 and XAD-4 are isolated with 0.1 N NaOH, and effluent of XAD-8/4 contains 0.1 N HCl), which is, sometimes, problematic for downstream use (i.e., ionic strength of the feed water is relatively high with little dilution when using each NOM fraction as the feed water for NOM in membrane filtration).

1.2.5 NOM Functionality

The charge density (or functionality) of NOM is an important factor in NOM rejection and reduction in flux involving the membrane since electrostatic interactions between NOM (with acidic functional groups) and the membrane (with a negatively charged surface) play an important role in rejection and fouling [25-26]. The charge density of NOM in bulk natural water cannot be easily measured using base titration due to various inorganic weak acids present in the natural waters. Instead, hydrophobic acids (XAD-8 resin isolate) are used for potentiometric titration (pH 3-8) to measure carboxylic acidity [27], or twice the amount of NaOH titration, and pH 8-10 was used as an estimate for determining phenolic acidity [11]. The same procedure is applicable for measuring the charge density of transphilic NOM (or hydrophilic acids) (XAD-4 resin isolate). It should be noted that NOM concentration in the titration sample should be high enough to avoid experimental errors that are commonly observed in a blank test (titration with NOM-free DI water) since very small amounts of NaOH is used for potentiometric titration. A better understanding of NOM transport characteristics in NF and tight-UF membranes may be facilitated by considering the charge density of NOM, since most commercially available membranes are negatively charged [28-29].

1.2.6 Colloidal NOM

Colloidal NOM is an important NOM fraction as it serves as the DBP precursor with high DBP formation potential, causes severe flux decline of membranes, and easily degraded in the

distribution system. Colloidal NOM was isolated using a 3.5 KDa dialysis bag involving several purifications and precipitation steps [9]. The comprehensive approach to NOM isolation presented by Leenheer identified most of the "missing NOM" as being in the colloidal NOM isolated by membrane dialysis. In this research, colloidal NOM was spectrally characterized as N-acetyl amino-sugars. Recent research shows that colloidal NOM, possessing large MW includes amino sugars and/or polysaccharide-like substances, and is neutral or positively-charged in natural waters (pH 6-8) [30].

1.2.7 Membrane Characterization

Membrane characterization, including pore size, hydrophobicity, and surface charge is needed to determine NOM transport characteristics in NF and tight-UF membranes since the mass transfer of NOM in the concentration polarization layer and through the membrane pores is affected by either hydrophobic or electrostatic interactions between NOM and the membrane (i.e. back diffusive transport of NOM in the concentration polarization layer may be accelerated when electrostatic repulsion between NOM and membrane surface is strong, while decreases when hydrophobic interaction is strong). It should be noted that although these parameters (pore size, hydrophobicity, and surface charge) describe that membrane characteristics affect NOM transport, they are not intrinsic properties of the membrane because they depend on the chemical and physical conditions in which the membrane is tested. This section presents an overview of the fundamental concepts of membrane characterization and a brief discussion of related research.

1.2.8 Pure Water Permeability and Salt Removal

Pure water permeability and average salt removal of a membrane are most common membrane properties. Pure water permeability is an intrinsic property determined using DI water (neither pH nor ionic strength adjustments) and it depends solely on temperature. It is determined based on the relationship between trans-membrane pressure (ΔP) and permeate flux (J). It is derived from the slope (X-axis: ΔP, Y-axis: J) of the relationship. Membrane hydraulic resistance (R_m) is inversely related to pure water permeability ($L_p = (\text{kinematic viscosity} \times R_m)^{-1}$). Salt removal of a membrane, and chemical, physical, and hydrodynamic conditions under

which the experiment is performed are recorded. In case of reverse osmosis (RO) and UF membranes, the type of salt (mono- or multi-valent) does not affect average salt rejection significantly (most salt are retained by RO membranes and most transmit through UF membranes) [31], while it significantly affects NF membrane, particularly as 'Donnan Exclusion' plays an important role in salt removal by NF membranes unless the concentration in the feed is very high [32-33].

1.2.9 Nominal and Effective Membrane MWCO

Membrane molecular weight cutoff (MWCO) is directly related to NOM transport through membrane pores, and affects NOM transport in the concentration polarization (CP) layer since suction through a membrane affects the formation of a CP layer. Pore size and its distribution has been determined using various methods, including the bubble point method, liquid displacement, solute probe techniques [34], and many others [35-36]. As inferred form the definition, the concept of MWCO is applied to NF and tight-UF (or UF) membranes since RO membranes are assumed to be non-porous and microfiltration (MF) membranes do not retain macromolecules. The nominal MWCO value of membranes provided by manufacturers are generally based on the solute removal test results using uncharged macromolecules such as dextran and polyethylene glycols (PEGs). However, the rejection of PEGs by charged membranes is influenced by solution chemistries, such as pH and ionic strength [37, 12]. Based on these observations, a new method was developed for determining membrane pore size distributions (PSDs) using a fractional rejection of non-ionic and charged macromolecules, and how these factors, including pH, ionic strength, divalent cations, and hydrodynamic, affect membrane pore size and its distributions by introducing the concepts of "absolute PSDs" and "effective PSDs" was demonstrated [38].

1.2.10 Membrane Hydrophobicity

Membrane hydrophobicity is an important factor affecting NOM transport characteristics in the CP layer, and also through NF and tight-UF membranes from the hydrophobic interactions between NOM and membrane surface (or pores). Membrane hydrophobicity can be evaluated based on membrane material and contact-angle measurement. However, the evaluation of membrane hydrophobicity in terms of membrane material should

be supported by contact-angle measurement. This is important because, there are many commercial membranes produced after surface-pore modification resulting in altered membrane hydrophobicity and surface charge. For instance, a polysulfone (PSF) membrane that is hydrophobic in terms of its material can become hydrophilic with the addition of sulfonic groups to its original PSF structure to make a sulfonated PSF membrane, and by deleting the methyl groups from the original PSF structure to make a polyethersulfone membrane [32]. In terms of its material properties, cellulose, a polysaccharide is relatively hydrophilic, an aromatic polyamide and is relatively hydrophobic, while, PSF is the most hydrophobic membrane [32].

Contact angle is the angle (measured through the denser fluid) formed at the junction of a solid surface and two immiscible fluid phases [39]. When a drop of water is placed on a membrane surface in the open atmosphere, the angle between the membrane surface and the air-water interface (measured through water) is the contact angle. Contact angle is a measure of the wetting tendency of the water on the membrane surface [40]. The concept of contact angle is closely related to surface tension with the exception that surface tension represents the interfacial tension between two phases, whereas contact angle describes the interface between three phases [41]. When a drop of water is present on a membrane, interfacial energy arises from the competing tendencies of the drop to spread on the membrane surface and to form round shape to minimize its area [40]. The most widely used techniques for measuring the contact angle of a membrane are the sessile drop and adhering gas bubble [42]. In both cases, a direct measurement of the contact angle is made from the drop (or bubble) profile. For the sessile drop technique, a drop of liquid is placed on a dry membrane surface, while a bubble of gas is placed underneath the submerged membrane surface for the adhering gas bubble technique. Numerous studies have shown consistency between the two methods. However, the adhering gas bubble method offers a significant advantage for measurements on membrane surface since that contact angle can be measured in the aqueous phase at a desired solution chemistry [43]. Measuring dry membranes is likely to introduce systematic errors; hence *in situ* measurements are preferable [44]. Contact-angle hysteresis, which is the difference between advancing and receding angles, relates to flux decline and recovery ratio of cellulose acetate and PSf membranes with proteins and dextran [45]. Membranes with smaller hysteresis exhibit minimal flux decline and good recovery. Even though the contact angle is considered the most convenient and reliable index of membrane hydrophobicity, it is controversial, in that

if hydrophobicity of the pore surface of a membrane is the same as that of the membrane surface measured by the contact angle.

1.2.11 Membrane Surface Charge

In this study, the results obtained from the NOM transport experiment and the diffusion cell tests are discussed based on electrostatic interactions between acidic functional groups of NOM and the negatively-charged surface of NF and tight UF membranes. A fundamental understanding of the surface (or pore) charge of a membrane and electrostatic interactions between NOM and the membrane is important. A polymeric membrane acquires surface charge when in contact with an aqueous medium (water). This charge influences the distribution of ions at the membrane-solution interface. Co-ions are repelled from the membrane surface while counter-ions are attracted to the surface. Consequently, an electrical double layer forms at the membrane surface. The distribution of ions in this layer have been described in several ways [41, 46-51].

Fundamental to all methods of the electrical double layer is the concept of a plane of shear. This plane separates the fixed part of the electrical double layer from the mobile part. The electrical potential at the shear plane is the zeta (or electrokinetic) potential. This potential is lower than the surface potential and is of significance, because the actual surface potential cannot be determined experimentally [41, 47, 48, 51]. Zeta potential can be determined from one of the following electrokinetic measurements: streaming potential, sedimentation potential, electro-osmosis, or electrophoresis [41, 47, 48]. Streaming potential has been the most widely used technique, as it is suitable for flat membrane surfaces [1, 29, 47, 52-53]. The effects of NOM and ionic species on membrane surface charge using both electrophoresis and streaming potential techniques was reported [54].

There have been numerous studies related to the surface charge of a membrane and factors governing, such as solution chemistry, adsorption of charged and non-charged macromolecules, and type of electrolytes. Zeta potential decreased and reached negative values with increasing pH [29, 53, 54]. Zeta potential of membranes with adsorbed protein or humic acids were less negative than those of clean membranes before adsorption [1, 53]. When using Suwannee River humic acid (SRHA) solution as a background electrolyte for zeta potential measurement, zeta potential was more negative compared to those measured without SRHA. Shim and co-workers (2002) attributed such differences in the roles of NOM to the surface

charge of the membrane that depends on the intrinsic surface charge of the membrane (i.e., a membrane with relatively high negative surface charge becomes less negative due to NOM adsorption, while a membrane with neutral or slightly charged (negatively) becomes more negative due to the role of NOM as a background electrolyte) [54].

There is considerable debate about the fact that surface charge should decrease negatively under high ionic strength because the double layer of the membrane surface is compressed by the higher ionic strength. The effect of ionic strength on PEG removal by sulfonated PSF [37] and polyamide thin-film-composite [38] membranes resulted in increased PEG removal with higher ionic strength, suggesting that the higher ionic strength reduced the pore radii of the membrane. This result provided indirect evidence of the charge of the membrane surface. Zeta potential comparison for different ionic strengths (conductivity) is not always reliable, however, the relative zeta potential of different membranes with the same ionic strength are comparable to assess the relative surface charge.

1.2.12 Other Characteristics

Other techniques applied to membrane characterization include FIIR spectrum (to identify functional groups of membrane surfaces), direct titration (to determine the amount of ionizable functional groups of membrane surface and pores), and AFM (to estimate roughness of membrane surface). Using FTIR spectrum, Kim et al. characterized a protein-fouled UF membrane and compared it to a virgin membrane [55]. Cho et al. compared the IR spectra of clean and NOM-fouled NF and UF membranes to demonstrate differences in functional groups, and observed noticeable differences in both, the absorbance intensity and IR peak between clean and NOM-fouled membranes [25]. The main idea of direct titration is similar to that of potentiometric titration used for determining charge density of NOM: very small and tiny pieces of a membrane (instead of hydrophobic or transphilic NOM) are placed in DI water after removing the supporting material, followed by pH adjustment, and titrated with acidic or basic ionic solutions [54, 56]. Both quantitative (amount) and qualitative (identification) analyses of ionizable functional groups in the membranes are expected when direct titration and FTIR spectrum are used together.

Hirose et al. suggested a linear relationship between membrane surface roughness and permeate flux for cross-linked aromatic polyamide RO membranes, where permeability increased with increasing surface roughness [57]. The linear relationship was attributed to

surface unevenness of the RO membrane skin layer, which resulted in enlargement of the effective membrane area. Vrijenhoek et al found that during the initial stages of fouling, more particles were deposited on the rough membrane than on the smooth membrane [58]. This was attributed to the supposition that particles preferentially accumulated in the "valleys" of rough membranes, resulting in "valley clogging", which caused severe flux decline than those in smooth membranes. However, it is still ambiguous whether or not surface roughness of membranes affect the long-term flux decline (after valleys are filled with particles). It is likely that long-term fouling is affected by foulant-foulant interactions rather than by foulant-membrane interactions.

1.2.13 Membrane Process

In this section, an overview of the fundamental theories and models needed to understand water treatment membrane processes (or pressure driven membrane processes) is provided. Detailed descriptions, discussions, and considerations about theories and models, refined to determine NOM transport characteristics in the CP layer, and through NF and tight-UF membranes are included.

1.2.14 Membrane Performance

Permeate flux and observed solute rejection are common parameters used for determining membrane performance. Permeate flux represents the quantity of water produced by the membrane process and is represented by Eq. 1-1, and it is assumed that no solute permeates through the membrane [32]:

$$J_w = L_p(\Delta P - \Delta \Pi) \tag{1-1}$$

where, J_w is the water flux (volume of water passing through a unit area of membrane per unit time), L_p is the pure water permeability (also defined as the hydrodynamic permeability coefficient), ΔP is the trans-membrane pressure, and $\Delta\Pi$ is the osmotic pressure difference across the membrane. In practice, NF and tight-UF membranes are a slightly permeable to low molecular solutes, and hence the '*real*' osmotic pressure difference across the membrane is not $\Delta\Pi$ but $\sigma\Delta\Pi$, where, σ is the reflection coefficient of the membrane for that particular solute. When observed solute removal is not 100%, then $\sigma < 1$ and Eq. 1-2 now becomes [32]:

$$J_v = L_p(\Delta P - \sigma\Delta\Pi) \quad (1\text{-}2)$$

where, J_w (Eq. 2-1) is replaced by J_v because the flux now is the solvent (water and solute) flux (J_w may also be used instead of J_v since most processes are operated in dilute conditions). However, the '*effective*' osmotic pressure difference across the membrane (which should be overcome by the trans-membrane pressure to produce water) may not be $\sigma\Delta\Pi$ but $\sigma\Delta\Pi_m$, where, $\Delta\Pi_m$ is the osmotic pressure difference between the membrane surface (not the feed bulk) and permeate, since concentration polarization, in practice, is an inevitable phenomenon in a pressure-driven membrane process [59]. Therefore, Eq. 1-3 becomes:

$$J_v = L_p(\Delta P - \sigma\Delta\Pi_m) \quad (1\text{-}3)$$

In case of MF and loose-UF membrane processes for particles and colloids rejection, the osmotic pressure produced by particles and colloids is negligible. Hence, the mechanical resistance of those accumulated (or polarized) at the membrane surface (which also results from the concentration polarization) is thought to determine the flux. In other cases with tight-UF (pore sizes range from 5 to 1 nm) and NF membrane processes for the separation of NOM (or other low MW macromolecules), consideration of both, the osmotic pressure and the mechanical resistance is needed to accurately determine the flux. In addition, it is difficult to define the solvent flux with one simple equation when natural water is directly filtered by a membrane without proper pre-treatment. This is because natural water includes all the solutes mentioned above in addition to various ionic species (although flux decline due to fouling is excluded, solvent flux at steady-state should be represented by various parameters including pure water permeability, trans-membrane pressure, effective osmotic pressure difference, and various mechanical resistance produced by polarized NOM, colloids, and particles). Based on the above considerations, the solvent (only contains water and NOM) flux of NF and tight-UF membrane processes may be defined as:

$$J_v = \frac{\Delta P - \sigma\Delta\Pi}{\mu(R_m + R_{CP})} \quad (1\text{-}4)$$

where, R_m is the membrane hydraulic resistance (R_m is identical to the pure water permeability, L_p), R_{CP} is the mechanical resistance produced by NOM accumulated (or polarized) in the CP layer, and $\sigma\Delta\Pi$ is the effective osmotic pressure produced by the accumulation of ionic salt at the membrane surface.

The selectivity of a membrane for a given solute is a measure of the quality of the water produced by the membrane process and is expressed by the observed solute removal R_{obs} [32]:

$$R_{obs} = (C_b - C_p)/C_b \quad (1\text{-}5)$$

where, C_b and C_p are the solute concentrations of the bulk feed solution and permeate, respectively. As mentioned above, the solute concentration at the membrane surface (C_m) is higher than that of the bulk feed solution due to CP. Hence, the true solute removal (R) by the membrane is expressed as [32]:

$$R_{obs} = (C_m - C_p)/C_m \quad (1\text{-}6)$$

The other important parameter remaining is the solute flux (often expressed as J_s), which links the solvent flux and the observed solute removal. To illustrative, the solute transport characteristics through a membrane, consider that in a diffusion-dominant membrane processes (solute transport though a membrane is mainly affected by the concentration difference across the membrane rather than the trans-membrane pressure), the trans-membrane pressure affects the solvent flux but hardly affects the solute flux, whereas both the solvent and solute flux are affected by the trans-membrane pressure in a convection-dominant membrane process. Most RO processes are diffusion-dominant (the observed salt removal increases with increasing trans-membrane pressure [31-32], while MF and loose-UF processes are convection-dominant), and the observed particle or colloid removal decreases with increasing trans-membrane pressure [60-61].

1.2.15 Concentration polarization and fouling

Membrane performance can change significantly with time, and often a typical flux-time behavior may be observed: the flux through the membrane decreases over time owing to

CP and fouling [32]. CP differs from fouling (pore-blocking, surface and pore adsorption, cake layer formation, or gel layer formation), since it is reversible for pressure release (i.e., CP disappears when the trans-membrane pressure reaches zero). Also, CP reaches steady-state as the convective transport of solute to the membrane equals the sum of the permeate flow plus the diffusive back transport of the solute (in case of salt, steady-state is reached within a few minutes), whereas fouling is a time-dependent phenomenon (it could reach steady-state ultimately, however, cleaning is often carried out prior to it reaching steady-state). Although CP and fouling are different phenomena, both are not completely independent of each other, given that fouling often results from CP.

1.2.16 Flux decline due to concentration polarization

Polyamide thin-film-composite (TFC) NF membranes were used to determine the mechanical resistance of polarized NOM with salt-free feed water containing only NOM (colloids and particles were removed with pre-filtration prior to flux decline tests) [62]. Flux decline due to polarized NOM at the membrane surface itself was insignificant compared to that of pure water flux, however, severe flux decline was observed when the feed water ionic strength was increased (zero to 10 mM) (owing to osmotic pressure build-up) as well as small amounts of calcium (0.1 mM) was added to the feed water (due to either NOM adsorption at the membrane surface or increase in the mechanical resistance). This indicates that NOM does not lead to significant osmotic pressure, and the mechanical resistance of polarized NOM layer is smaller than that of the NF membrane hydraulic resistance itself unless fouling occurs. Another possible reason for this observation is the electrostatic repulsion between NOM and negatively-charged NF membrane surface which was used. Moreover, the condition of no salt (or no calcium) in the feed water favors enhanced electrostatic repulsion.

1.2.17 Flux decline due to fouling

Several studies have investigated the influence of pH, ionic strength, and calcium concentration on the flux decline of NF and UF membranes due to NOM fouling [2, 12, 37, 63]. Even though each study used a different membrane and NOM, the common observation was that the flux declined severely with decreasing pH, increasing ionic strength and calcium concentration. Electrostatic interaction played an important role in NOM fouling. Hydrophobic interactions also influenced flux decline due to NOM fouling, and the results indicate that a

hydrophobic NOM (XAD-8 isolate) exhibited more flux decline than the hydrophilic NOM (the effluent of XAD-8 resin) [2]. Based on the results of Cho et al. [25], non-charged NOM fractions are considered important foulants for both relatively hydrophilic and hydrophobic NOM-source waters. Flux decline was severe when NOM contained polysaccharides or polysaccharide-like substances (hydrophilic neutral component included in the effluent of XAD-4 resin). Furthermore, fouled membranes were verified using FTIR. Various studies have shown that hydrophobic membranes (based on contact angle measurements) were easily fouled by NOM compared to hydrophilic membranes [25, 64-65]. The influence of hydrodynamic conditions (in terms of initial permeation drag [63, 66] and J_0/k ratio (the ratio of water molecule transport by permeate flux to NOM molecule transport by back diffusion) [12, 67] on flux decline due to NOM fouling was investigated. The results revealed a large flux decline with increase in the initial permeation drag and J_0/k ratio. Based on previous studies, we can postulate that flux decline due to NOM fouling is reduced by increasing electrostatic repulsion, decreasing hydrophobic interaction, and adjusting hydrodynamic conditions.

1.2.18. Donnan equilibrium in charged membranes

A dynamic equilibrium occurs when a charged membrane is placed in a salt solution. The counter-ion (opposite in charge of the fixed charge in the membrane) concentration is higher while the co-ion (same charge type as the fixed membrane charge) concentration is lower in the membrane phase than in the bulk solution, thus creating a Donnan potential. This potential prevents the diffusion of the counter-ion from the membrane phase to the bulk solution, and the diffusion of the co-ion from the bulk solution to the membrane phase. A potential also occurs when an applied pressure gradient forces water flow through the membrane. The effect of Donnan potential is repulsion of the co-ion from the membrane, and because of electroneutrality requirements, the counter-ion is also rejected. The fixed charged groups in most charged nanofiltration membranes are carboxylic, sulfonic, and amino groups.

Three important features in Donnan equilibrium are (1) unequal distribution of ions, (2) osmotic pressure, and (3) the potential difference between the membrane and bulk solution phases. Considering the concentration differences at the interface between the membrane and the external dilute solution, the Donnan equilibrium can be simply assumed as shown in Eq. (1-7). The Donnan potential differences ψD on both sides of the membrane are determined to satisfy the electroneutrality in the membrane and in the external solutions is expressed as Eqs.

(1-8) and (1-9), respectively, based on assumed activity coefficient γ_i = 1.

$$\left(\frac{\gamma_i c_i}{\gamma_i^o C_i}\right)^{1/z_i} = exp\left(-\frac{F\Delta\psi_D}{RT}\right) \quad (1\text{-}7)$$

$$\sum z_i c_i + \varphi X = o \quad (1\text{-}8)$$

$$\sum z_i C_i = o \quad (1\text{-}9)$$

where, Ci and ci = solute concentrations in external solution and membrane respectively, F = Faraday number, R = gas constant, T = temperature, zi .= valence of the solute, and φ X = effective charge density of membrane.

The model predicts that the rejection is a function of the membrane charge density, feed solute concentration, and the charge of the ions. While it does provide a qualitative description of solute rejection, this model does not take into account diffusive and convective fluxes; these are also important in the charged membrane process.

1.3 Hypothesis and objectives

The surface charge properties of membranes in contact with aqueous media are induced by the ionization of surface functional groups (e.g., –COOH, $–NH_2$, and $–SO_3H$) as indicated below [68–73]:

$$R–COOH \leftrightarrow R–COO^- + H^+ \quad (1\text{-}7)$$

$$R–NH_2^+ \leftrightarrow R–NH + H^+ \quad (1\text{-}8)$$

$$R–SO_3H \leftrightarrow R–SO_3^- + H^+ \quad (1\text{-}9)$$

Therefore, the ζ (zeta) potential of the membrane surface, as determined by electrokinetic measurements, is widely used as a surrogate parameter to represent the surface charge properties of membranes. It theoretically corresponds to the electric potential at the shear plane between the stern and diffuse layers, according to the electrical double layer theory [74]. However, ζ potential cannot accurately represent the surface charge properties of the membranes because of the distance between the surface and the shear plane of the electrical double layer. Hence, ζ potential is typically lower than the local surface potential calculated using the diffuse double layer theory (Fig. 2) [75]. In addition, the accurate measurements of ζ potential values can be hindered by cation species in the electrolyte solutions entering the diffuse layer, as electrokinetic measurements generally employ electrolytes (e.g., NaCl or KCl) with a streaming potential to drive the pressure or electrophoretic mobility of particles [74, 76-80].

To overcome these limitations, an approach capable of accurately representing the surface charge properties of the membranes is required. In this context, potentiometric titration analysis is a well-established method to quantify the ionized functional groups present in organic materials [81]. Therefore, potentiometric titrations have been employed to evaluate the complexation of natural organic matter (NOM) with heavy metals and other minerals [82-84]. As positively charged ions and particles have been found to readily complex with NOM, the electrostatic repulsion between NOM and membrane surfaces that influence membrane fouling could also be estimated using potentiometric titrations [85]. Although, some studies have investigated the differences in the surface charge properties of the membranes based on potentiometric titration and electrophoresis, the potentiometric titration method has not yet been applied to determine surface charge properties of membranes and subsequent prediction

of the performance of membrane processes [80, 86]. Thus, the objective of this study is to investigate the membrane fouling mechanism and the performance of the membranes, based on electrical transport of natural organic matter (NOM) and ions at the membrane surface using electrophoresis and potentiometric titration methods.

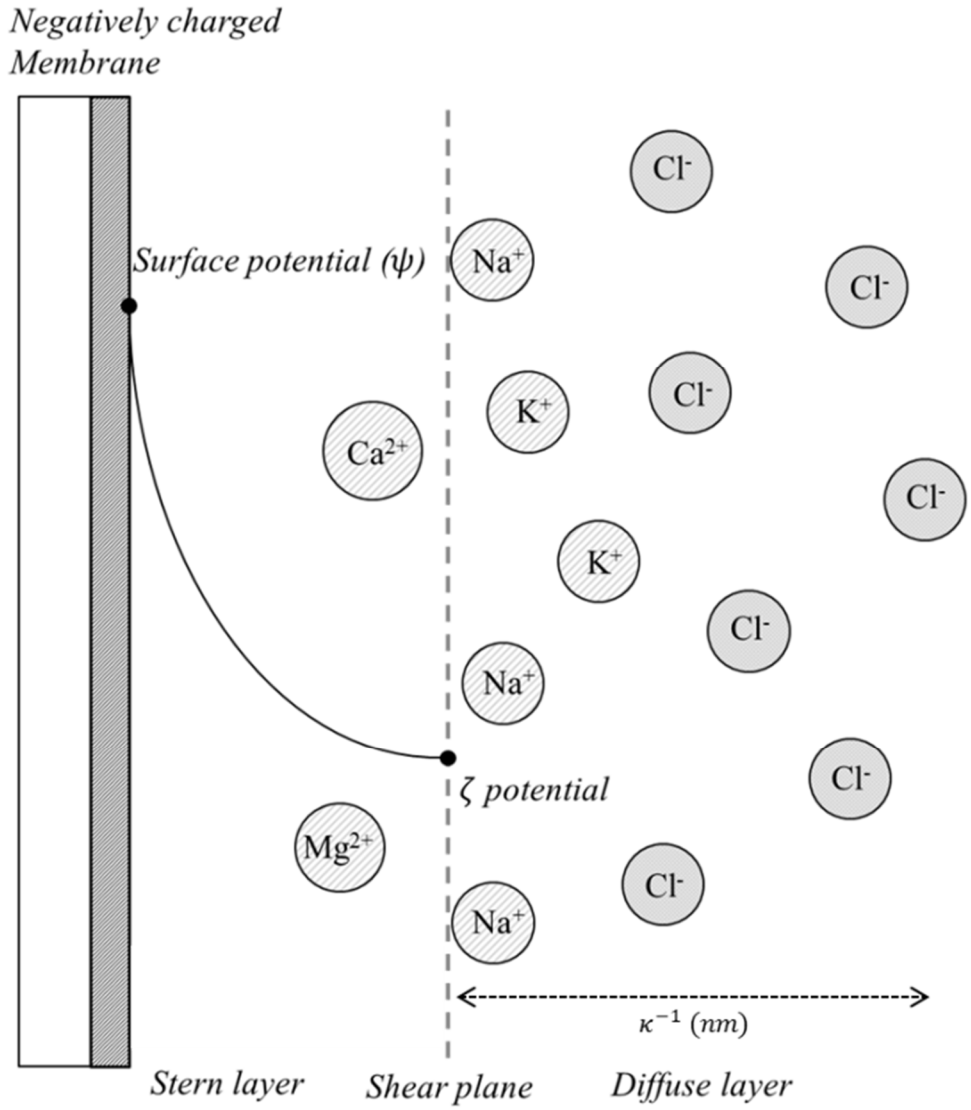

Figure 1-1. Schematic of surface potential and zeta potential in the electrical double layer theory.

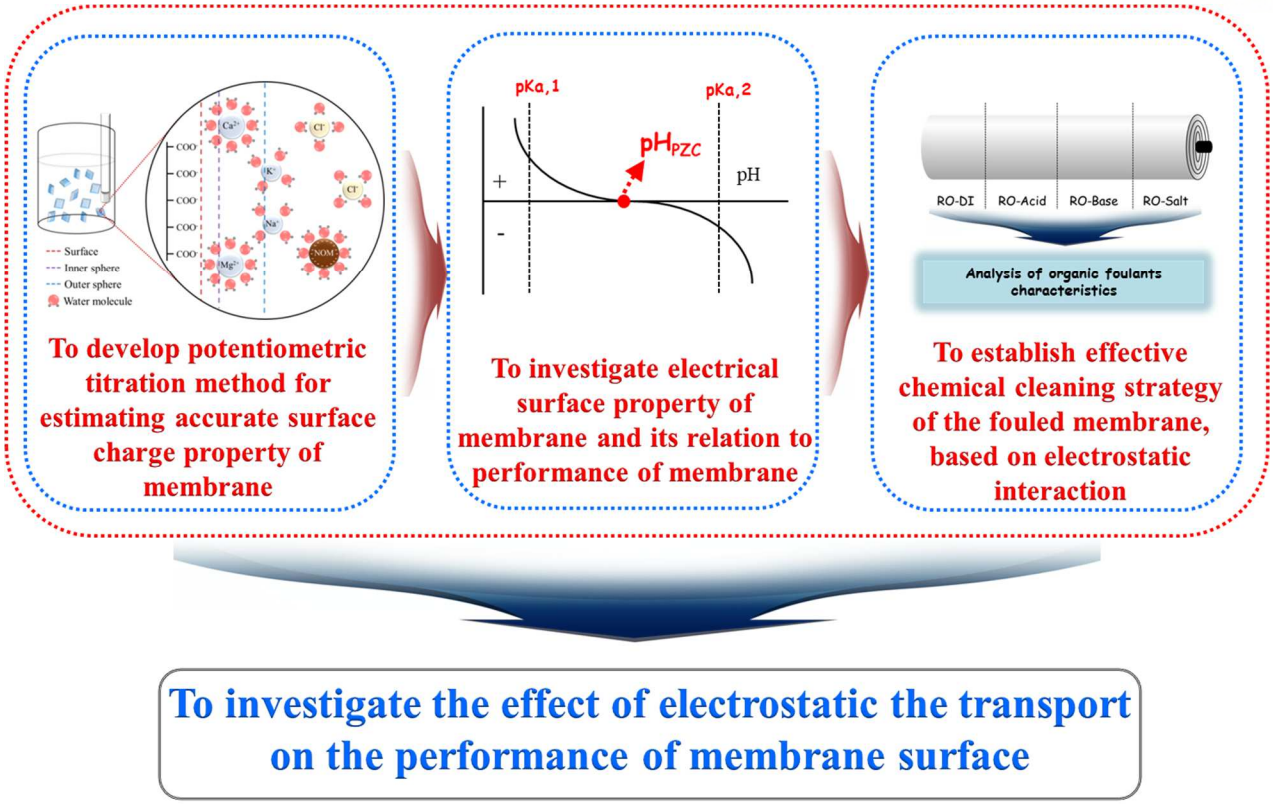

Figure 1-2. Concept schematic of surface potential and zeta potential in the electrical double layer theory.

2.0 Surface charge characterization of nanofiltration membranes by potentiometric titrations and electrophoresis: Functionality vs. zeta potential

2.1 Introduction

During recent decades, great progress has been made in the field of membrane technologies, which has enabled their use in practical applications, including drinking water production, wastewater treatment, seawater desalination, and energy recovery [87-90]. However, the efficient operation of membrane processes is still hindered by membrane fouling, which significantly influences their performance in terms of salt rejection and permeate flux decline [91]. Indeed, the surface charge properties of the membranes are considered as key factors affecting their salt rejection and permeate flux decline. For example, electrostatic interactions between charged solutes and membrane surfaces (known as Donnan exclusion) can have a significant effect on the salt rejection [92-94]. Furthermore, membranes electrostatically repel charged organic materials, colloids, and particles due to their charged surfaces at neutral pH values, which ultimately plays a critical role in the accumulation of potential foulants on the membrane surfaces which is associated with the decline of permeate flux [95-97]. To address these issues, many researchers have investigated the surface charge properties of membranes and their relationship to the electrostatic transport at the surfaces, which in turn determines their salt rejection and fouling mechanisms [98-101].

The main purpose of this study was to validate a potentiometric titration method based on the quantification of ionized functional groups (termed as functionality) to estimate the surface charge properties of nanofiltration (NF) membranes. Therefore, the functionality and ζ potential were rigorously characterized using potentiometric titrations and electrophoresis at various pH and ionic strength conditions, and directly correlated to the performance of the NF membranes in terms of salt rejection and fouling propensity.”

2.2 Materials and methods

2.2.1. Physicochemical properties of the NF membranes

Two different types of thin-film composite (TFC) NF membranes, namely NE20 (nominal molecular weight cut-off (MWCO) = 1000 Da) and NE70 (nominal MWCO = 350 Da) (Toray Chemical, Seoul, Republic of Korea), were employed to compare their functionality and ζ potential measurements. The physicochemical properties of the selected NF membranes are listed in Table 2-1. Although both membranes contain piperazine-based polyamides, their pore sizes in relation to the polymer-linking structures differed significantly from one another [80]. Prior to all experiments, the virgin NF membranes were soaked in deionized (DI) water for 1 day to remove the coating materials from the membrane surfaces. The functional group compositions of the NF membranes were identified using attenuated total reflection-Fourier transform infrared (ATR-FTIR) spectroscopy (Vertex70, Bruker, MA, USA) utilizing a ZnSe crystal at an incident angle of 45° over a scanning wavelength of 550–1800 cm^{-1} with a resolution of 0.4 cm^{-1} [101].

Table 2-1. The physicochemical properties of the NF membranes.

Classification	NF	
Membrane code	NE20	NE70
Manufacturer	Toray chemical, Seoul, Republic of Korea	
Membrane Type	Thin-film composite	
Membrane materials	Polyamide	
Water Soluble monomer	Piperazine	
Nominal MWCO (Da)	1000	350

2.2.2. Surface charge characterization of the membranes using electrophoresis

The ζ potential values of the NF membranes were measured by electrophoresis in a quartz cell. Due to the accumulation of cations in the electrolyte solution on the membrane surface, an asymmetric electroosmotic flow occurs through the membrane surface, which allows the monitoring particles to pass through the electrophoresis chamber. The ζ potential values of the NF membranes can therefore be calculated from the electrophoretic mobility of the monitoring particles using the Smoluchowski equation [92, 102]:

$$\zeta = 4\pi\eta U/\varepsilon_r\varepsilon_0 \quad (2\text{-}1)$$

where ζ is the ζ potential measured by electrophoresis (mV), U is the electrophoretic mobility of a monitoring particle ($cm^2\ V^{-1}\ s^{-1}$), η is the liquid medium viscosity (0.89×10^{-3} Pa s), ε_r is the liquid medium permittivity (78.38), and ε_0 is the vacuum permittivity (8.854×10^{-12} s m^{-1}). In this study, the ζ potential values of the NF membranes were determined using a commercial electrophoresis analyzer (ELSZ-2000, Otsuka Electronics, Osaka, Japan) with polystyrene latex particles (diameter = 520 nm) coated with hydroxypropyl cellulose (HPC, molecular weight (MW) = 300,000 Da) as a mobility monitoring particle.

As the ζ potential values of membranes vary significantly depending on the pH and ionic strength of the solution, the effects of pH on the ζ potential measurements were identified using a 10.0 mM NaCl solution between pH 2.0 and 11.0. In addition, the dependence of the ζ potential values on ionic strength at each pH (pH = 2.0, 4.0, 5.5, 7.0, 9.0, and 11.0) was investigated under 4 different ionic strength conditions (NaCl concentrations = 0.1, 1, 5, and 10.0 mM). The pH of each samples was adjusted using 0.1 M of NaOH and HCl solutions and then its ζ potential value was subsequently measured using the electrophoresis method in 30 seconds. For all experiments, the electrophoresis cell constant was calibrated using a 10.0 mM NaCl solution and was used to compare the relative ζ potential values under different ionic strength conditions, as the electric field intensity, which is closely associated with the electrophoresis cell constant, varied significantly according to the ionic strength of the electrolyte solution.

2.2.3. Surface charge characterization of the membranes using potentiometric titrations

Prior to carrying out functionality measurements using potentiometric titrations, the supporting layer was completely detached from each NF membrane coupon (only TFC membranes are applicable) and the membrane coupons were soaked in DI water for 1 d (active surface area = $0.0031 \pm 0.0002\ m^2$). The soaked membrane coupons were cut into small pieces (~1.5 mm × 1.5 mm) and then immersed in a 10 mM NaCl solution (40 mL). The pH of the solution was adjusted to 2.0 using 0.1 M HCl solution and the solution was titrated from pH 2.0 to 11.0 using an automatic microtitrator (702 SM, Metrohm, Herisau, Switzerland) with a 0.5 N NaOH solution to quantify the ionized carboxylic and amine functional groups present on the active layers. Although the back side of the active layer contained dibenzyl sulfone moieties, these groups did not influence the functionality measurements of the membranes as

their acid dissociation constant ($pK_a \approx 23.9$) is significantly higher than the pH values of the tested electrolyte solutions (pH = 2.0–11.0) [103]. After subtracting the background functionality of DI water from the titration curves, the membrane functionalities were determined as follows:

$$\text{Membrane functionality (meq/m}^2\text{ membrane)} = \frac{(V_a - V_b) \times C_s}{A} \quad (2\text{-}2)$$

where V_a is the volume of NaOH solution consumed during titration of the active layer (mL), V_b is the NaOH volume consumed in a blank test with DI water (mL), C_s is the concentration of NaOH (N), and A is the surface area of the active layer (m^2).

The point of zero charge (PZC) determined at the pH value where the functionality of the membrane is independent on the ionic strength is defined as the point of zero salt effect in the titration curves. Therefore, these values were obtained by titrating the active layers of the membranes (sample volume = 40 mL) using a 0.05 N NaOH solution under different pH (4.0 – 9.0) and ionic strength conditions (NaCl concentrations = 0.1, 1.0, 5.0, and 10.0 mM [103-107]. On the basis of the PZC, the consumed volume of the NaOH solution during the titration was calculated from hexaplicate measurements. The difference between the concentration of acid and the concentration of base ($\Gamma_{H^+} - \Gamma_{OH^-}$) can be described as follow:

$$(\Gamma_{H^+} - \Gamma_{OH^-})(meq/m^2) = A_{PZC} - A_{pH} \quad (2\text{-}3)$$

where A_{PZC} is the membrane functionality at pH_{pzc} (meq/m^2), and A_{pH} is the membrane functionality as a function of pH (meq/m^2). The standard deviation was less than ±0.040 meq/m^2 for all the samples.

2.2.4. A bench-scale cross-flow NF membrane unit

The bench-scale cross-flow NF membrane unit was comprised of a flat-sheet filtration cell (effective surface area = 96 cm^2; channel height = 0.04 cm), a magnetic gear pump (Micropump, Vancouver, WA, USA), and a feed water reservoir (Fig. 2-1). Prior to carrying out the filtration tests, the NF membrane unit was stabilized using DI water over 2 h. The cross-

flow NF membrane unit was operated under recirculation mode at 20 ± 0.7°C. During the salt rejection and fouling experiments, the feed water pressure was maintained at 900 kPa constantly with a cross-flow velocity of 0.25 L min^{-1} (the initial water flux of the NE20 membrane =15.7 L m^{-2} h^{-1}; the initial water flux of the NE70 membrane = 14.7 L m^{-2} h^{-1}).

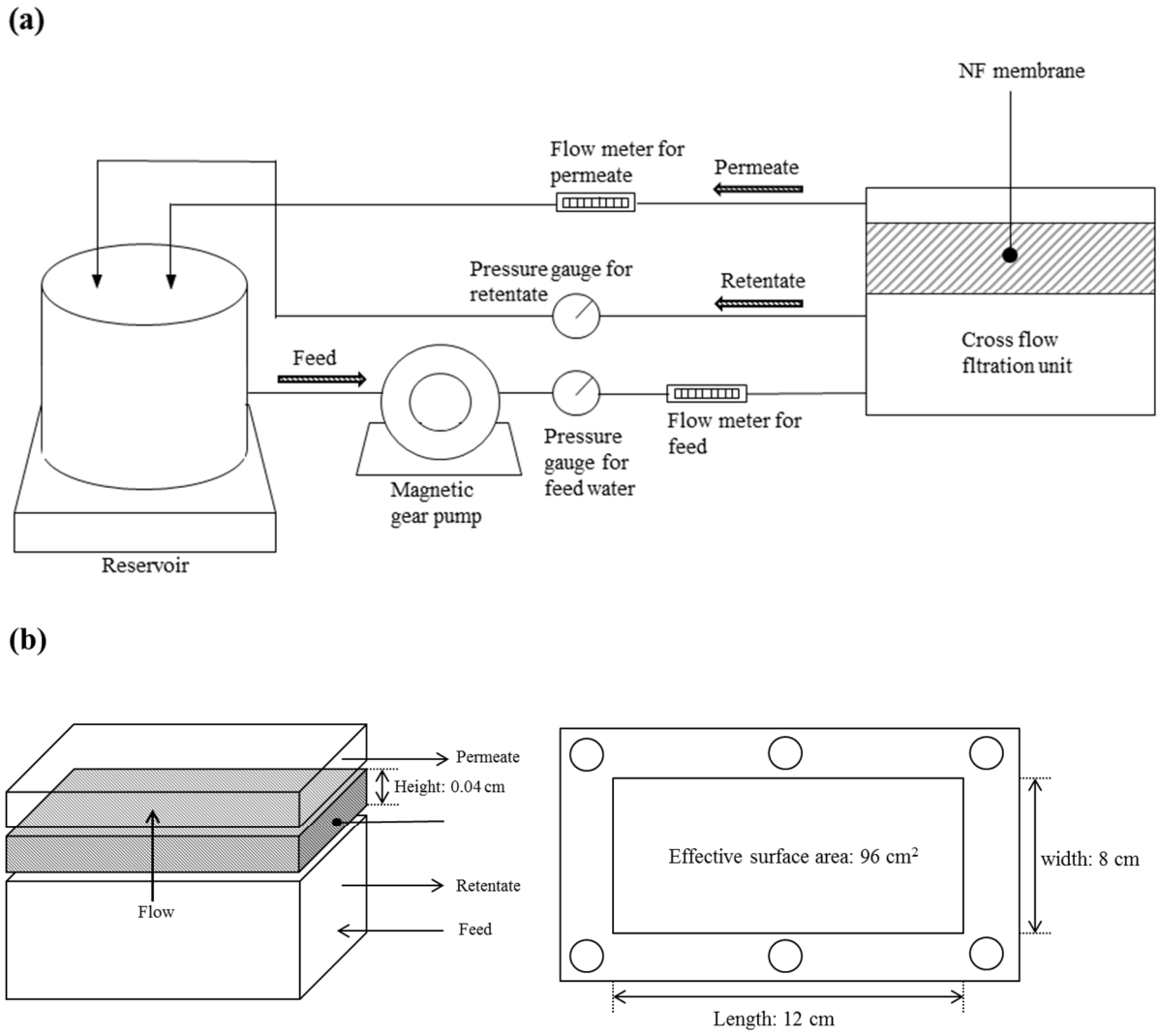

Figure 2-1. Schematic diagram of the laboratory-scale crossflow nanofiltration unit.

2.2.5. Salt rejection tests

The effects of the surface charge properties on the salt rejection of the NF membranes were investigated using a 10.0 mM NaCl solution at pH 5.0, 7.0, 9.0, and 11.0 (. Following stabilization for 1 h under the desired conditions, the permeate was collected and the concentrations of Na^+ and Cl^- ions in the feed and permeate samples were measured using ion

chromatography (DX-120, ICS-90, Dionex, Sunnyvale, CA, USA) equipped with IonPac CS12A and IonPac AS14 columns (Dionex, Sunnyvale, CA, USA). The rejection rates of NaCl by the NF membranes were calculated using the following equation:

$$\text{Salt rejection rate (\%)} = \left(1 - \frac{C_p}{C_f}\right) \times 100 \quad (2\text{-}4)$$

where C_f and C_p are the NaCl concentrations in the feed and permeate samples, respectively.

2.2.6. Preparation and characterization of an organic foulant

Humic acid purchased from Sigma-Aldrich (MO, USA) was selected as the organic foulant, and was pre-treated at pH 2.0 using a bench-scale NF unit equipped with an NE20 membrane (nominal MWCO = 1000 Da), as organic materials with MWs less than the MWCO of the membrane are often rejected due to electrostatic repulsion between the organic materials and the membrane surface [109]. The pre-treated foulant sample was then filtered using a 0.45 μm mixed cellulose ester membrane filter (Millipore, Bedford, MA, USA) to remove any suspended solids. The MW distributions of the untreated and pre-treated foulant samples were identified using high-performance size-exclusion chromatography (HPSEC) equipped with a Protein-Pak 125 column (Waters, Milford, MA, USA), and UVA and fluorescence detectors to confirm both the removal of organic foulants with small MW values (MW < 1000 Da) and the effective MWCO of the NE20 membrane (2620 Da) (Fig. 2-2) [110, 111]. The dissolved organic carbon (DOC) concentrations of the pre-treated foulant sample was adjusted to approximately 7.1 mg-C L^{-1} (determined using a total organic carbon (TOC) analyzer, TOC-$V_{CPH,}$ Shimadzu, Kyoto, Japan), and its ionic strength was adjusted to 10 mM by the addition of NaCl solid The hydrophobicity and functionality values of the pre-treated foulant sample determined using Amberlite XAD-8/4 resins (Supelco, Bellefonte, PA, USA) and potentiometric titrations are listed in Table 2-2 [112].

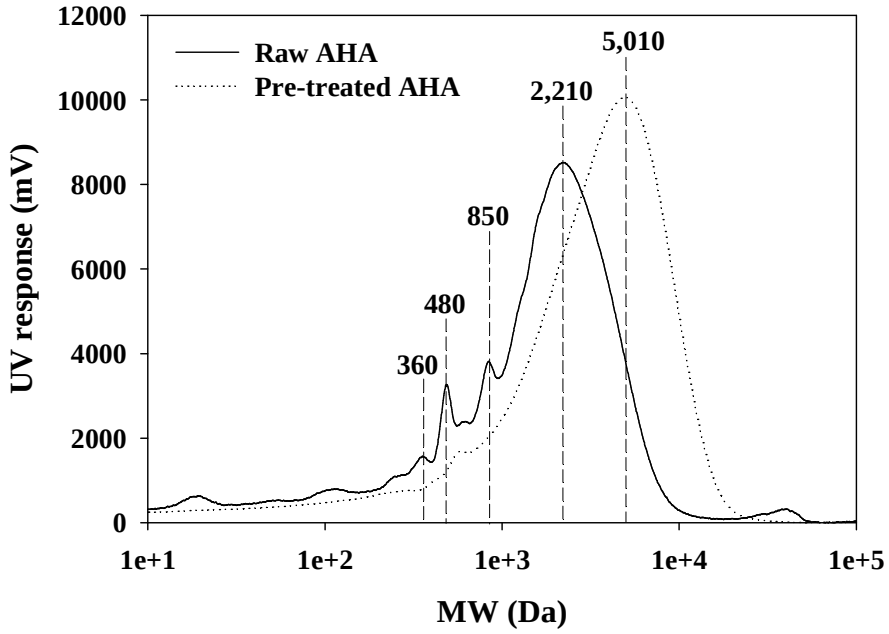

Figure 2-2. MW distribution of the untreated and pre-treated foulant samples at pH 2.0 using the NE 20 membrane (MWCO = 1,000 Da).

Table 2-2. Characteristics of pre-treated aldrich humic acid as a model foulant.

Property		Value
Dissolved Organic Carbon (DOC)		7.1 mgC/L
Manufacturer		Aldrich, USA
Acidity (meq/gC)	Total	16.6
	Carboxylic	12.2
	Phenolic	4.4
Relative polarity (%)	Hydrophobic	59
	Transphilic	17
	Hydrophilic	23

2.2.7. Fouling experiments

The fouling potentials of the pre-treated foulant towards the NF membranes were

investigated at different pH values (i.e., pH 2.0, 4.0, 5.5, 7.0, 9.0, and 11.0) to assess the suitability of the functionality and ζ potential values as surrogate parameters for predicting the fouling propensities of the NF membranes (determined by the amount of foulant desorbed from the membrane surface). To determine the effects of the surface charge properties on the formation of initial fouling layers by organic materials, each fouling test was conducted over 1 h. After the fouling experiments, the accumulated foulant on the membrane surface was desorbed using a 0.1 N NaOH solution, and the pH of the desorbed samples were immediately adjusted to 5.5. using a 0.1 N HCl solution to avoid oxidation of the humic substances. The amount of foulant desorbed from the membranes were then calculated from triplicate measurements using the following equation:

$$\text{Amount of desorbed foulant (mg-C/m}^2) = \frac{C_t \times V}{A} \quad (2\text{-}5)$$

where C_t is the DOC concentration (mg-C L^{-1}), V is the sample volume (L), and A is the membrane surface area (m^2). The standard deviation was less than ±9.3 mgC/m^2 for all the samples.

2.3. Results and discussion

2.3.1. Characterization of the NF membranes

The functional group composition of the NF membranes was investigated using ATR-FTIR spectroscopy (Fig. 2-3). The NE20 and NE70 membranes exhibited almost identical ATR-FTIR spectra, although there were slight differences in the intensities of the IR peaks. For both samples, the C=O bands of the carboxylic acids were observed in the range of 1700–1650, 1280–1200, and 1320–1210 cm^{-1}. In addition, the IR peaks in the range of 1600–1550 and 1500–1460 cm^{-1} indicated the presence of aromatic C=C moieties, while ketone C–CO–C stretches were observed in the range of 1150–1050 cm^{-1}, and the N–H bonds of the aliphatic amides produced a IR peak in the range of 750–700 cm^{-1} [113, 114]. These results imply that the NE20 and NE70 membranes are predominantly composed of both carboxylic and amide

functional groups, and had similar functional group compositions.

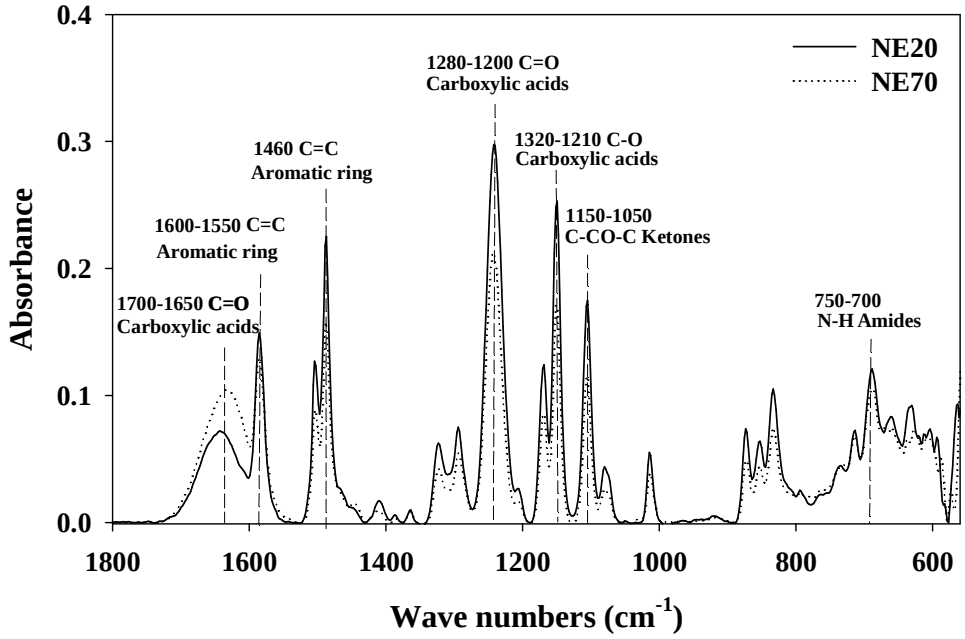

Figure 2-3. ATR-FTIR spectra of the virgin NE20 and NE70 membranes.

2.3.2. Effects of pH and ionic strength on the ζ potential measurements

The variations in the ζ potential values of the NF membranes between pH 2.0 and 11.0 (ionic strength = 10.0 mM NaCl) are illustrated in Fig. 2-4. As shown, the NE20 and NE70 membranes exhibited the positive ζ potential values when the solution pH was lower than the membrane iso-electric point (IEP; the pH where the ζ potential value = 0, IEP of the NE20 membrane = ~5.0; IEP of the NE70 membrane = ~3.0), while the negative ζ potential values were obtained when the solution pH was higher than the membrane IEP values. These amphoteric curves thereby confirm that the tested polyamide TFC NF membranes consist of bear carboxyl and amine functional groups on their surfaces when in contact with an aqueous solution [83]. In addition, the lower IEP and more negative ζ potential values of the NE70 membrane compared to the NE20 membrane can be attributed to its higher density of carboxylic functional groups ($pK_a \approx 3$). Despite the deprotonation of the amine functional groups ($pK_a \approx 9$) occurring above pH 9.0, negligible increases in the negative ζ potential values were observed for both the NE20 and NE70 membranes between pH 7.0 and 11.0. This observation therefore implies that the ζ potential measurements cannot truly reflect the deprotonation of the amine functional groups on the membrane surfaces.

The effects of ionic strength on the ζ potential values of the NF membranes under different pH conditions (ionic strength = 0.1, 1.0, 5.0, and 10.0 mM) are demonstrated as shown in Fig. 2-5. As indicated, the negative ζ potential values of the NF membrane surfaces were deceased with increasing the solution ionic strength, which can be explained by the electrical double layer compaction theory [89]. Indeed, the negative ζ potential values of the NF membranes can be reduced due to the decrease in the electrophoretic mobility of the monitoring particles with increasing the solution ionic strength [94]. Similarly, a reduction in the negative ζ potential values with increasing the solution ionic strength may reduce electrostatic interactions between the membrane surface and the organic materials [115]. As previously mentioned (Fig. 2-4), the ionization of amine functional groups was not responsible for the increased negative ζ potential values of the NF membranes under high ionic strength conditions (i.e., 10.0 mM NaCl). However, the substantial negatively increases in the ζ potential values of the NF membranes, corresponding to the ionization degree of the amine functional groups, was observed under low ionic strength conditions (i.e., 0.1 mM NaCl, Fig. 2-5). In addition, although the IEP values of the NF membranes should theoretically be independent from the

solution ionic strength, slight shifts were observed for both the NE20 and NE70 membranes. These results support the assumption that the Na^+ ions of the electrolyte solutions that enter the diffuse layer of the membrane surfaces under high ionic strength conditions may interfere with accurate assessment of the membrane surface charge properties by electrophoresis.

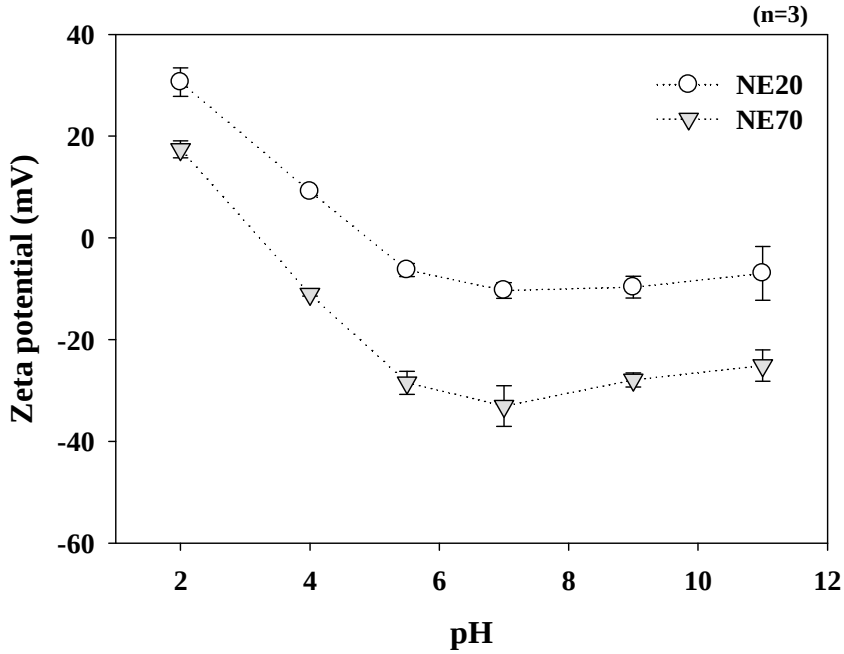

Figure 2-4. The ζ potential of the virgin NE20 and 70 membranes as a function of pH (pH = 2.0, 4.0, 5.5, 7.0, 9.0, and 11.0) at the ionic strength of 10mM NaCl.

(a)

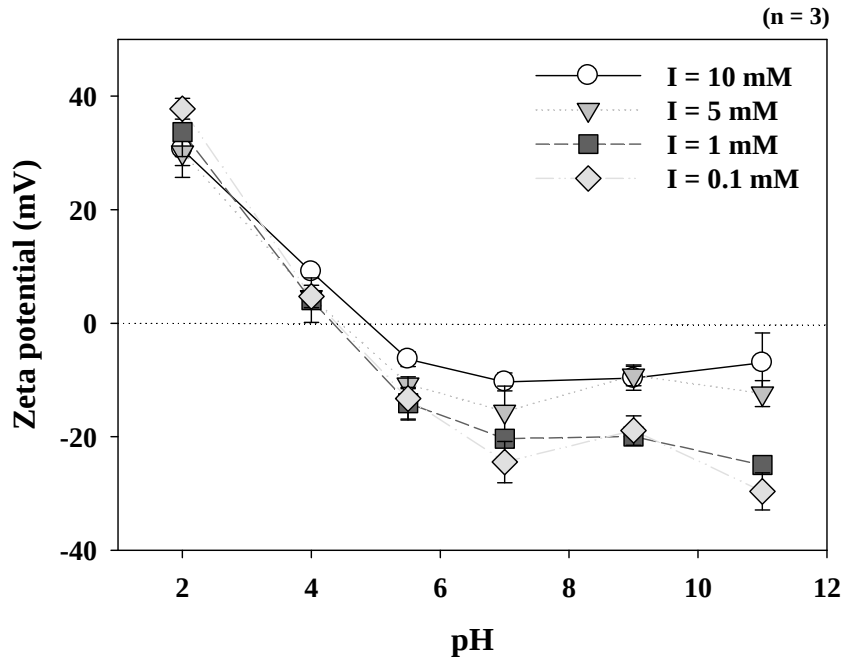

(b)

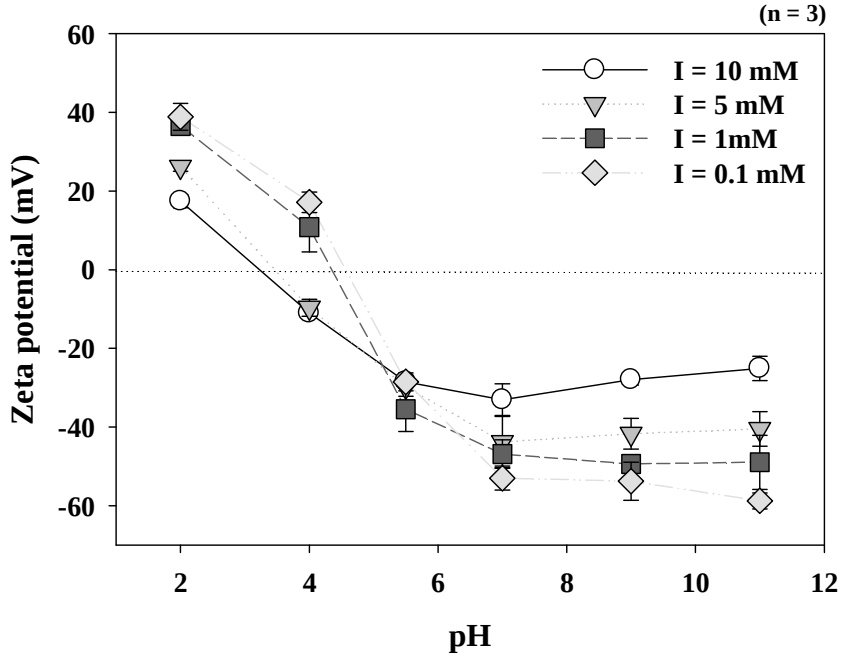

Figure 2-5. Ionic strength effects on the ζ potentials of the virgin (a) NE20 and (b) NE70 membranes as a function of pH (pH = 2.0, 4.0, 5.5, 7.0, 9.0, and 11.0).

2.3.3. Effect of ionic strength on the functionality measurements

The variations in the functionalities of the NE20 and NE70 membranes under different pH conditions (ionic strength = 10.0 mM NaCl) are depicted in Fig. 2-6. As expected from the ζ potential results, the NE70 membrane exhibited a higher functionality than the NE20 membrane because of its higher density of ionizable functional groups. In addition, the functionalities of the NE20 and NE70 membranes were gradually increased in the pH range of 2.0 – 4.0 due to the ionization of the carboxylic functional groups ($pK_a \approx 3$), while the functionalities became stable between pH 3.0 and 9.0. In contrast to the results obtained from the surface charge analyses of the NF membranes using electrophoresis, the functionalities of both the NE20 and NE70 membranes were significantly increased in pH range of 9.0 – 11.0 due to the deprotonation of the amine functional groups ($pK_a \approx 9$).

The potentiometric titration curves of the NF membranes under different ionic strength conditions are compared in Fig. 2-7. The functionalities of the NE20 and NE70 membranes were decreased with increasing the solution ionic strength, which corresponded to the previously mentioned electrical double layer compaction theory [89]. In addition, the NE20 and NE70 membranes were positively charged when the solution pH was lower than their PZC values (the PZC of NE20 membrane ≈ 7.0; the PZC of NE70 membrane ≈ 6.5) and their surfaces became negatively charged when the solution pH was above their PZC values. The lower PZC value observed for the NE70 membrane compared to the NE20 membrane can be explained by the differences in the ionization degree of the surface functional groups (i.e., the carboxylic functional groups). Unlike the IEP values, the PZC values were closely associated with the intrinsic pK_a values of the membrane surfaces governing the electrostatic transport at the membrane surfaces. These observations indicate that the functionality measurements may offer significant insights into the differences in the surface charge properties of the NE20 and NE70 membranes induced by the ionization degree of the surface functional groups.

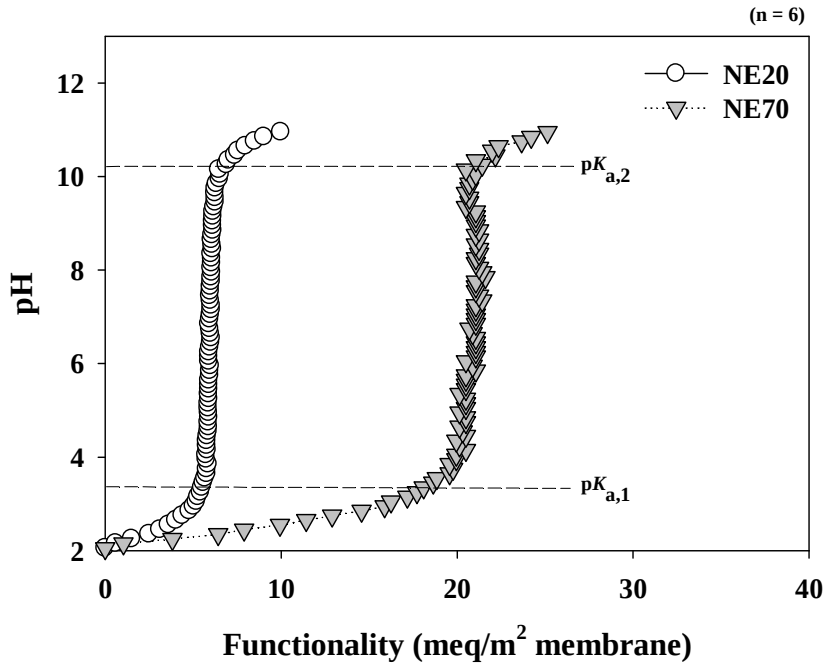

Figure 2-6. Functionality of virgin NE20 and 70 membranes estimated with 10 mM of NaCl electrolytes.

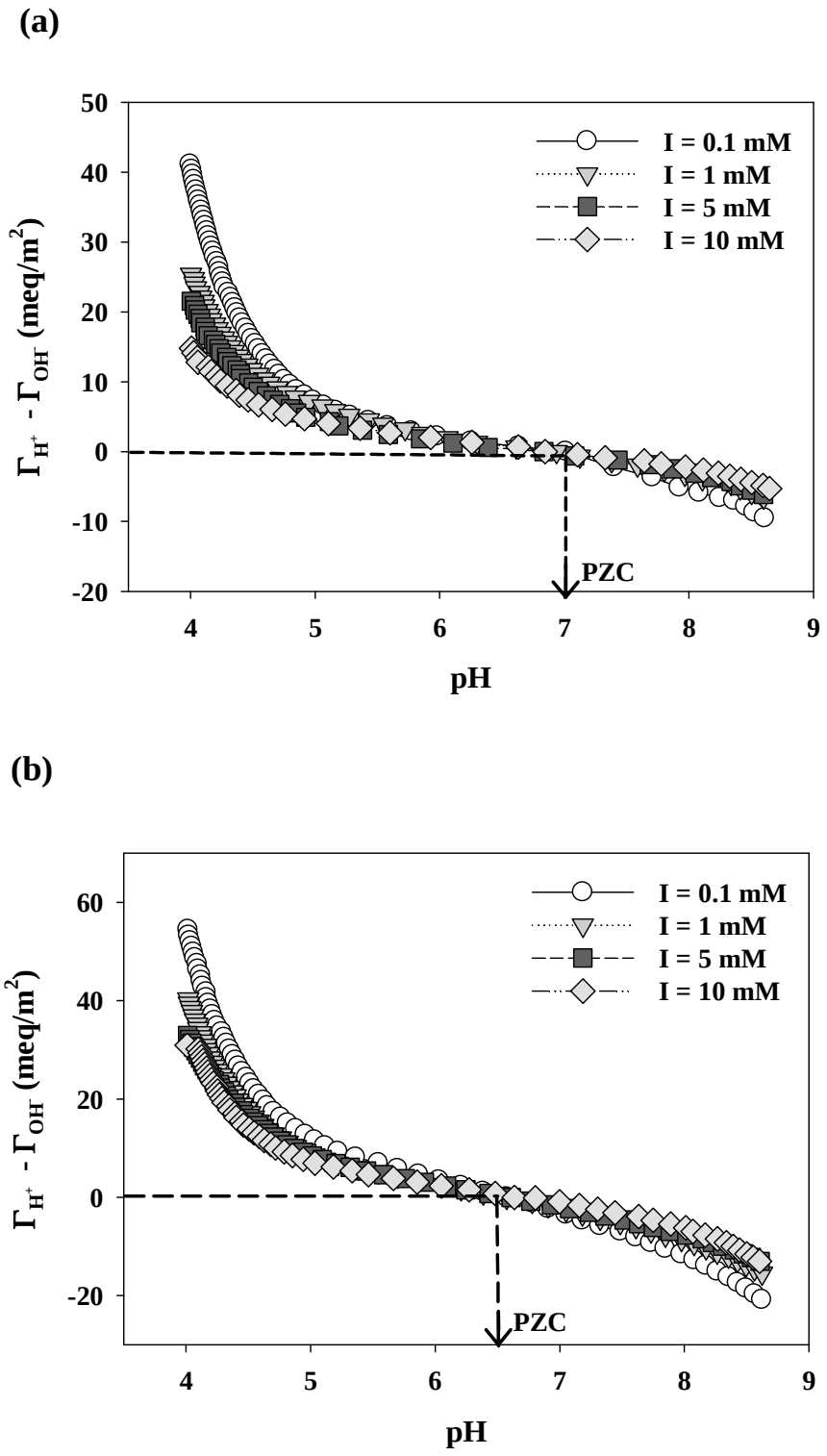

Figure 2-7. Potentiometric titration curves of (a) NE20 and (b) NE70 membranes as a function of ionic strengths to determine PZC of membrane (PZC of NE20 membrane: 7.0 PZC of NE 70 membrane: 6.5).

2.3.4. Effect of pH on salt rejection

The rejection rates of NaCl (concentration = 10.0 mM) by the NF membranes were evaluated under different pH conditions (i.e., pH = 5.0, 7.0, 9.0, and 11.0). As shown in Fig. 2-8, the NE20 and NE70 membranes exhibited their highest rejection rates of Na^+ ions at pH 5.0, whereas the highest rejection rates of Cl^- ions were observed at pH 11.0, which can be attributed to the dependence on the electrostatic repulsions between the membrane surfaces and the charged ions according to their PZC values (the PZC of NE20 membrane ≈ 7.0; the PZC of NE70 membrane ≈ 6.5) rather than their IEP values (the IEP of NE20 membrane ≈ 5.0; the IEP of NE70 membrane ≈ 3.0). The lowest rejection rates of both the Na^+ and Cl^- ions by the NE20 and NE70 membranes were observed at approximately pH 7.0, likely due to the absence of the electrostatic repulsions between the membrane surfaces and the charged ions. Furthermore, the rejection rates of NaCl by the NE70 membrane were significantly higher than those by the NE20 membrane due to the smaller MWCO value of the NE70 membrane (MWCO of NE70 = 350 Da; MWCO of the NE20 = 1000 Da) and its higher density of ionizable functional groups (i.e., carboxylic functional groups). These observations indicate that the functionality measurements based on potentiometric titrations for determining the PZC values of NF membranes can accurately predict the electrostatic transport of charged ions at the membrane surfaces in association with salt rejection.

(a)

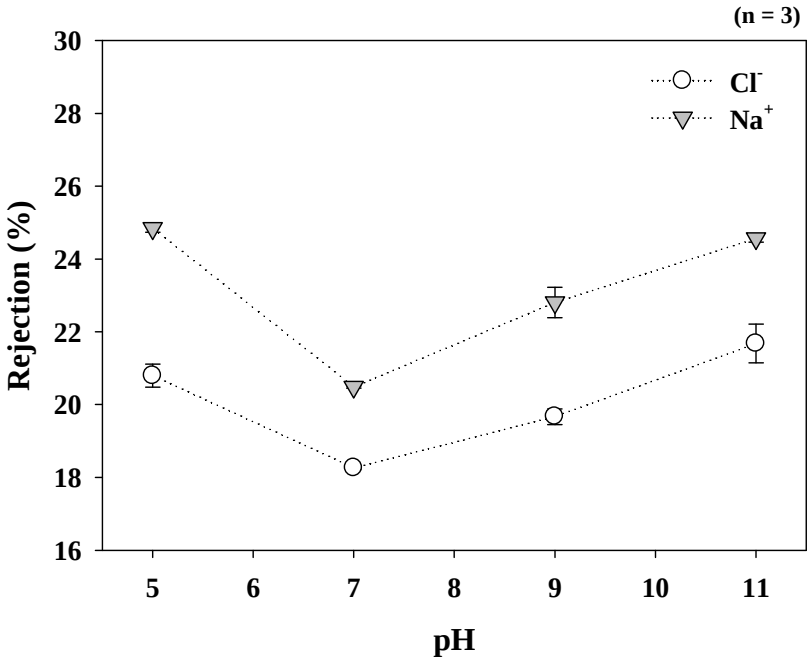

(b)

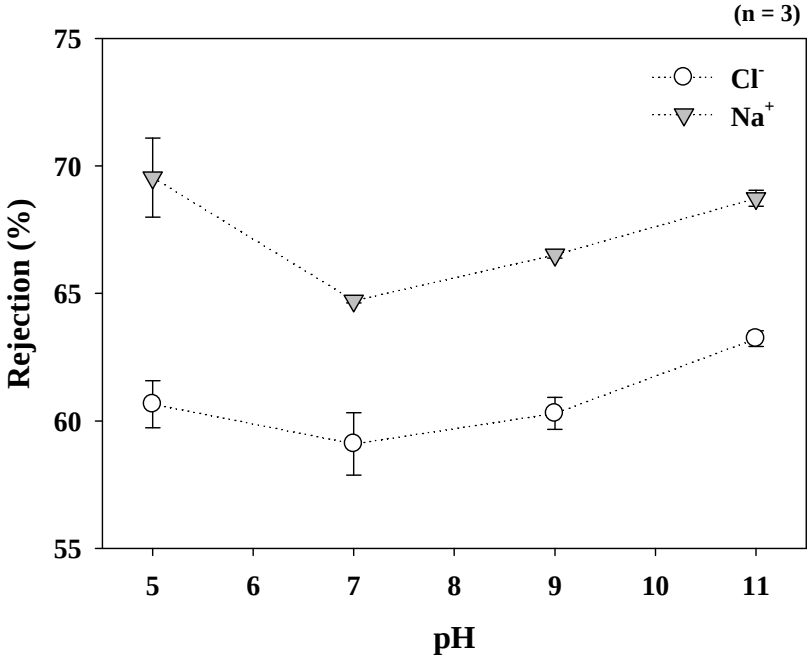

Figure 2-8. The rejection rates of chloride (Cl^-) and sodium (Na^+) by (a) NE20 and (b) NE70 membranes as a function of the pH (pH = 5.0, 7.0, 9.0, 11.0).

2.3.5. Correlation between the surface charge properties and the fouling propensity

Fig. 2-9 shows the amount of organic foulant desorbed from the NF membrane surfaces after conducting fouling experiments under different pH conditions (i.e., pH 2.0–11.0) over 1 hour. As shown, the amount of desorbed organic foulant from the NE20 and NE70 membranes decreased with increasing the solution pH. In addition, the organic foulant exhibited higher fouling potentials (in terms of the amount of desorbed foulant from the membrane surface) for the NE70 membrane than for the NE20 membrane over all pH values examined. These results imply that the surface charge properties of the NF membranes induced by the ionization of the surface functional groups play a critical role in the initial formation of fouling layers on the membrane surfaces due to the presence of charged organic materials.

The correlations between the ζ potential values and the fouling propensities of the NF membranes are illustrated in Figs. 2-10a and 2-10b (pH = 4–11). The amount of desorbed organic foulants from the NE20 (ζ potential = 0.2 × (amount of desorbed organic foulant, R^2 = 0.92) and NE70 (ζ potential = 0.4 × (amount of desorbed organic foulant) − 40.4, R^2 = 0.99) membrane surfaces were increased proportionally to the decrease in their ζ potential values, as determined by the solution pH. This observation supports the conclusion that the enhanced electrostatic interactions between organic materials and membrane surfaces produced by increasing the solution pH values result in a reduced fouling potential of the NF membranes towards organic materials. In addition, Fig. 2-10c shows the differences in the ζ potential values of the NE20 and NE70 membranes (Δζ potential) plotted against the differences in the amount of the desorbed organic foulant from their surfaces (Δ amount of desorbed organic foulant). As indicated, the Δζ potential values were poorly correlated to the change in the amount of desorbed organic foulant (Δζ potential = −1.8 × (Δ amount of desorbed organic foulant) + 45.9, R^2 = 0.07). This observation implies that the ζ potential measurements are not suitable to predict the differences in the fouling propensities of the NE20 and NE70 membranes.

The relationship between the functionalities and fouling propensities of the NF membranes is represented in Fig. 2-11 (pH = 4–9). The amount of desorbed organic foulant from the NE20 (functionality = −0.006 × (amount of desorbed organic foulant) + 6.2, R^2 = 0.93) and NE70 (functionality = −0.023 × (amount of desorbed organic foulant) + 21.5, R^2 = 0.89) membranes were linearly correlated with the decrease in membrane functionality under a range of pH conditions (see Figs. 11a and 11b). However, the R^2 values decreased significantly when their

linear regressions were plotted between pH 4 and 11 (Fig. 2-12.), since the ionized amine moieties ($–NH_2^+$) on the membrane surfaces were transformed into neutral amine moieties (–NH) above pH 9 ($pK_a \approx 9$), which rendered the membrane surfaces more negative but decreased the electrostatic repulsions between the positively charged functional groups of the membrane surfaces and the positively charged moieties of the organic materials. Furthermore, a strong linear correlation was observed for the relationship between the changes in the functionality and the variations in the amount of the desorbed organic foulant (Δ functionality = −1.2 × (Δ amount of desorbed organic foulant) + 2.6, $R^2 = 0.99$) (Fig. 2-11c). A possible explanation for these observations is that that the functionality measurements reflect the electrostatic transport properties of not only negatively but also positively charged organic materials at the membrane surfaces.

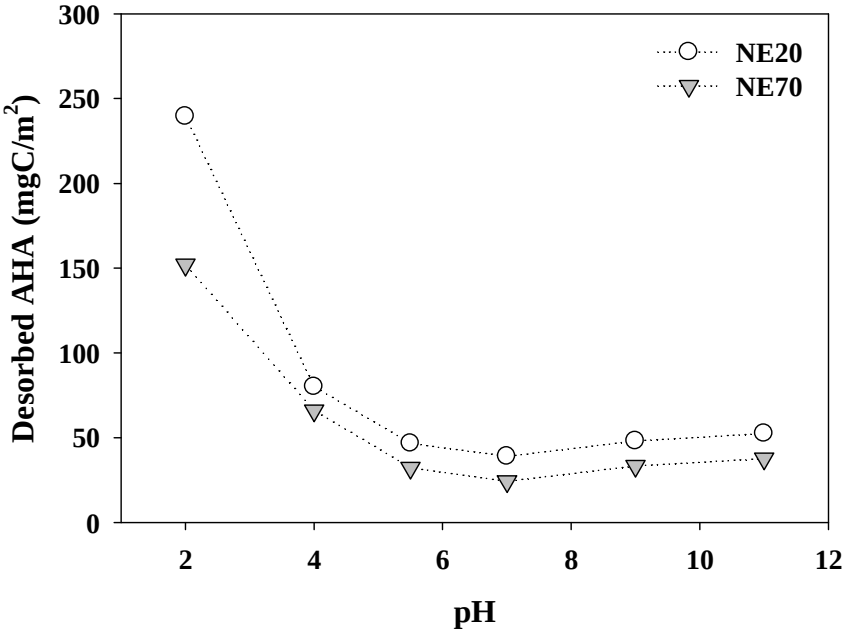

Figure 2-9. The amount of desorbed AHA from the fouled NE20 and 70 membranes as a function of pH (pH= 2.0, 4.0, 5.5, 7.0, 9.0, 11.0) using 0.1 N of NaOH desorbed solution.

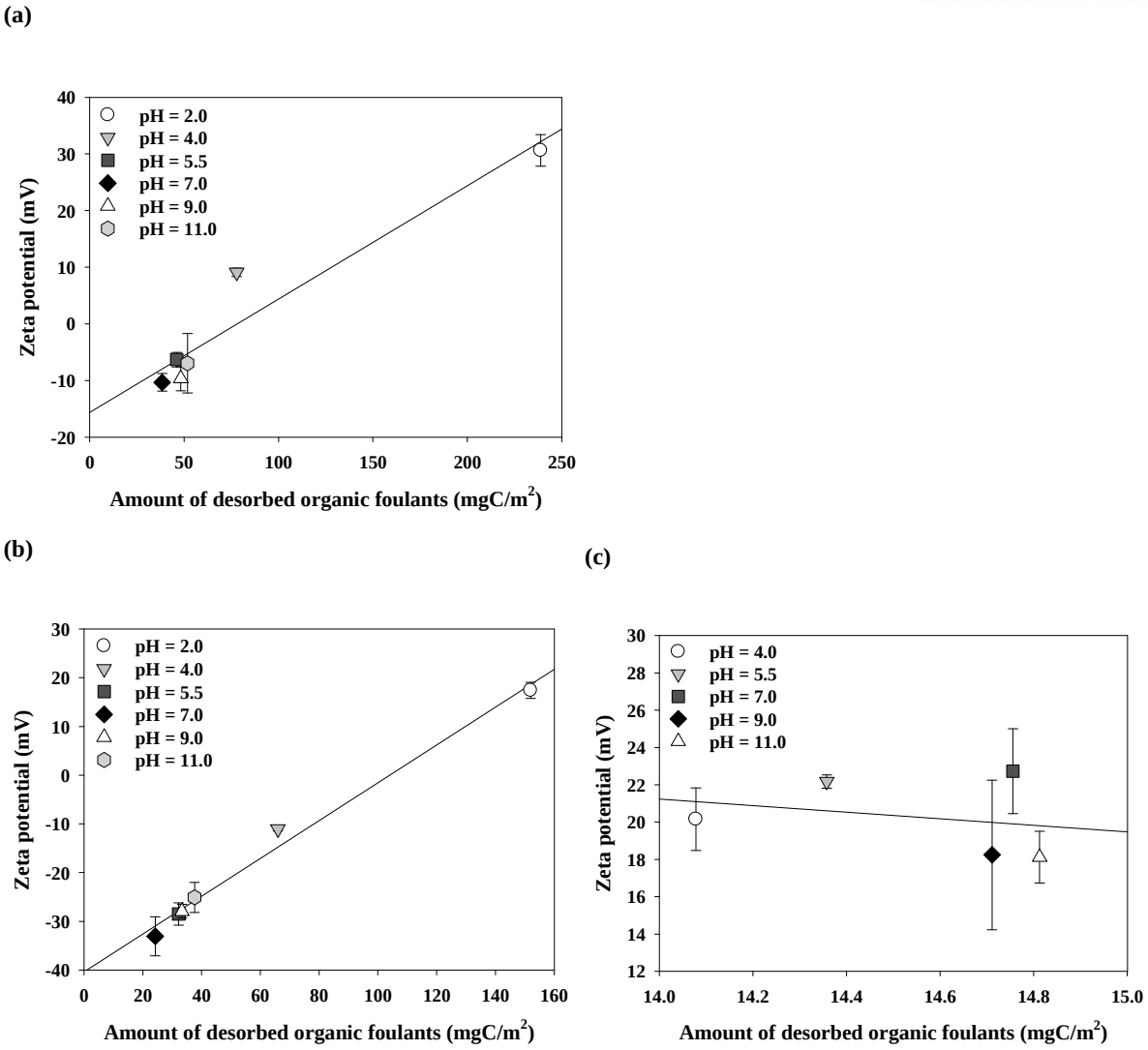

Figure 2-10. Correlation between the ζ potentials of the NE20 and NE70 membranes and the amount of desorbed organic foulants from the fouled membranes as a function of pH: (a) the ζ potential of the NE20 and the amount of desorbed AHA from the NE20 membrane (ζ potential = 0.2 × (amount of desorbed organic foulants) – 15.6, R^2 = 0.92) (b) the ζ potential of the NE70 and the amount of desorbed AHA from the NE70 membrane (ζ potential = 0.4 × (amount of desorbed organic foulants) – 40.4, R^2 = 0.99) (c) the difference in the ζ potential between the NE20 and NE70 membranes and the difference in the amount of desorbed organic foulants between the NE20 and NE70 membranes (Δ ζ potential = –1.8 × (Δ amount of desorbed organic foulants) + 45.9, R^2 = 0.07).

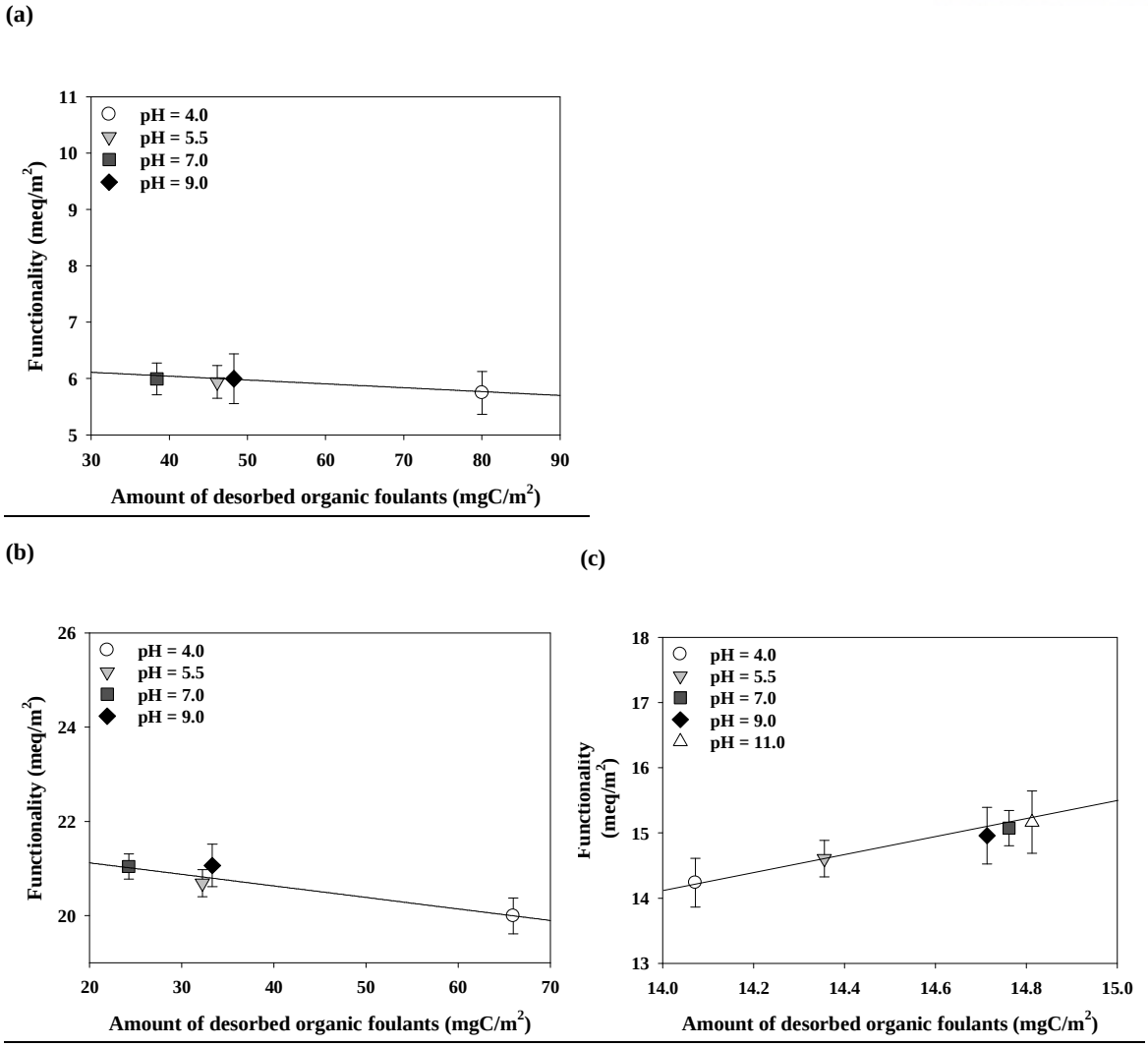

Figure 2-11. Correlation between the functionality of the NE20 and NE70 membranes and the amount of desorbed organic foulants from the fouled membranes as a function of pH: (a) the functionality of the NE20 and the amount of desorbed organic foulants from the NE20 membrane (functionality = –0.006 × (amount of desorbed organic foulants) + 6.2, R^2 = 0.93) (b) the functionality of the NE70 and the amount of desorbed AHA from the NE70 membrane (functionality = –0.026 × (amount of desorbed organic foulants) + 21.7, R^2 = 0.89) (c) the difference in the functionality between the NE20 and NE70 membranes and the difference in the amount of desorbed AHA between the NE20 and NE70 membranes (Δ functionality = 1.197 × (Δ amount of desorbed organic foulants) – 2.61, R^2 = 0.99).

(a)

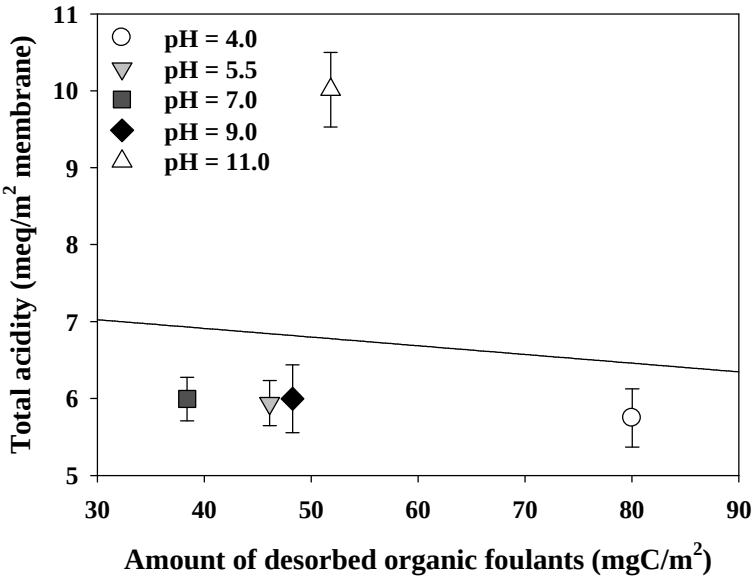

(b)

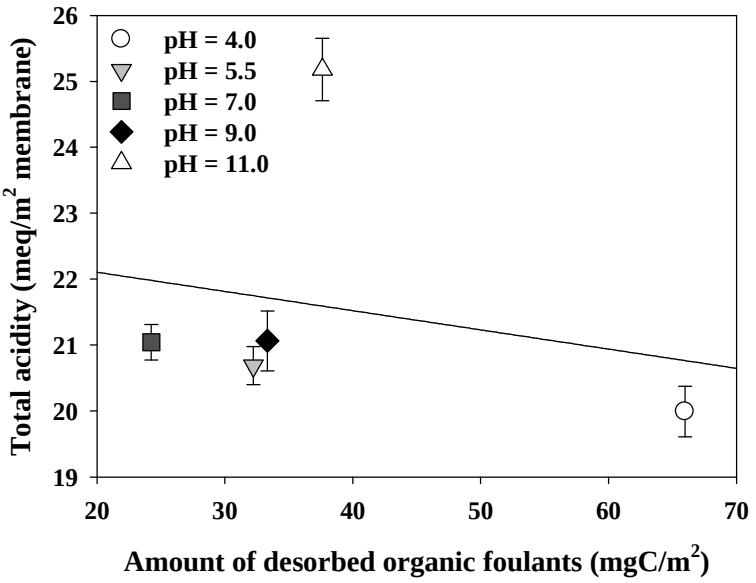

Figure 2-12. Correlation between the acidity of the NE20 and NE70 membranes and the amount of desorbed organic foulants from the fouled membranes as a function of pH: (a) the functionality of the NE20 and the amount of desorbed organic foulants from the NE20 membrane (functionality = –0.011 × (amount of desorbed organic foulants) + 7.4 R^2= 0.1) (b) the functionality of the NE70 and the amount of desorbed AHA from the NE70 membrane (functionality = –0.029 × (amount of desorbed organic foulants) + 22.7 R^2 = 0.23)

2. 4. Summary

The surface charge properties of the two different NF membranes (i.e., functionality and ζ potential) were characterized using potentiometric titrations and the electrophoresis method at a wide range of pH values and under varying ionic strength conditions with regard to the performance of the membranes (i.e., salt rejection and fouling propensity). The lowest rejection rates of Na^+ and Cl^- ions by the NE20 and NE70 membranes were observed at pH values close to their PZC values, as determined by potentiometric titrations; however, the obtained values were not consistent with their IEP values determined using electrophoresis measurements. These results demonstrate that the use of potentiometric titrations to quantify the ionized functional groups (i.e., functionality) present on the surfaces of NF membranes can be an effective method to assess the electrostatic transport of charged ions at the membrane surfaces (i.e., salt rejection). In addition, the decrease in the fouling potential of the membranes towards organic materials caused by increased electrostatic repulsive forces between the membrane surfaces and the organic materials with increasing solution pH depends highly on the ζ potential values of the NE20 and NE70 membranes, as determined by electrophoresis measurements. However, the intrinsic differences in the fouling propensities of the NE20 and NE70 membranes governed by the ionization degree of the surface functional groups could not be adequately predicted by their ζ potential values. In contrast, the electrostatic transport properties of both negatively and positively charged organic materials at the membrane surfaces could be determined by potentiometric titrations (only TFC membranes are applicable), as the functionalities of the NF membranes were indicative of the ionization degree of the surface functional groups. These observations confirm that the functionality measurements provide new insights into the role of surface charge properties in the salt rejection and fouling mechanisms of the NF membranes. Therefore, these results confirm the development of a novel approach to effectively determine the surface charge properties of membranes, which will ultimately aid in the development of efficient membrane processes with reduced membrane fouling and enhanced membrane performance.

3.0 Influence of the organic matter polarity on the intrinsic electrical surface property (pK_a) of negatively charged nanofiltration membrane

3.1 Introduction

Nanofiltration (NF) membranes are increasingly being used for drinking water treatment because they meet both the strict water quality regulations and water production requirements. However, successful application of NF membranes is often limited by natural organic matter (NOM) fouling. To overcome this limitation, numerous studies to increase membrane NOM removal efficiency and to decrease membrane fouling are ongoing. The surface charge properties of the membranes are considered to be key factors affecting their salt rejection and permeate flux decline. For example, electrostatic interactions between charged solutes and membrane surfaces (known as Donnan exclusion) can have significant effects on salt rejection [24–26]. Furthermore, membranes electrostatically repel charged organic materials, colloids, and particles due to their charged surfaces at neutral pH values, which ultimately plays a critical role in the accumulation of potential foulants on the membrane surfaces that are is associated with the decline of permeate flux [27–29]. To address these issues, many researchers have investigated the surface charge properties of membranes and their relationship to the electrostatic transport at the surface. These determine their salt rejection and fouling mechanisms [30–33].

In our previous study, the point of zero charge (PZC) was determined at the pH value where the functionality of the membrane is independent of the ionic strength, and was defined as the point of zero salt effect (PZSE) in the titration curves. Therefore, the objectives of this study were to determine intrinsic pK_a values of virgin- and fouled-NF membranes with three types of organic matters possessing different charge properties (positive, negative, and neutral charge) and to investigate their reversibility using chemical cleaning (HCl, NaOH, NaCl, and DI water).

3.2 Material and methods

3.2.1 Fouling experiment with bench scale of NF unit

3.2.1.1. Characteristics of target foulants

Commercial *m*-Phenylenediamine (MPD, Aldrich, USA), coumarin-3-carboxylic acid (CCA, Aldrich, USA) and D-(+)-glucose (DG, Aldrich, USA) were used as model organic foulants to investigate the fouling aspects of membrane surface in terms of the electrical polarity. MPD and CCA are positively and negatively charged, respectively, when in contact with neutral aqueous media via ionization of their functional groups (i.e., carboxylic and amine functional groups). Alternatively, DG which does not possess ionizable functional groups is used as an electrically neutral compound. The selected model organic foulants have similar molecular weight (MW; MPD: 108.14 $g \cdot mol^{-1}$, CCA: 190.15 $g \cdot mol^{-1}$, DG: 180.16 $g \cdot mol^{-1}$), thus, it is appropriate to investigate the fouling aspects in terms of the electrical polarity of foulants on the membrane surface.

5 g of each of the selected foulants were added into 5 L of deionized (DI) water, and 2.93 g of NaCl powder was added to adjust to 10 mM of ionic strength (IS). The concentrations of the organic foulant solutions were quite high for accelerating irreversible organic fouling of the membrane surface. Prior to the fouling experiments, the three different solutions were filtered using a mixed cellulose ester membrane filter (0.45 μm, Millipore, USA) to remove the suspended solids. The dissolved organic carbon (DOC) concentration, and water quality (i.e., pH and conductivity) were determined using a total organic carbon (TOC) analyzer (Shimadzu, TOC-V_{CPH}, Japan), and a pH and conductivity portable meter (Thermo, Orion 3 star, USA), respectively.

3.2.1.2. Physicochemical property of NF membrane

A commercial polymeric NF membrane with *m*-Phenylenediamine-based polyamide thin-film composite (TFC), NE90 (Toray Chemical Korea Inc., Seoul, Republic of Korea), with a molecular weight cut-off (MWCO) of 210-310 Da was selected for this study (Table 3-1.). Prior to all experiments, the virgin NF membrane was rinsed overnight with DI water to remove any coating material from the membrane surface. The virgin, fouled, and chemically-cleaned membranes were dried in a desiccator for 2 days, and then their physicochemical properties (i.e., zeta potential, hydrophobicity and/or hydrophilicity, functional groups composition and

surface morphological features) were determined to investigate the fouling and chemical cleaning aspects of the membrane surface, in terms of electrical polarity of the target foulants. The surface zeta potential values of the membranes were analyzed using an electrophoretic light scattering spectrophotometer (ELSZ-2000, Otsuka Electronics, Japan) with 10 mM of NaCl electrolyte solution, and pH range 3-11. The hydrophobicity and/or hydrophilicity of the membranes were determined by contact angle measurement (sessile drop method) using a goniometer (Phoenix, SEO, Republic of Korea). The difference in the functional group composition of the virgin, fouled and chemically cleaned NF membranes was identified by attenuated total reflection-Fourier transform infrared (ATR-FTIR) spectroscopy (Nicolet iS10, Thermo Scientific, Waltham, MA, USA). A field emission electron microscope (FE-SEM; S-4700, Hitachi, Tokyo, Japan) coupled to an energy dispersive X-ray (EDX) spectrometer (7200-H, Horiba, Kyoto, Japan) was used to examine the surface morphological features of the virgin, fouled, and cleaned NF membranes, as well as the composition of inorganic materials accumulated on the membrane surfaces.

Table 3-1. Physicochemical properties of the NF membranes.

Classification	NF
Membrane code	NE90
Manufacturer	Toray Chemical Korea Inc., Seoul, Republic of Korea
Membrane type	Thin-film composite
Membrane materials	Polyamide
Water soluble monomer	Meta-phenylene diamine
Nominal MWCO (Da)	200

3.2.1.3. Bench-scale of NF membrane system description

A schematic representation of the bench-scale cross flow NF membrane unit containing a flat-sheet-type membrane cell for the membrane performance tests is presented in

Fig. 3-1. The NF membrane filtration unit (surface area = 56.25 cm^2, channel height = 0.04 cm) is equipped with the NF membrane, a magnetic gear pump (Micropump, Vancouver, WA, USA), and a reservoir for feed water. The permeated water was recirculated to the feed water tank to minimize changes to the feed water concentration. The temperature of the reservoir for feed water was adjusted by refrigerated temperature circulator. Prior to the experiment, the membranes were stabilized in the membrane test unit with deionized water for 2 h for compaction. The performance test conditions were 17 (±1.3)°C, 20 bar, and 5.3 $cm \cdot s^{-1}$ of cross flow velocity.

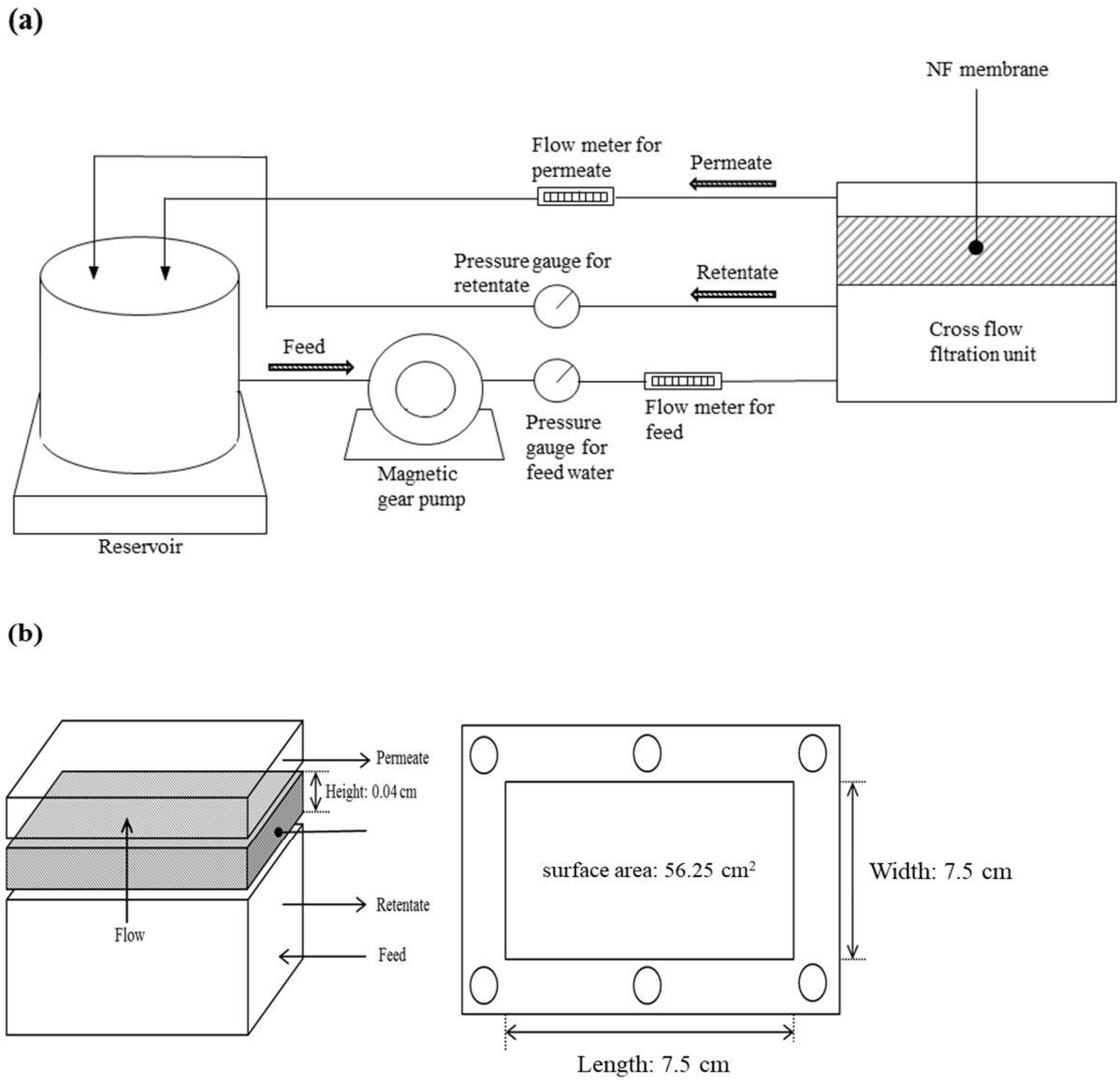

Fig. 3-1. Schematic of a laboratory-scale crossflow nanofiltration unit.

3.2.2 Determination of membrane PZC and pK_a

Membrane PZC was determined in our previous study [72]. The polyamide membranes generally have two ionizable functional groups (i.e., carboxylic and amine functional groups); thus, electrical surface property of a solid can be represented by the PZC of surface. The PZC of the virgin and fouled membranes were determined using PZSE method with various concentrations of NaCl solution [desalination]. Furthermore, electrical surface property (i.e. intrinsic pKa) of virgin and fouled NF membranes was determined using the PZC values. Generally, polyamide membranes have two ionizable functional groups (carboxylic and amine functional groups), thus two equilibrium constants, $K_{a,1}$ and $K_{a,2}$ can be described as in these equations:

$$K_{a,\,1} = \frac{\{COO^-\}\,[H^+]}{\{COOH\}} \tag{3-1}$$

$$K_{a,\,2} = \frac{\{NH\}\,[H^+]}{\{NH_2^+\}} \tag{3-2}$$

and the consumption of titration solution can be calibrated as consumption of acid and consumption of base, based on the pH_{pzc}. The difference in consumption of acid (Ca) and consumption of base (Cb), Q, can be described as per the following equation, based on the charge balance:

$$C_A - C_B = Q = [\equiv NH_2^+] - [\equiv COO^-] + [H^+] - [OH^-] \tag{3-3}$$

additionally, functionality of the membrane can be described as per the following equation based on mass balance:

$$Functionality = [\equiv COOH] + [\equiv COO^-] + [\equiv NH_2^+] + [\equiv NH] \tag{3-4}$$

where, the pH is below the pH pzc, Ca-Cb Q is the concentration of protonated carboxylic groups, and when pH is higher than pHpzc, Q is the concentration of deprotonated amine groups.

$$Q \cong \{COOH\}\, for\, pH < pH_{pzc}\ ;\ Q \cong \{NH\}\, for\, pH > pH_{pzc} \tag{3-5}$$

Thus, the following equation used to determine intrinsic pK_a values of the membranes can be established by substituting equations (3-3) and (3-4) with equations (3-1) and (3-2):

$$K_{a,1} = \frac{(Functiionality-Q)[H^+]}{Q} \quad (3\text{-}6)$$

$$K_{a,2} = \frac{Q\,[H^+]}{(Functiionality-Q)} \quad (3\text{-}7)$$

3.2.3 Reversibility of fouled membrane by chemical cleaning

The reversibility of fouled membrane was investigated with a laboratory-scale cross-flow RO filtration unit using various chemical cleaning solutions (0.1 N HCl, 0.1 N NaOH, 0.1 N NaCl, and DI). Four coupons of the fouled NF membranes were soaked in 500 mL of each cleaning solution for 10 h under moderate stirring conditions (150 rpm). This unit comprised of a flat-sheet filtration cell (effective surface area = 56.25 cm^2; channel height = 0.04 cm), a high-pressure pump (CAT pumps, model 1050 10 GPM 2200, Minneapolis, MN, USA), and a feed water reservoir. Prior to all filtration tests, the RO filtration unit was stabilized for 2 hours using DI water. The RO filtration unit was operated in recirculation mode at 17 (±1.3)°C. During the filtration tests, feed water pressure was maintained at 20 bar with a cross-flow velocity of 5.3 cm s^{-1}. The rejection rates of NaCl by the RO membranes and their permeate fluxes were calculated using the following equations:

$$\text{Salt rejection rate (\%)} = \left(1 - \frac{C_p}{C_f}\right) \times 100 \quad (3\text{-}8)$$

$$\text{Permeate flux (L } m^{-2}h^{-1}) = \frac{Q}{A} \quad (3\text{-}9)$$

where, C_f and C_p are NaCl concentrations in the feed and permeate water, Q is the permeate flow (L h^{-1}), and A is the membrane surface area (m^2).

3.3.0 Results and discussions

3.3.1. Water quality of target foulants

Water quality parameters (i.e., pH and conductivity), TOC, and TN of three target foulants in the feed and permeate waters were identified to assess the performance of the tested NF membranes (Table 3-2.). The NF membranes had effectively reduced conductivity, TOC, and TN of the target foulants. However, TOC rejection of DG with abundant neutral polarity was relatively low. This implies that the rejection mechanism of organic matter in NF membrane is dominated by the electrostatic repulsion between charged organic matter and membrane surface, rather than by size exclusion.

Table 3-2. Water characteristics of feed and permeate water of target foulants.

Sample	MW (g mol^{-1})	pH		TOC (mgC L^{-1})	TN (mgN L^{-1})	Conductivity (μS cm^{-1})
MPD	108.14	7.3	Feed	655.1 (±5.2)	245.5 (±3.8)	878 (±2.0)
			Permeate	4.9 (±1.2)	2.1 (±0.7)	83.3 (±1.3)
			Rejection (%)	99.2	99.1	90.5
CCA	190.15	6.7	Feed	635.3 (±3.1)	B.D.	890 (±1.0)
			Permeate	3.3 (±0.8)	B.D.	81.7 (±0.3)
			Rejection (%)	99.5	B.D.	90.8
DG	180.16	7.1	Feed	463.7 (±4.9)	B.D.	851 (±4.0)
			Permeate	15.2 (±1.7)	B.D.	80.8 (±1.2)
			Rejection (%)	96.7	B.D.	90.5

3.3.2. Fouling behavior with various organic matters of the NF membranes

Fig. 3-2 shows the decline of the normalized water flux after conducting fouling experiments using three organic foulants with different polarities. Large flux declines occur especially with CCA, the next most potent foulant being MPD, followed by the least fouling DG. The NF membrane exhibited a permeated flux decline of 40% over 30 h for MPD, and 90% and 50% over 30 h with CCA and DG, respectively. The molecular weight (MW) of MPD was the highest. These result were consistent with fouling with MW.

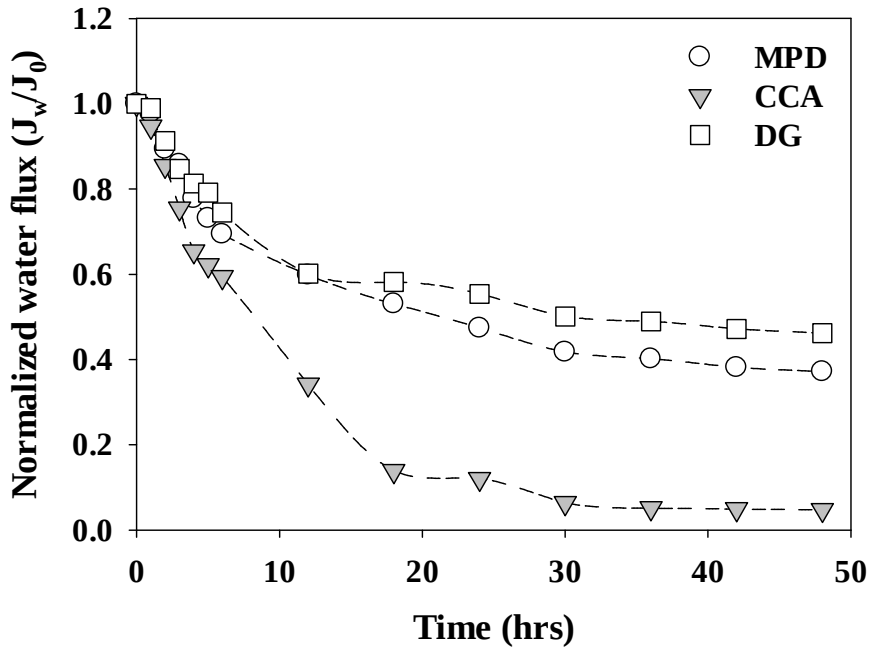

Figure 3-2. Permeate flux decline of NE90 membrane in terms of the target foulants.

Variations in the ζ potential values of the NF membranes in terms of three different foulants are illustrated in Fig. 3-3. As shown, the virgin and fouled NF membranes exhibited positive ζ potential values when the solution pH was lower than the iso-electric point of the membrane, while the negative ζ potential values were obtained when the solution pH was higher than the IEP values of the membrane. These amphoteric curves thereby, confirm that the tested polyamide TFC NF membranes consist of bear carboxyl and amine functional groups on their surfaces when in contact with an aqueous solution. Negative ζ potential values of the NF membranes surface decreased with membrane fouling. The ionization of carboxylic functional groups was not responsible for ζ potential values of the fouled membrane with CCA, and the ionization of the amine functional groups was not responsible for ζ potential values of the membrane fouled with MPD. Ionization of both carboxylic and amine functional groups were not responsible for ζ potential values fouled with DG. These results support the assumption that the MPD was adsorbed onto the carboxylic functional groups on the NF membrane surface, while, CCA was adsorbed onto the amine functional groups, and DG was adsorbed onto both, the carboxylic and amine functional groups on the NF membrane.

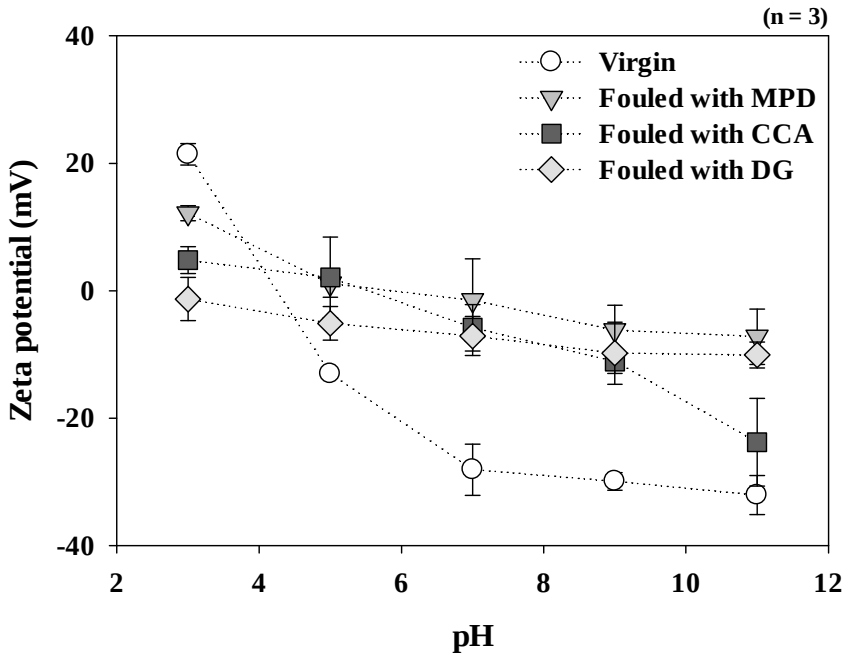

Figure 3-3. Surface zeta potential of virgin and fouled NE90 membranes as determined by electrophoresis method (ionic strength = 10 mM NaCl).

The ATR-FTIR spectra of the virgin and fouled NF membranes are shown in Fig. 3-4. The identical ATR-FTIR spectra were detected for the virgin and fouled NF membranes. However, the intensities of the IR peaks were related to amide functional groups originating from the microbial cell lysis, and alcohol functional groups derived from cell-wall polysaccharides of microorganisms, which differed considerably amongst them. After formation of MPD fouling layers onto the NF membrane surface, the intensities of IR peaks associated with carboxylic acid (1320–1210 cm^{-1}), and C-O alcohols (1075–1000 cm^{-1}) were substantially decreased. After formation of CCA fouling layers onto the membrane surface, the intensities of IR peaks associated with N-H amides (1700–1630 cm^{-1}), and CNH amides (1490–1430 cm^{-1}) were substantially decreased. In addition, the intensities of IR peaks associated with N-H amides (1700–1630 cm^{-1}), CNH amides (1490–1430 cm^{-1}), carboxylic acid (1320–1210 cm^{-1}), and C-O alcohols (1075–1000 cm^{-1}) were also substantially decreased. These results supported the assumption that the MPD was adsorbed onto carboxylic functional groups on the NF membrane surface, CCA was adsorbed onto amine functional groups, and DG was adsorbed onto both carboxylic and amine functional groups on the NF membrane.

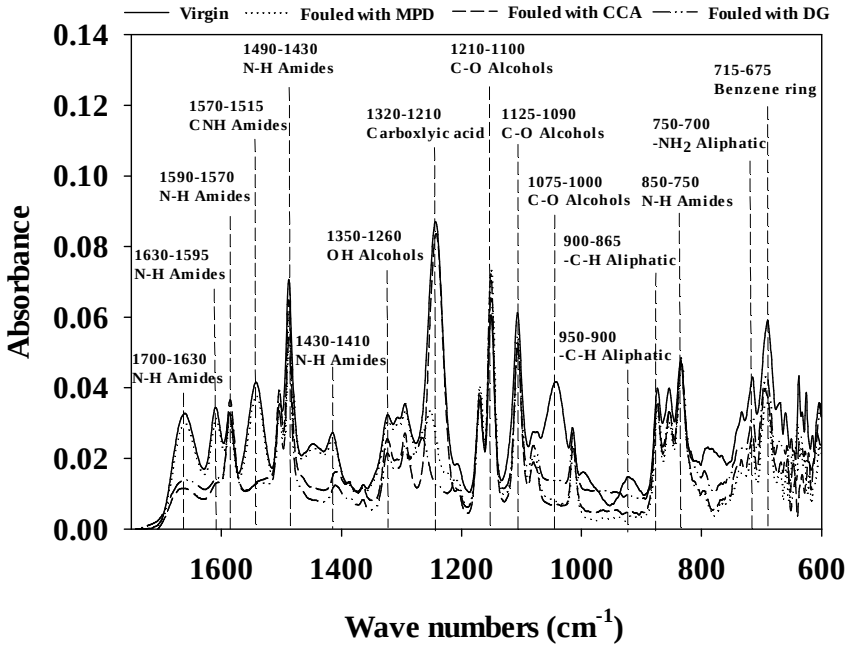

Figure 3-4. ATR-FTIR spectra of the virgin and fouled NE90 membranes.

Table 3-3. Surface features of virgin and fouled NE 90 membranes.

	Surface zeta potential at pH 7 (mV)	Contact angle (°)
Virgin	–28.1 (±1.6)	48.3 (±2.2)
Fouled with MPD	–1.4 (±6.5)	34.6 (±4.7)
Fouled with CCA	–5.8 (±3.6)	31.7 (±3.4)
Fouled with DG	–7.2 (±3.1)	38.3 (±2.6)

3.3.3. Electrical surface property (PZC and pK_a) of the NF membranes

The functionalities of virgin and fouled NF membranes in terms of pH are illustrated in Figure 3-5. The functionalities of virgin and fouled membranes were gradually increased in the pH range of 2–4 due to the ionization of the carboxylic functional groups (pKa ≈ 3), while the functionalities became stable between pH 3 and 9. In addition, the functionalities of the membranes were significantly increased in pH range of 9–11 due to the deprotonation of the amine functional groups (pKa ≈9). The lowest amount of deprotonation of carboxylic group was observed in the membrane fouled with MPD. The lowest amounts of deprotonation of amine groups was observed in the membrane fouled with CCA, while no significant changes in the deprotonation of both carboxylic and amine functional groups were observed in the

membrane fouled with DG. These results supported the assumption that the MPD was adsorbed onto the carboxylic functional groups on the NF membrane surface, while, CCA was adsorbed onto the amine functional groups, and DG was adsorbed onto both, the carboxylic and amine functional groups on the NF membrane.

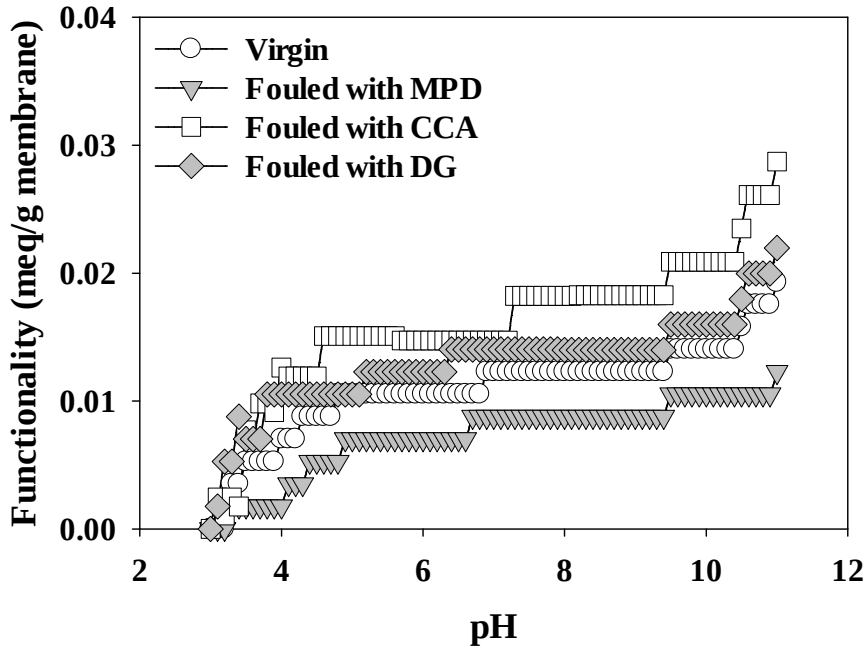

Figure 3-5. Functionality of virgin and fouled NE90 membrane (ionic strength= 10 mM NaCl).

The potentiometric titration curves of virgin and fouled membranes under different ionic strength conditions are compared in Fig. 3-6. The virgin and fouled membranes were positively charged when the pH of the solution was lower than their PZC values (the PZC of virgin NF membrane ≈6.3; the PZC of fouled with MPD ≈6.1; the PZC of fouled with CCA ≈6.9; the PZC of fouled with DG ≈6.3) and their surfaces became negatively charged when the pH of the solution was above their PZC values. The lower PZC value observed for membrane fouled with MPD compared to virgin NF membrane can be explained by the adsorption of positively charged foulants on the negatively charged membrane surface. In addition, the higher PZC value was observed for membrane fouled with CCA due to the adsorption of negatively charged foulants on the negatively charged membrane surface. Moreover, no significant changes to PZC values was observed for membrane fouled with DG. This is due to the adsorption of neutral foulants on the negatively charged membrane surface. These observations indicate that the PZC measurements may offer significant insights into the differences in PZC

values in terms of membrane foulant properties based on the degree of ionization of the surface functional groups.

(a)

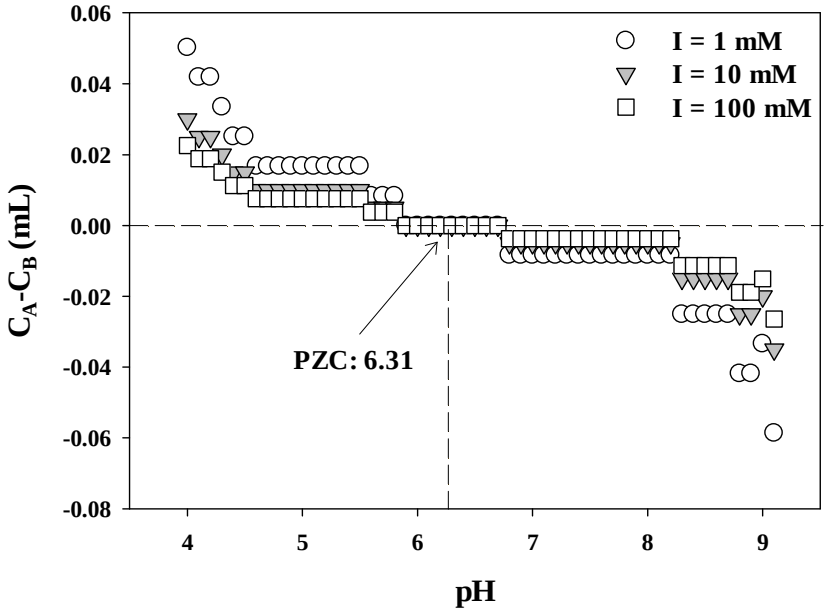

(b)

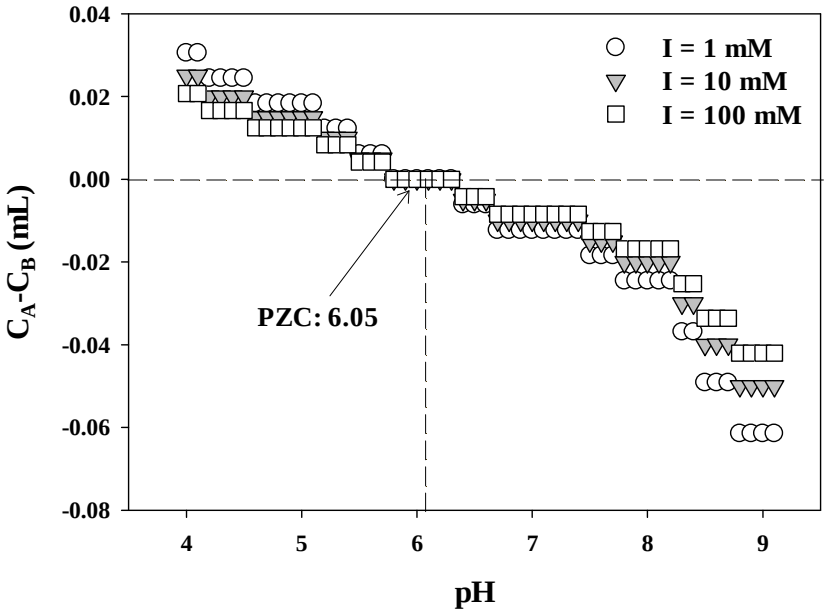

(c)

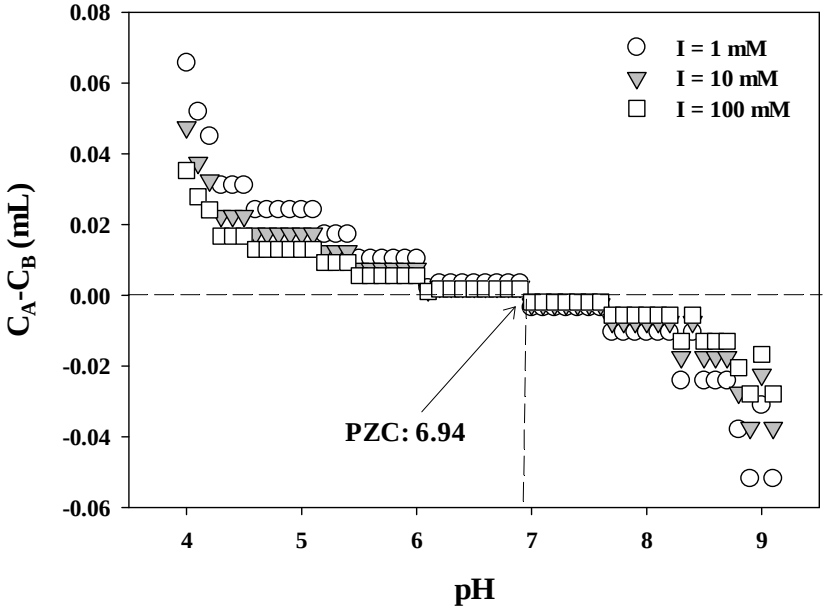

(d)

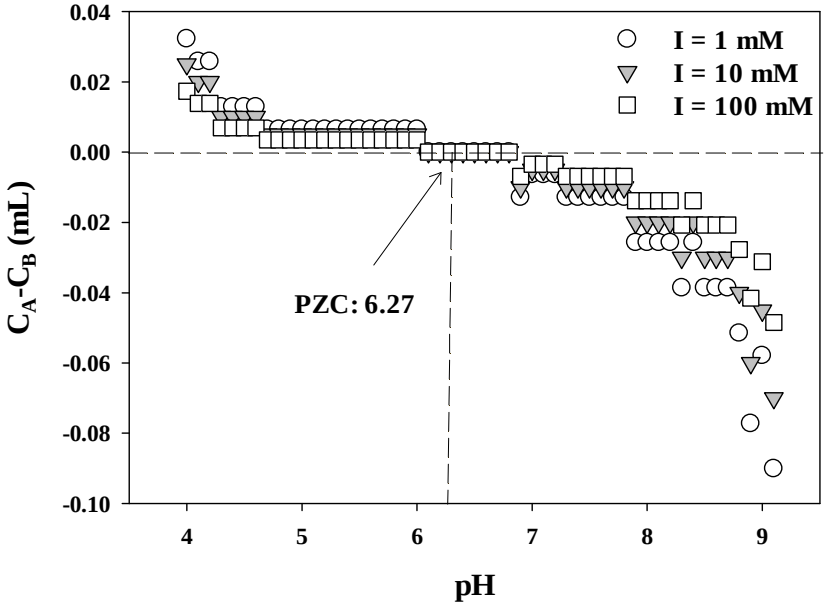

Figure 3-6. Potentiometric titration curves of (a) virgin, (b) fouled with MPD, (c) fouled with CCA, and (d) fouled with DG NE90 membranes as a function of ionic strength.

The electrical surface property (intrinsic pK_a value) of virgin and fouled NF membranes with three target foulants are compared in Fig. 3-7. It was observed that the p$Ka,_1$ and p$Ka,_2$ of virgin membrane were 3.41 and 9.23, respectively. This is because the two ionizable functional groups (carboxylic and amine functional groups) comprised of the NE 90 membrane. After membrane fouling with MPD, it was observed that its p$Ka,_1$ value was substantially increased, while p$Ka,_2$ value was significantly decreased. In contrast, its p$Ka,_1$ value was substantially decreased and p$Ka,_2$ value was significantly increased compared to the virgin membrane. However, no significant changes in p$Ka,_1$ and p$Ka,_2$ of fouled membrane with DG was observed. These observations indicate that the intrinsic pKa measurements may offer significant insights regarding the characteristics of membrane fouling.

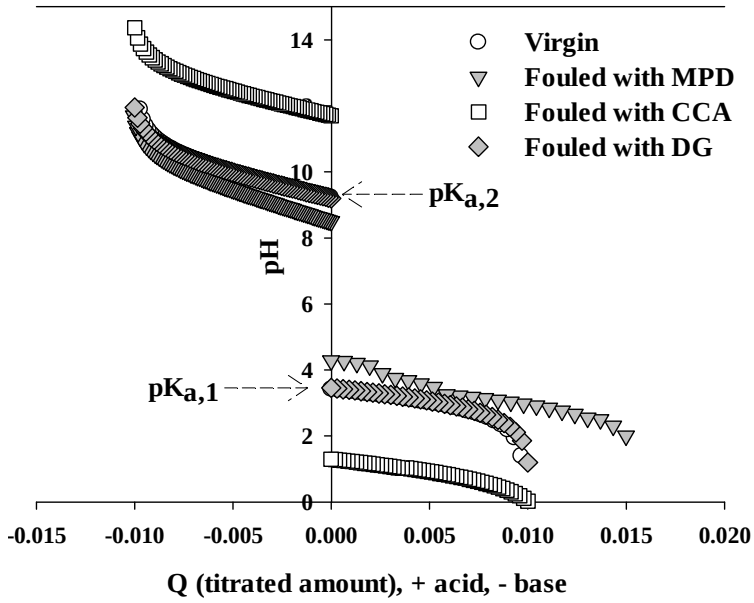

Figure 3-7. Determination of intrinsic pKa,1, and pKa,2 of virgin and fouled NE90 membranes.

Table 3-4. Electrical surface property of virgin and fouled NF membranes as determined by PZSE method.

	Virgin	**Fouled with MPD**	**Fouled with CCA**	**Fouled with DG**
$pKa,_1$	3.41	4.28	1.3	3.46
$pKa,_2$	9.23	8.5	11.7	9.2
PZC	6.31	6.05	6.94	6.27

3.3.4 Reversibility of fouled NF membranes

Salt rejection (NaCl = 0.1 M) and permeate flux (feed: DI water) of the virgin, fouled, and cleaned NF membranes under controlled conditions (feed water pressure = 20 bar; cross flow velocity = 5.3 $cm \cdot s^{-1}$; effective surface area = 56.25 cm^2; channel height = 0.04 cm; temperature = 17 ± 1.3ºC) are compared in Fig. 3-7. The fouled NF membranes exhibited a much lower permeate flux (MPD: 6.3 L $m^{-2} h^{-1}$; CCA: 2.7 L $m^{-2} h^{-1}$; DG: 6.9 L $m^{-2} h^{-1}$) than that of the virgin NF membrane (17.3 L $m^{-2} h^{-1}$) due to formation of membrane foulants.

Moreover, a significant decrease was observed for the salt rejection rate of the fouled NF membranes (MPD: 83.2%; CCA: 75.1%; DG: 81.1%) compared to the virgin NF membrane (90.1%). There may be two possible reasons: 1) The interactions between CP and cake layer formed is highly dependent on the intrinsic properties of the cake layer formed (e.g., porosity, thickness). The formed cake layer can cause cake-enhanced CP, which can increase salt passage through the NF membranes; 2) increased salt concentration on the NF membrane surface (due to the hindered back diffusion of salts from the NF membrane surface by forming colloidal cake layers on the surface) can increase the passage of salts through the RO membranes [34].

All the applied desorbing agents were effective in recovering salt rejection and permeate flux. However, the recovery rates varied markedly according to the type of desorbing agent. The recovery rates of the salt rejection and permeate flux due to cleaning using DI water, acid, base, and salt solutions in the fouled membrane with MPD were in the order of cleaned with S (salt rejection = 85.1%; permeate flux 9.1 L $m^{-2} h^{-1}$) > cleaned with DI (salt rejection = 84.7%; permeate flux 11.3 L $m^{-2} h^{-1}$) > cleaned with B (salt rejection = 84.1%; permeate flux = 12.1 L $m^{-2} h^{-1}$) > cleaned with A (salt rejection = 87.3%; permeate flux = 15.7 L $m^{-2} h^{-1}$). In addition, the recovery rates of the salt rejection and permeate flux in the membrane fouled with CCA were in the order of cleaned with A (salt rejection = 82.7%; permeate flux 13.4 L $m^{-2} h^{-1}$) > cleaned with DI (salt rejection = 83.1%; permeate flux 13.5 L $m^{-2} h^{-1}$) > cleaned with S (salt rejection = 84.1%; permeate flux = 13.7 L $m^{-2} h^{-1}$) > cleaned with B (salt rejection = 88.3%; permeate flux = 16.3 L $m^{-2} h^{-1}$).

The recovery rates of the salt rejection and permeate flux in the fouled with DG membrane were in the order of cleaned with DI (salt rejection = 81.1%; permeate flux 11.7 L $m^{-2} h^{-1}$) > cleaned with A (salt rejection = 82.7%; permeate flux 12.3 L $m^{-2} h^{-1}$) > cleaned with B (salt rejection = 84.1%; permeate flux = 14.1 L $m^{-2} h^{-1}$) > cleaned with S (salt rejection =

88.3%; permeate flux = 15.1 L m^{-2} h^{-1}). These observations suggest that acid cleaning, base cleaning and salt cleaning can effectively recover the performance of the fouled NF membranes with positively- or negatively-charged, and neutral organic foulants, respectively [26].

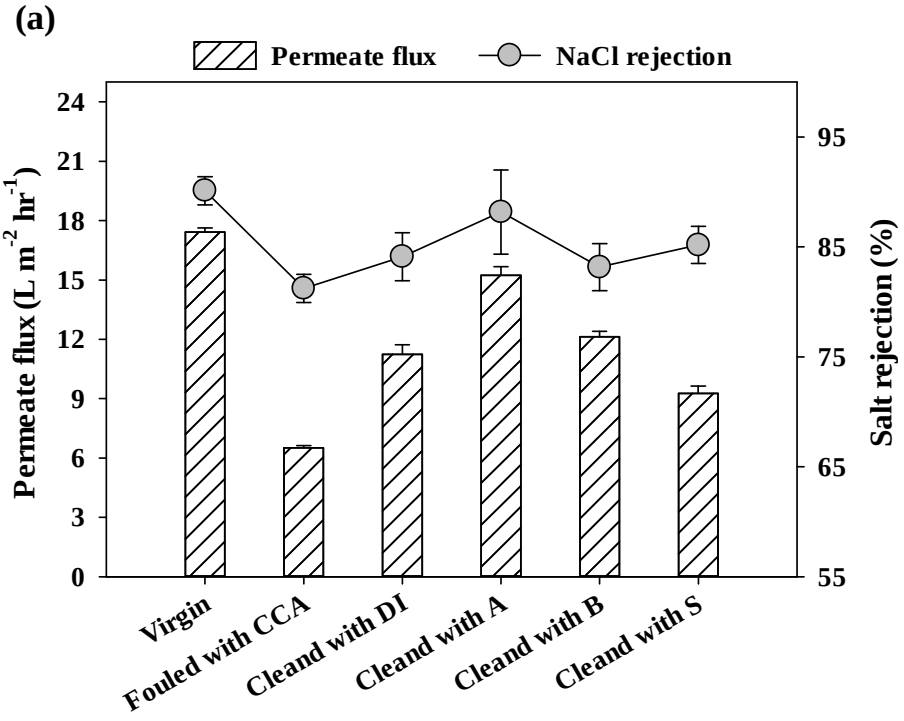

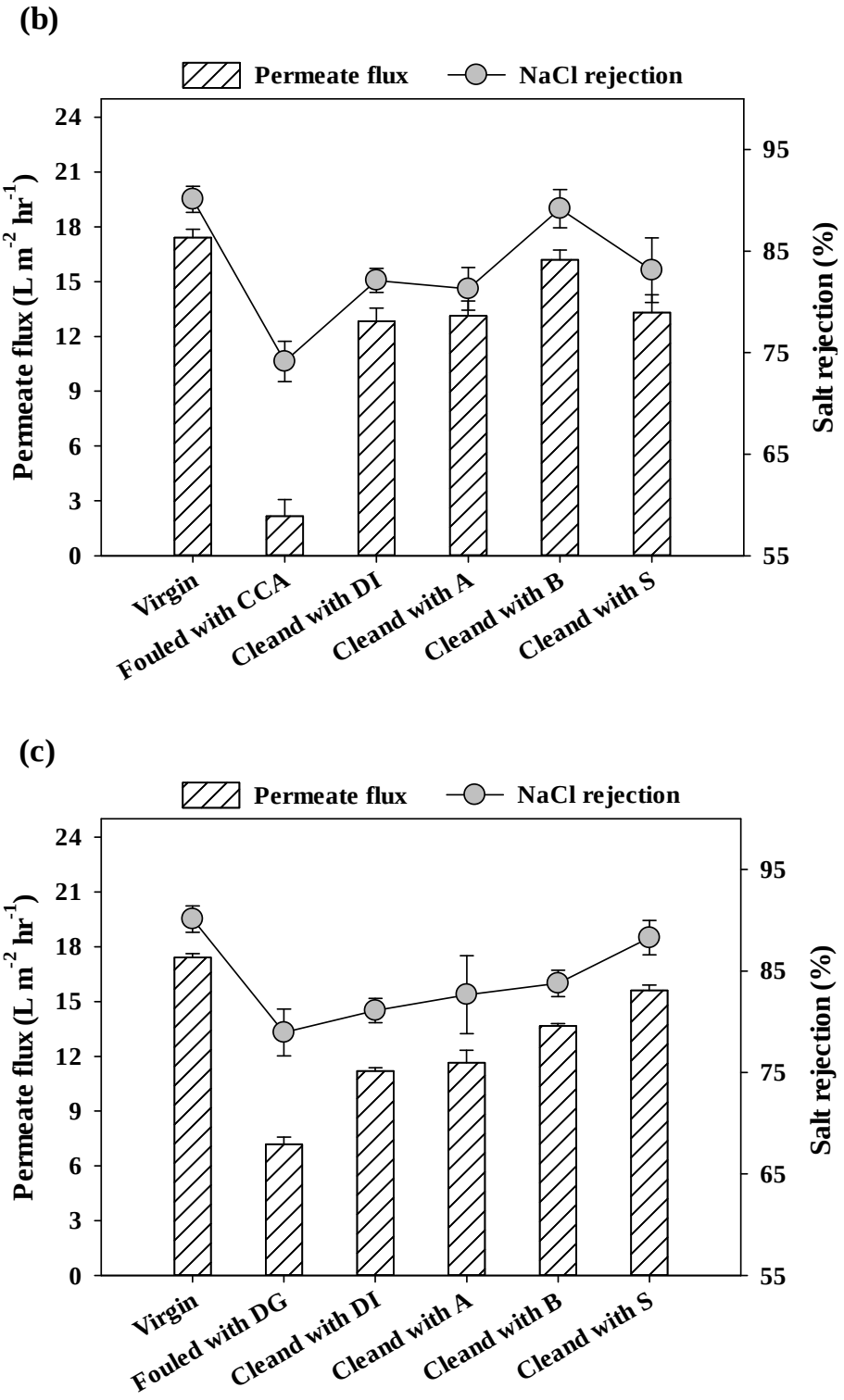

Figure 3-8. Permeate flux (feed water: DI water) and salt rejection (NaCl = 0.1 M) of the virgin, fouled, and cleaned RO membranes under controlled conditions. (a): fouled with MPD, (b): fouled with CCA, (c): fouled with DG; surface area = 56.25 cm^2; channel height = 0.04 cm; temperature = 17 (±1.3)°C; feed pressure = 20 bar; cross flow velocity = 5.3 $cm \cdot s^{-1}$).

3.4 Summary

The electrical surface properties (pK_a and PZC) of virgin and fouled NF membranes were determined using potentiometric titrations method with regard to the reversibility of the membranes (i.e., salt rejection and permeate flux). The lower PZC value observed for fouled with MPD membrane compared to virgin NF membrane can be explained by the adsorption of positively charged foulants on the negatively-charged membrane surface. In addition, the higher PZC value was observed for membrane fouled with CCA by the adsorption of negatively charged foulants on the negatively charged membrane surface. Moreover, no significant changes to PZC values were observed for membrane fouled with DG. This is due to adsorption of neutral foulants on the negatively charged membrane surface. These observations indicate that the PZC measurements may offer significant insights into the differences in PZC values regarding the properties of membrane foulants based on the ionization degree of the surface functional groups. All the applied desorbing agents were effective in recovering salt rejection and permeate flux. However, the recovery rates varied markedly according to the types of desorbing agents. The recovery rates of the salt rejection and permeate flux through cleaning using DI water, acid, base, and salt solutions in the membrane fouled with MPD were in the order of cleaned with S (salt rejection = 85.1%; permeate flux 9.1 L m^{-2} h^{-1}) > cleaned with DI (salt rejection = 84.7%; permeate flux 11.3 L m^{-2} h^{-1}) > cleaned with B (salt rejection = 84.1%; permeate flux = 12.1 L m^{-2} h^{-1}) > cleaned with A (salt rejection = 87.3%; permeate flux = 15.7 L m^{-2} h^{-1}). In addition, the recovery rates of the salt rejection and permeate flux in the fouled with CCA membrane were in the order of cleaned with A (salt rejection = 82.7%; permeate flux 13.4 L m^{-2} h^{-1}) > cleaned with DI (salt rejection = 83.1%; permeate flux 13.5 L m^{-2} h^{-1}) > cleaned with S (salt rejection = 84.1%; permeate flux = 13.7 L m^{-2} h^{-1}) > cleaned with B (salt rejection = 88.3%; permeate flux = 16.3 L m^{-2} h^{-1}). The recovery rates of the salt rejection and permeate flux in the fouled with DG membrane were in the order of cleaned with DI (salt rejection = 81.1%; permeate flux 11.7 L m^{-2} h^{-1}) > cleaned with A (salt rejection = 82.7%; permeate flux 12.3 L m^{-2} h^{-1}) > cleaned with B (salt rejection = 84.1%; permeate flux = 14.1 L m^{-2} h^{-1}) > cleaned with S (salt rejection = 88.3%; permeate flux = 15.1 L m^{-2} h^{-1}). These observations suggest that the electrical surface properties can be a promising tool for effective selection of cleaning agents (acid cleaning, base cleaning and salt cleaning) to recover the performance of the fouled NF membranes.

4.0 An autopsy study of a fouled reverse osmosis membrane used for ultrapure water production

4.1 Introduction

During recent decades, the demand for ultrapure water (UPW) has risen continuously in a variety of industrial applications, such as power generation, pharmaceutical formulations, and semiconductor manufacturing [116]. The use of UPW is essential for improving energy efficiencies of power generation plants and boiler facilities which produce a huge amount of steam [117, 118]. In addition, UPW is considered a key determinant of the quality and performance of high value-added industrial products, including pharmaceuticals and semiconductors, which require a high degree of accuracy in manufacturing processes [119]. Therefore, UPW production has received considerable attention as an emerging water market throughout the world. Global Water Intelligence (GWI) reported that UPW accounted for approximately 20% of the world water market in 2011, and is anticipated to increase to 4 billion dollars by 2025, which is equivalent to the proportion of seawater desalination in the world water market [119].

The production of UPW aims to remove all types of contaminants, including suspended solids, salt ions, organic and inorganic materials, particulate and colloidal matters, bacteria, dissolved gases (i.e., CO_2 and O_2), and trace ions, leaving only water molecules [116]. However, the required degree of purity of UPW varies considerably depending on its specific uses. For UPW used as cooling water, it is important to eliminate potentially corrosive substances and scale-forming materials from source water, as deposits via chemical precipitation promote corrosion and/or scaling on the surfaces of heat-exchangers, which may decrease thermal and mechanical efficiencies of heat-exchangers in power generation plants and boiler facilities [120]. Removal of bacteria and endogenous pyrogens from source water is crucial for pharmaceutical formulations, since UPW is utilized as a diluent or solvent [121]. In the semiconductor industry, contamination by particulate and/or ionic materials and the formation of native oxide layers in the presence of dissolved oxygen (> 0.1 μg L^{-1}) on surfaces of the silicon wafers during rinsing procedures may lead to poor performance and low yields

of semiconductor devices [122-124]. Therefore, UPW used in semiconductor manufacturing requires at least 18 MΩ cm of the electrical resistivity at 25 ºC and extremely low concentrations of all water contaminants [1].

The UPW production systems typically combine 5 to 10 different unit processes (e.g., coagulation/flocculation, ion-exchange adsorption, gas separation, membrane, and oxidative processes), since there is no unit process which can solely eliminate all contaminants from source water [125, 126]. Consequently, the purity degree of UPW is largely dependent on synergistic effects from the combination of various unit processes. The UPW production systems have progressed in conjunction with advances in membrane technologies [125-127]. Early UPW production systems in the 1970s contained anion and cation exchange resin filters, followed by a mix-bed deionizer to remove inorganic materials where removal of ionic materials relied on anion and cation exchange resin filters. In the early 1980s, reverse osmosis (RO) membranes were adopted for UPW production to eliminate total dissolved solids, particulate matters, and dissolved organic carbon (DOC). In the mid-1980s, ultrafiltration (UF) membranes were introduced as a polishing stage for the removal of microorganisms and macromolecules before providing UPW to end users [116]. More recently, the combination of RO-mix-bed deionization-UF processes has replaced anion and cation exchange resin filters coupled with a mixed-bed deionizer as a mainstream feature of UPW production systems, due to great advances in membrane technologies associated with water recovery, chemical usage for cleaning, and water qualities [126, 128-130].

In recent years, RO membranes have increasingly been considered a core technology of UPW production systems as they enable the removal of most contaminants from source water. The previous study demonstrated that the use of the RO membranes as a primary stage of UPW production systems could result in produced UPW having the maximum electrical resistivity of 2 MΩ cm [131]. However, very little is known about the RO membranes used for UPW production (i.e., removal of ionic materials and formation of membrane fouling) compared to the electrodeionization (EDI) processes [117, 118, 121]. The majority of previous studies on UPW production have focused on removing ionic materials using EDI processes for achieving high demineralization levels [118, 132]. Although a recent study has emphasized the importance of the RO membranes in UPW production systems with the latest trends occurring in the world water market, there has been no comprehensive research on fouling characteristics of the RO membranes used for UPW production [116, 118, 119, 121].

The primary objective of this study is to provide insights into fouling and cleaning behaviors of the RO membranes fed with tap water for UPW production. Dissolved organic matter (DOM) in feed and treated waters, foulants, and deposited on the RO membrane surfaces, were rigorously analyzed using a variety of characterization techniques to identify effects of DOM properties on fouling formation of the RO membranes. In addition, surface features of virgin, fouled, and cleaned RO membranes were investigated through membrane autopsies and straightly correlated to observed fouling characteristics of the RO membranes and effects of desorbing agents (i.e., deionized (DI) water, acid, base, and salt solutions) on the fouled RO membranes. This enabled elucidation of the cleaning mechanisms of the RO membranes used as a pre-treatment of ion-exchange resin (IER) filters in the UPW production system.

4. 2. Materials and Methods

4.2.1. Description of the UPW production system

A lab-scale UPW production system consisting of a microfiltration cartridge (MFC) filter, two RO membranes, and two IER filters was operated intermittently for nearly 3 years (Fig. 4-1). Tap water from a drinking water treatment plant (DWTP, Ulju-gun, Ulsan, Republic of Korea) was filtered using a MFC filter with a nominal pore size of 0.5 μm (SP32410, SpectraPure, Tempe, AZ, USA). This was operated in ‘dead-end mode’ (recovery rate = 97%) and further treated by two serially connected spiral-wound thin-film composite polyamide RO membrane modules (recovery rate = 15%; effective surface area of each module = 0.4 m^2) with a nominal pore size < 0.005 μm (RE-1812-50, Toray Chemical Korea, Republic of Korea). The physicochemical characteristics of the MFC filter and the RO membrane are summarized in Table 1. The RO permeate was polished with two serially connected IER filters (Dowex Monosphere MR-450 UPW, Dow Chemical, Midland, MI, USA). Each IER filter had the H^+ exchange capacity of 1.9 eq L^{-1} and the OH^- exchange capacity of 1.0 eq L^{-1} (Table 4-1). The specifications of the IER filter are provided in Table 4-2.

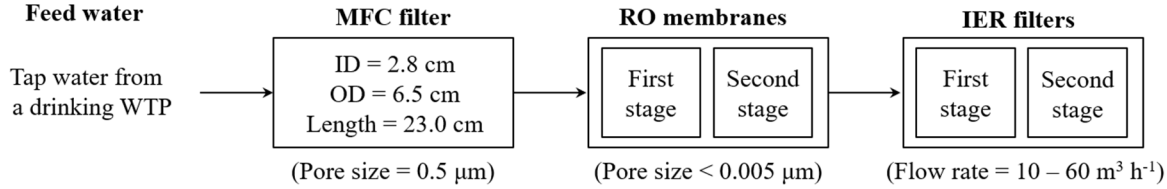

Figure 4-1. Schematic diagram of the UPW production system comprising a MFC filter, RO membranes, and IER filters.

Table 4-1. Physicochemical properties of the MFC filter and RO membranes

Type	**MFC filter**	**RO membrane**
Manufacturer	SpectraPure	Toray Chemical Korea
Membrane code	SP32410	RE-1812-50
Materials	Polypropylene	Thin-film composite polyamide
Nominal pore size (μm)	0.5	< 0.005
Roughness (μm)	N.A.	0.04
Inner diameter (cm)	2.8	N.A.
Outer diameter (cm)	6.5	N.A.
Length (cm)	23.0	N.A.
Effective surface area (m^2)	N.A.	0.4

N.A.: not available.

Table 4-2. Specifications of the IER filter.

Specifications	**H^+**	**OH^-**
Materials	Styrene-divinylbenzene	
Functional groups	Sulfonic acid and quaternary ammonium	
Total exchange capacity (eq L^{-1}) [a]	1.9	1.0
Water content (%)	46 – 53	45 – 53
Averaged particle size (μm)	360	590
Uniformity coefficient (μm) [b]	1.1	1.1
Particle density (g mL^{-1})	1.22	1.08
Cationic resin conversion rate to H^+ (%) [a]	99.7	-
Anionic resin conversion rate to OH^- (%) [a]	-	95.0

[a] Minimum.

[b] Maximum.

4.2.2 Preparation of water and foulant samples

4.2.2.1 Water samples

Four different water samples were obtained from the tested lab-scale UPW production system to investigate the removal of organic, inorganic materials, and ionic species and variations in physicochemical properties of DOM in feed and treated waters: (i) the tap water from the DWTP (feed), (ii) the permeate of the MFC filter (MFC permeate), (iii) the permeate of the RO membranes (RO permeate), and (iv) the permeate of the IER filters (IER permeate). All water samples were pre-filtered using 0.45 μm mixed cellulose ester membrane filters (Millipore, Bedford, MA, USA) prior to analyses.

4.2.2.2. Foulant samples

Foulants were extracted from the fouled RO membranes after 3-years operation using

four different desorbing agents: (i) DI water (RO-DI), (ii) an acid (0.1 N HCl) solution (RO-A), (iii) a base (0.1 N NaOH) solution (RO-B), and (iv) a salt (0.1 N NaCl) solution (RO-S). Four coupons of the fouled RO membranes (effective surface area of each coupon = 0.04 m^2) collected from the first stage of the RO membrane modules were soaked in 500 mL of each desorbing solution for 10 hours under moderate stirring conditions (150 rpm). The pH of the foulant samples extracted using acid and base solutions was maintained at approximately 6.5 by the addition of NaOH and HCl. All foulant samples were pre-filtered using 0.45 μm mixed cellulose ester membrane filters.

4.2.3. Virgin, fouled, and cleaned RO membranes

The virgin RO membranes were rinsed several times using DI water and soaked in DI water overnight to remove membrane-coating materials (i.e. humectants) from membrane surfaces. The soaked, fouled, and cleaned RO membranes using DI water (cleaned RO-DI), acid (cleaned RO-A), base (cleaned RO-B), and salt (cleaned RO-S) solutions were dried in a desiccator overnight. Their surface characteristics and performance were analyzed to investigate effects of DOM properties on fouling formation of the RO membranes.

4.2.4. Lab-scale cross-flow RO filtration unit

The performance of the virgin, fouled, and cleaned RO membranes (i.e., permeate flux and salt rejection) were investigated with a lab-scale cross-flow RO filtration unit using 0.1 M NaCl solution. This unit was comprised of a flat-sheet filtration cell (effective surface area = 96 cm^2; channel height = 0.04 cm), a high-pressure pump (CAT pumps, model 1050 10 GPM 2200, Minneapolis, MN, USA), and a feed water reservoir. Prior to all filtration tests, the RO filtration unit was stabilized for 2 hours using DI water. The RO filtration unit was operated in re-circulation mode at 20 ± 1 ºC. During filtration tests, feed water pressure was maintained at 1000 kPa with a cross-flow velocity of 8.68 cm sec^{-1}. The rejection rates of NaCl by the RO membranes and their permeate fluxes were calculated using the following equations:

$$\text{Salt rejection rate } (\%) = \left(1 - \frac{C_p}{C_f}\right) \times 100 \quad (4\text{-}1)$$

$$\text{Permeate flux (L } m^{-2}h^{-1}) = \frac{Q}{A} \quad (4\text{-}2)$$

where C_f and C_p are NaCl concentrations in the feed and permeate water, Q is the permeate flow (L h^{-1}), and A is the membrane surface area (m^2).

4.2.5 Analytical methods

Dissolved organic carbon (DOC) and total nitrogen (TN) concentrations in water and foulant samples were measured using a total organic carbon analyzer (TOC-V_{CPH}, Shimadzu, Kyoto, Japan) equipped with a TN analyzer (TNM-1, Shimadzu, Kyoto, Japan). The aromatic carbon contents of DOM were evaluated using a UV/Vis spectrometer (UV-1601, Shimadzu, Kyoto, Japan) with a 1 cm quartz cell (Hellma, Mülheim, Germany) at UV absorbance at 254 nm (UVA_{254}); specific UV absorbance (SUVA) values were determined as the ratio of UVA_{254} to DOC concentration. Concentrations of inorganic materials in water and foulants samples were quantified using an inductively coupled plasma-optical emission spectrophotometer (700-ES, Varian, Walnut Creek, CA, USA).

The three-dimensional fluorescence excitation-emission matrix (3D FEEM) and molecular weight (MW) distributions of DOM were confirmed using fluorescence spectroscopy (RF-5301, Shimadzu, Kyoto, Japan), high-performance size-exclusion chromatography (HPSEC) equipped with a Protein-Pak 125 column (Waters, Milford, MA, USA), with fluorescence detection at excitation (Ex) wavelength 278 nm and emission (Em) wavelength 353 nm (RF-10AXL; Shimadzu, Kyoto, Japan) and UV detection at 254 nm (SPD-10AVP; Shimadzu, Kyoto, Japan), and phosphate buffer(96 mM NaCl + 2.4 mM NaH_2PO_4+ 1.6 mM Na_2HPO_4, ionic strength 0.1 M, pH 6.8), with a flow rate of 0.7 ml/min and an injection volume of 200 μl [131, 134]. An electrophoretic light scattering spectrophotometer (ELSZ-2000, Otsuka Electronics, Osaka, Japan) and a goniometer (Phoenix Multi/Tilting, SEO, Gyeonggi-do, Korea) were applied to identify differences in surface ζ potential and contact angle of the virgin, fouled, and cleaned RO membranes. Prior to analyze surface feature, the virgin, fouled and cleaned RO membranes were soaked with DI water for overnight and were dried in a vacuum desiccator for 48 hours. Functional group compositions of the virgin and fouled RO membranes were analyzed using attenuated total reflection-Fourier transform infrared (ATR-FTIR) spectroscopy (Vertex70, Bruker, MA, USA), utilizing a ZnSe crystal at

an incident angle of 45 º over a scanning wavelength of 750–1750 cm^{-1} with a resolution of 0.4 cm^{-1} [135, 136].

4.3 Results and discussions

4.3.1 Water quality analyses

Bulk water quality parameters (i.e., pH and conductivity), amounts and nature of DOM (i.e., DOC, TN, UVA_{254}, and SUVA), presence and concentrations of ionic species, and metals and metalloids in the feed and treated waters were identified to assess the performance of the tested UPW system (Table 4-3). The RO membranes were effective in reducing conductivity and DOC, TN, and UVA_{254} concentrations; the polishing stage using IER filters resulted in ultra-trace levels of all these parameters (conductivity = 0.55 μS cm^{-1}; DOC = 0.07 mg L^{-1}; UVA_{254} = 0.001 cm^{-1}; TN = 0.05 mg N L^{-1}). Similar to conductivity and DOM, most ionic species, metals, and metalloids in feed water were hardly removed using the MFC filter. However, there were significant decreases in these parameters after the RO membranes, and almost complete removal of conductivity, DOC, TN, and UVA_{254} from the RO permeate by the use of IER filters. Consequently, the achieved purity degree of UPW satisfied the electrical resistivity of the IER permeate (> 18.2 ΩM) at room temperature (~ 20ºC) that is required for semiconductor manufacturing [116].

Table 4-3. Characteristics of feed and treated waters in the UPW production system (n=3).

		Feed	MFC permeate	RO permeate	IER permeate
Bulk parameters	pH	7.3	7.3	7.5	6.3
	Conductivity (μS cm^{-1})	68.5	67.1	12.1	0.55
	TN (mgN L^{-1})	2.15 (±0.10)	2.08 (±0.06)	0.98 (±0.47)	0.05 (±0.01)[a]
	DOC (mgC L^{-1})	1.65 (±0.10)	0.81 (±0.13)	0.09 (±0.07)	0.07 (±0.02)[a]
	UVA_{254} (cm^{-1})	0.024 (±0.002)	0.018 (±0.001)	0.002 (±0.001)	0.001 (±0.000)
	SUVA	1.45 (±0.03)	2.22 (±0.20)	2.22 (±0.78)	1.37 (±0.28)

	($L\ mg^{-1}\ m^{-1}$)				
Ion species	Na^+ ($mg\ L^{-1}$)	6.47 (±0.21)	6.13 (±0.16)	0.21 (±0.01)	B.D.L.
	K^+ ($mg\ L^{-1}$)	2.19 (±0.22)	2.12 (±0.12)	0.41 (±0.01)	B.D.L.
	Mg^{2+} ($mg\ L^{-1}$)	3.26 (±0.12)	3.12 (±0.27)	0.29 (±0.09)	B.D.L.
	Ca^{2+} ($mg\ L^{-1}$)	14.48 (±0.21)	13.9 (±0.14)	1.54 (±0.13)	B.D.L.
	Cl^- ($mg\ L^{-1}$)	17.23 (±0.41)	15.82 (±0.35)	0.42 (±0.01)	B.D.L.
	NO_3^- ($mg\ L^{-1}$)	1.71 (±0.18)	1.64 (±0.25)	0.38 (±0.01)	B.D.L.
	SO_4^{2-} ($mg\ L^{-1}$)	11.23 (±0.32)	9.97 (±0.14)	0.12 (±0.01)	B.D.L.
Metals and metalloids	Al ($\mu g\ L^{-1}$)	19.17 (±0.13)	12.25 (±0.16)	1.98 (±0.09)	2.7 (±0.12)
	As ($\mu g\ L^{-1}$)	0.54 (±0.02)	0.18 (±0.03)	0.00 (±0.00)	0.00 (±0.00)
	Cd ($\mu g\ L^{-1}$)	0.01 (±0.01)	0.00 (±0.00)	0.00 (±0.00)	B.D.L.
	Co ($\mu g\ L^{-1}$)	0.02 (±0.01)	0.00 (±0.00)	0.00 (±0.00)	0.00 (±0.00)
	Cr ($\mu g\ L^{-1}$)	0.14 (±0.06)	0.00 (±0.00)	0.00 (±0.00)	0.00 (±0.00)
	Cu ($\mu g\ L^{-1}$)	1.15 (±0.03)	0.82 (±0.03)	0.28 (±0.02)	B.D.L.
	Fe ($\mu g\ L^{-1}$)	3.67 (±0.31)	1.23 (±0.18)	0.32 (±0.17)	1.3 (±0.02)
	Mn ($\mu g\ L^{-1}$)	2.16 (±0.02)	1.98 (±0.02)	0.35 (±0.02)	0.1 (±0.00)
	Pb ($\mu g\ L^{-1}$)	0.04 (±0.01)	0.03 (±0.01)	0.01 (±0.02)	B.D.L.

[a] n=2

B.D.L.: below the detection limit.

4.3.2 Characterization of DOM

The 3D FEEM of DOM in feed and treated waters are illustrated in Fig. 4-2. Two pairs of humic-like fluorophores were detected for the feed water at excitation wavelength (Ex) = 250 nm/emission wavelength (Em) = 430 nm (Feed I; the maximum intensity = 60 mV) and Ex = 300 nm/Em = 400 nm (Feed II; the maximum intensity = 60 mV) [138]. Despite the considerable decrease in DOC concentration, the intensities of humic-like fluorophores were slightly lower after treatment with the MFC filter (the maximum intensity of MFC permeate I at Ex = 250 nm/Em = 430 nm = 50 mV; the maximum intensity of MFC permeate II at Ex = 300 nm/Em = 400 nm = 50 mV). In addition, distinctive humic-like fluorophores were not observed for the RO and IER permeates due to the almost complete removal of DOM (DOC of RO permeate = 0.09 $mgC\ L^{-1}$; DOC of IER permeate = 0.07 $mgC\ L^{-1}$). These results were

in good agreement with the abatement trend of SUVA values through the UPW production system.

The MW distributions of aromatic and protein-like substances in DOM of feed and treated waters are presented in Fig. 4-3. The aromatic substances of DOM in feed water contained either low (960 – 1,780 daltons (Da)) or high MW fractions (31,290 Da), with the highest peak at 960 Da (Fig. 4-3a). After passing through the MFC filter, the high MW fraction was completely removed and the UVA intensities of the low MW fractions were substantially decreased. A low MW fraction was found only for the RO permeate at 1,220 Da, and its UVA intensity was mostly eliminated after the IER filters. Protein-like substances of DOM in feed water ranged from 150 Da to 48,640 Da, with the highest peak at 6,660 Da (Fig. 4-3b). Most MW fractions were effectively removed by the MFC filter, with the exception of the peak at 150 Da. No distinctive peaks were detected for the fluorescence chromatograms of RO and IER permeates. Although the fluorescence detection had higher sensitivity compared to the UVA detection, fluorescence intensities of DOM (the maximum intensity = 3,423 mV) were much lower than UVA intensities (the maximum intensity = 6,740 mV) [139, 140]. Based on these observations, it could be postulated that DOM in feed water is dominantly composed of hydrophobic components.

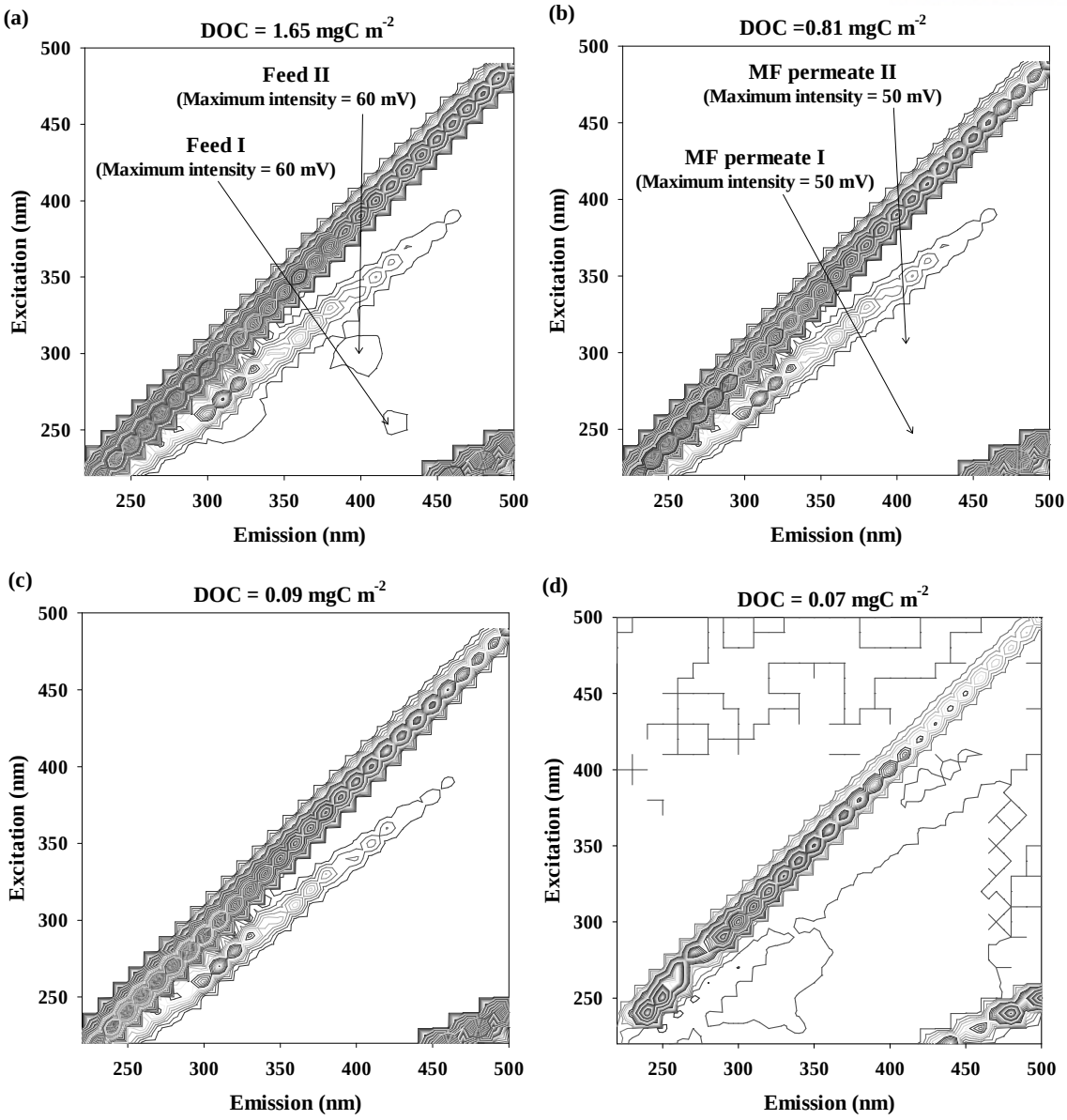

Figure 4-2. Fluorescence spectral characteristics of DOM in feed and treated waters of the UPW system: (a) feed, (b) MFC permeate, (c) RO permeate, and (d) IER permeate.

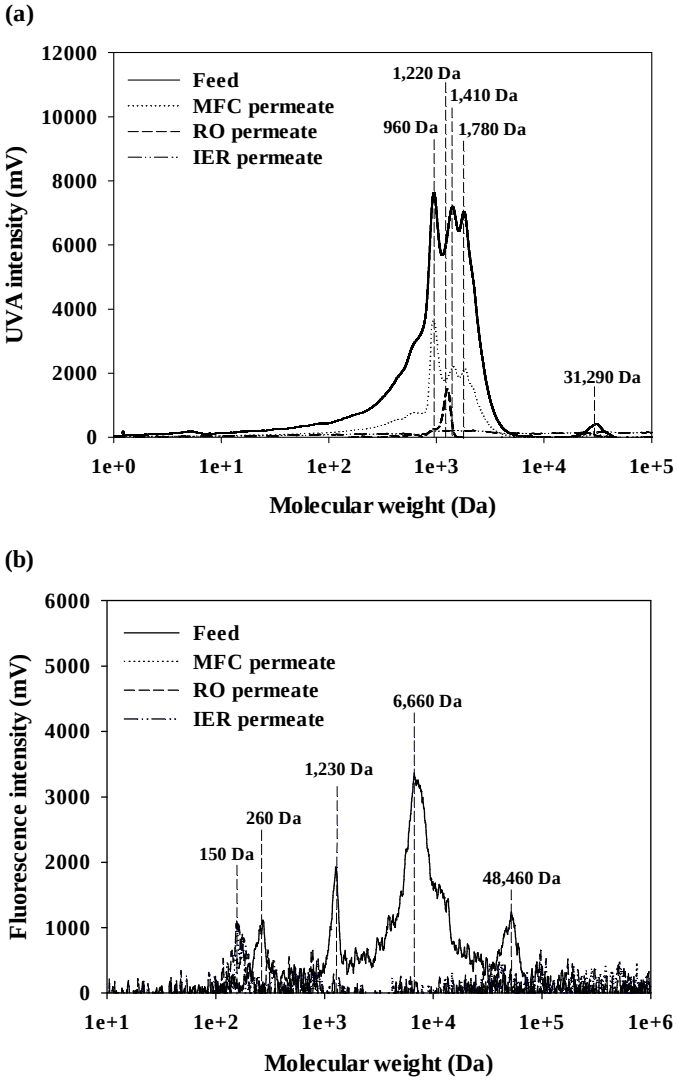

Figure 4-3. The MW distribution of DOM in the feed and treated waters of the UPW production system: (a) aromatic substance and (b) protein-like substances.

4.3.3. Characterization of the RO membrane foulants

4.3.3.1. Organic and inorganic contents

The composition of desorbed foulants from the RO membranes utilized in the UPW production system is listed in Table 4-4. The salt solution (0.1 N NaCl) was more effective than DI water, acid (0.1 N HCl) or base (0.1 N NaOH) solutions in desorbing DOC (RO-DI = 25.39 mgC m^{-2}; RO-A= 15.95 mgC m^{-2}; RO-B = 46.14 mgC m^{-2}; RO-S = 65.12 mgC m^{-2}) and TN (RO-DI = 2.71 mgN m^{-2}; RO-A= 2.72 mgN m^{-2}; RO-B = 2.85 mgN m^{-2}; RO-S = 3.57 mgN m^{-}

^{2}) foulants from the RO membranes. Moreover, the desorbed RO membrane foulants using the salt solution exhibited a lower SUVA value than the desorbed RO membrane foulants using other solutions (RO-DI = 2.17 L mg^{-1} m^{-1}; RO-A= 0.81 L mg^{-1} m^{-1}; RO-B = 4.96 L mg^{-1} m^{-1}; RO-S = 0.13 L mg^{-1} m^{-1}

This shows that the reduced the electrostatic interaction of charged membrane surface and NOM, leading to double layer compaction and charge screening due to structural variations in cross-linked fouling gel layers during exposure of the RO membrane surfaces to the salt solution may lead to the desorption of hydrophilic organic foulants [141]. Furthermore, some fraction of neutrals foulants can be easily desorbed by decreased hydrophobic/hydrophilic interaction with infiltrating sodium and chlorides ions into Stern layer [142-144].

In general, membrane fouling can be categorized into two groups according to the adhesion strength of foulants to membrane surfaces: (i) irreversible fouling (i.e., desorbable using chemical cleaning) and (ii) reversible fouling (i.e., desorbable using hydraulically cleaning) [138]. The sum of DOC of the desorbed RO membrane foulants using acid, base, and salt solutions was defined as irreversible membrane fouling, and the DOC of the desorbed foulants using DI water was defined as reversible membrane fouling. It is therefore evident that irreversible membrane fouling may govern fouling behavior and characteristics of the RO membranes used in UPW production systems.

The quantity of desorbed metals and metalloids from the RO membranes was highly variable depending on the type of desorbing agents. Furthermore, despite the relatively lower DOC concentration of RO-B (46.14 mgC m^{-2}) compared to RO-S (65.12 mgC m^{-2}), RO-B had higher Al, Ca, and Fe concentrations than RO-S, as most multivalent ions had a greater potential to form complexes with hydrophobic DOM components [140, 145]. This observation was strongly supported by the relatively higher SUVA value of desorbed foulants from RO-B compared to that of RO-S. Previous studies have demonstrated that accumulation of complexes with multivalent ions and hydrophobic DOM components onto membrane surfaces can intensify the formation of organic fouling in the RO membrane processes [146].

Table 4. Composition of the desorbed RO membrane foulants from the UPW production system using DI water, acid, base, and salt solutions (n=3).

		RO-DI	RO-A	RO-B	RO-S
Bulk Parameter	DOC (mgC m^{-2})	25.39 (± 0.35)	15.95 (± 0.38)	46.14 (± 0.94)	65.12 (± 1.51)
	UVA_{254} (cm^{-1})	0.087 (± 0.003)	0.017 (± 0.003)	0.289 (± 0.004)	0.011 (± 0.001)
	SUVA (L mg^{-1} m^{-1})	2.71 (± 0.09)	0.81 (± 0.14)	4.96 (± 0.05)	0.13 (± 0.04)
	TN (mgN m^{-2})	1.08 (± 0.41)	2.72 (± 0.34)	2.85 (± 0.18)	3.57 (± 1.95)
Metals and metalloids	Al (mg m^{-2})	0.24 (± 0.02)	4.89 (±0.09)	8.19 (± 0.06)	0.01 (± 0.01)
	As (μg m^{-2})	0.03 (± 0.01)	0.02 (± 0.01)	8.79 (± 0.01)	0.01 (± 0.01)
	Ca (mg m^{-2})	25.72 (± 4.83)	25.09 (± 0.55)	36.96 (± 2.45)	24.06 (± 2.37)
	Cd (μg m^{-2})	B.D.L.	B.D.L.	B.D.L.	B.D.L.
	Co (μg m^{-2})	B.D.L.	B.D.L.	B.D.L.	B.D.L.
	Cr (μg m^{-2})	0.01 (± 0.01)	0.01 (± 0.01)	0.06 (± 0.01)	0.00 (± 0.01)
	Cu (μg m^{-2})	0.04 (± 0.01)	0.65 (± 0.01)	0.25 (± 0.01)	0.04 (± 0.01)
	Fe (μg m^{-2})	0.62 (± 0.02)	0.38 (± 0.04)	1.92 (± 0.01)	0.01 (± 0.01)
	Mg (mg m^{-2})	12.82 (± 2.45)	10.29 (± 0.16)	9.73 (± 0.16)	9.89 (± 0.01)
	Mn (μg m^{-2})	0.16 (± 0.01)	0.47 (± 0.01)	0.1 (± 0.01)	0.09 (± 0.01)
	Pb (μg m^{-2})	0.02 (± 0.01)	0.47 (± 0.06)	0.23 (± 0.01)	N.D.

B.D.L.: below the detection limit.

4.3.3.2. Fluorescence spectroscopy

The fluorescence spectral properties of desorbed foulants from the RO membranes are depicted in Fig. 4-4. Three types of fluorophores were found for the desorbed RO membrane foulants using DI water, acid, base, and salt solutions. The RO-DI showed two pairs of humic-like fluorophores at Ex = 250 nm/Em = 410 nm (RO-DI I; the maximum intensity = 269 mV) and Ex = 290 nm/Em = 410 nm (RO-DI II; the maximum intensity = 269 mV). Three different fluorophores were found for RO-A at Ex = 230/Em = 260 nm (RO-A I; protein-like fluorophore, the maximum intensity = 156 mV), Ex = 250/Em = 360 nm (RO-A II; humic-like fluorophore, the maximum intensity = 175 mV), and Ex = 290/Em = 360 nm (RO-A III; humic-like fluorophore, the maximum intensity = 156 mV) while a relatively strong humic-like fluorophore was detected for the RO-B at Ex = 290 nm and Em = 400 nm (RO-B I; the maximum intensity = 1,345 mV). Despite having the highest DOC concentration, the RO-S exhibited two types of relatively weak fluorophores at Ex = 260 nm/Em = 310 nm associated with protein-like fluorophores (the maximum intensity = 93 mV) and Ex = 280 nm/Em = 380 nm, indicative of humic-like fluorophores (the maximum intensity = 113 mV). These results support the assumption that the salt solution is an effective agent to desorb hydrophilic organic foulants from the surfaces of the RO membranes used for UPW production [141].

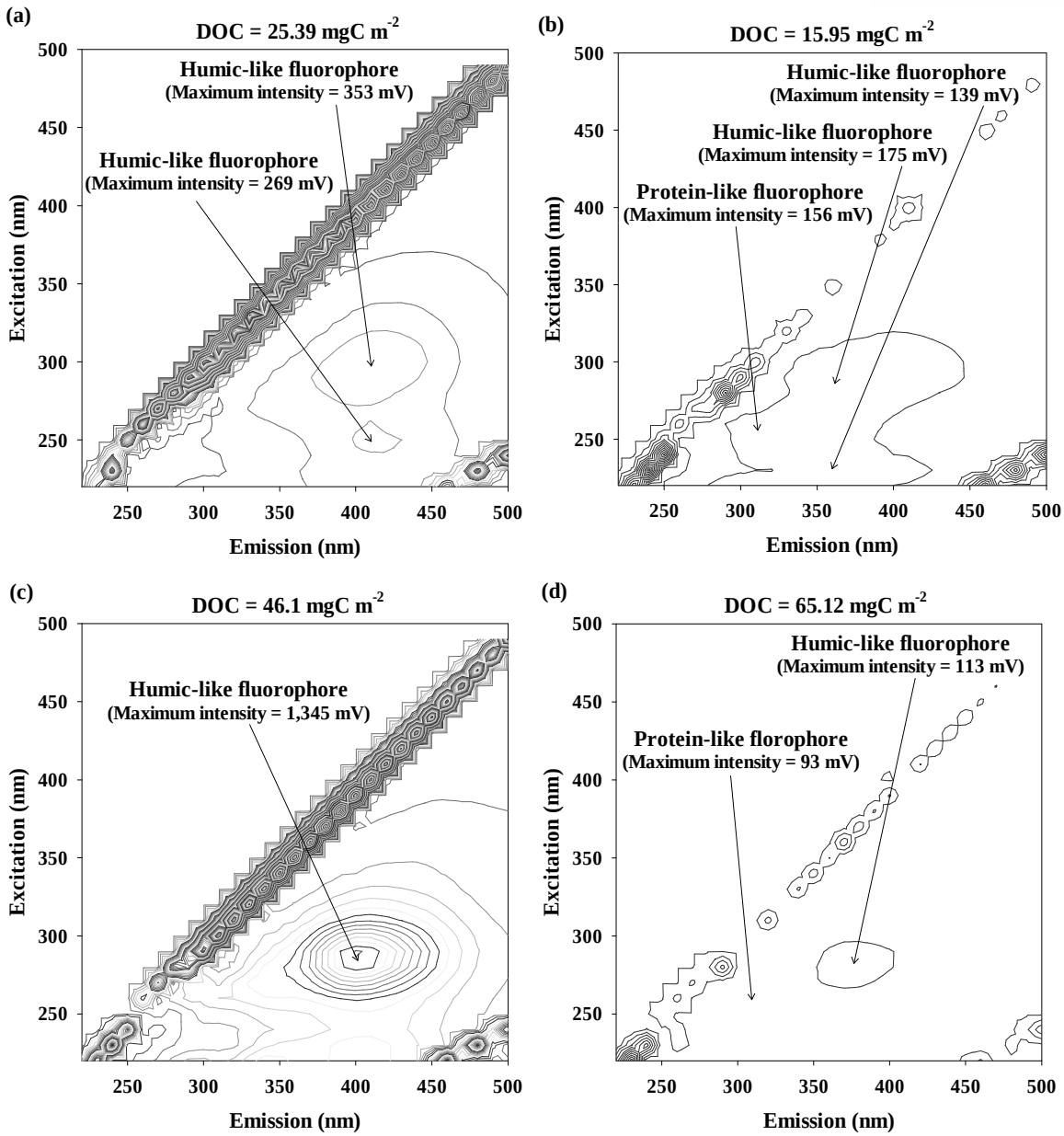

Figure 4-4. The 3D FEEM of the desorbed foulants from the RO membranes used for UPW production: (a) RO-DI, (b) RO-A, (c) RO-B, and (d) RO-S.

4.3.3.3. HPSEC analysis

The MW distributions of the desorbed RO membrane foulants using DI water, acid, base, and salt solutions, in terms of aromatic and protein-like substances, are shown in Fig. 4-5. There were no prominent MW peaks for aromatic substances in RO-A and RO-S (Fig. 4-5a). Even though aromatic substances of RO-B included both low (930 Da) and high MW fractions (13,500 Da and 26,800 Da), UVA intensities of high MW fractions (the maximum intensity at 13,500 Da = 1,806 mV; the maximum intensity at 26,800 Da = 2,018 mV) were negligible compared to that of low MW fractions the (maximum intensity at 930 Da = 41,787 mV). In addition, a relatively weak peak was observed for aromatic substances of RO-DI at 640 Da (the maximum intensity = 6,802 mV). The MW distribution patterns of the protein-like substances (Fig. 4-5b) were differed considerably from those of the aromatic substances (Fig. 4-5a), due to significant differences in the major foulant components according to the type of desorbing agent used. No distinctive MW peaks were observed for protein-like substances of RO-A and RO-B. However, the MW distribution of the protein-like substances in RO-S ranged from 1,530 Da to 15,700 Da, with the highest peak at 9,620 Da (the maximum intensity = 15,043 mV); RO-DI exhibited a very weak fluorescence peak at 850 Da (the maximum intensity = 3,398 mV). The absence of prominent UVA peaks and the relatively higher intensities of fluorescence peaks in RO-S clearly showed that RO-S is predominantly comprised of hydrophilic DOM components (i.e., polysaccharide-like and protein-like substances).

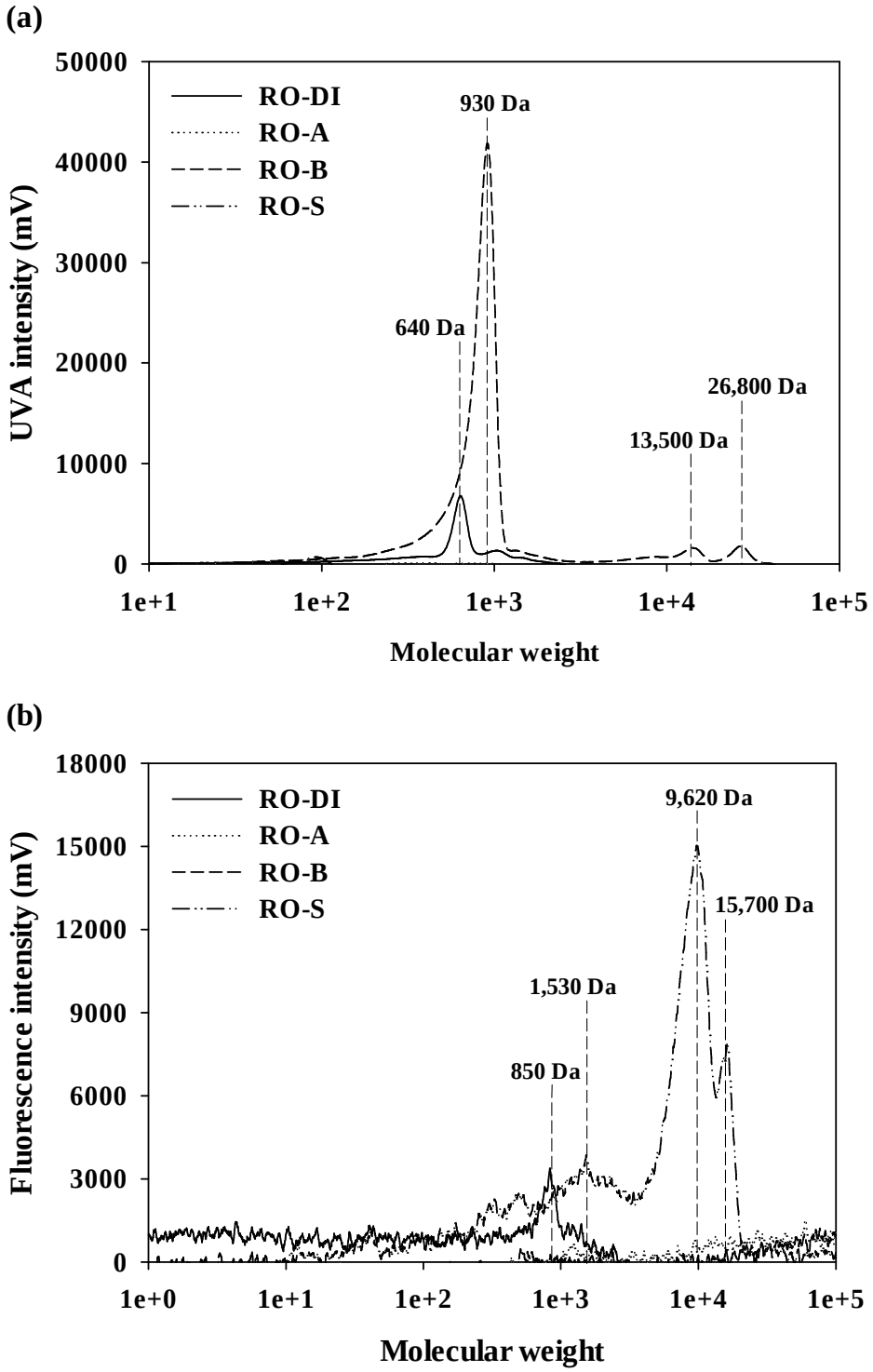

Figure 4-5. The MW distribution of the desorbed foulants from the RO membranes used for UPW production: (a) aromatic substance and (b) protein-like substances.

4.3.3.4 ATR-FTIR spectroscopy

The ATR-FTIR spectra of the virgin and fouled RO membranes are exhibited in Fig. S1, Supplementary information (SI). The identical ATR-FTIR spectra were detected for the virgin and fouled RO membranes. However, the intensities of the IR peaks related to amide functional groups originating from the microbial cell lysis, and alcohol functional groups derived from cell wall polysaccharides of microorganisms, differed considerably from each other [134, 138]. After formation of fouling layers onto the RO membrane surfaces, intensities of IR peaks associated with N-H stretching of amides (1700–1630 cm^{-1}, 1630–1595 cm^{-1}, and 1430–1410 cm^{-1}), the CNH band of secondary amides (1570–1515 cm^{-1}), the OH band of alcohols (1350–1260 cm^{-1}), the C-O stretching of alcohols (1075–1000 cm^{-1}), and –CH band of aldehydes (975–780 cm^{-1}) were substantially decreased. Conversely, the intensities of IR peaks indicative of the N-H stretching of amides (1590–1570 cm^{-1}, 1610–1500 cm^{-1}, and 850–750 cm^{-1}), the C-O stretching of carboxylic acids (1250–1050 cm^{-1}), and the C-O stretching of alcohols (1210–1100 cm^{-1}) were significantly increased [135, 147]. This may be attributed to deposition of either hydrophobic (i.e., humic-like substances) or hydrophilic DOM components (i.e., polysaccharide-like and protein-like substances) from feed water onto the RO membrane surfaces during operation of the UPW production system.

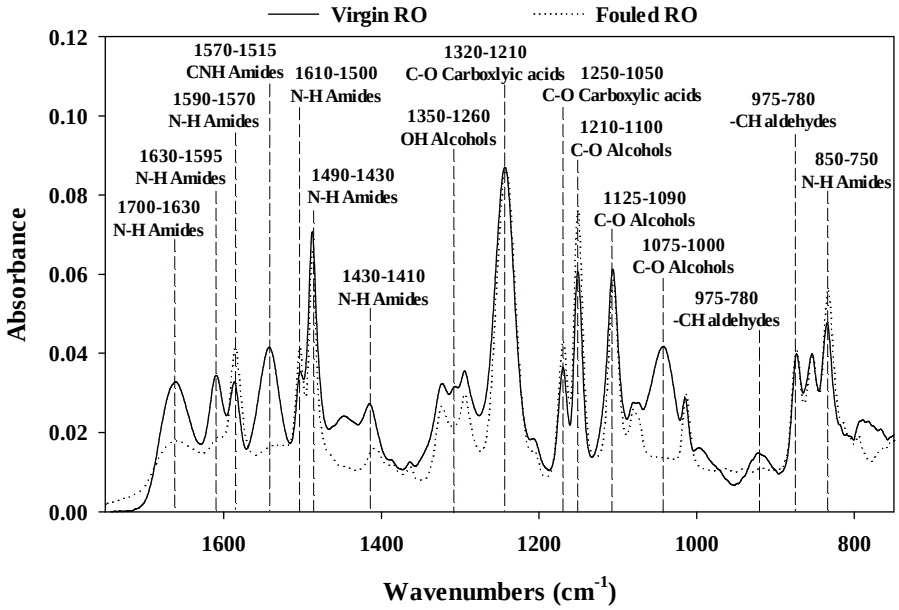

Figure 4-6 The ATR-FTIR spectra of the virgin and fouled RO membranes used in the UPW system.

4.3.4 Surface features of virgin, fouled and cleaned RO membranes

The physicochemical characteristics of the virgin, fouled, and cleaned RO membrane surfaces are summarized in Table 4-5. After formation of fouling layers on membrane surfaces, the negative surface ζ potential of the virgin RO membranes was considerably decreased (virgin RO membrane = –27.4 mV; fouled RO membrane = 1.7 mV), whereas the contact angle was slightly increased (virgin RO membrane = 58.3 º; fouled RO membrane = 65.1 º). Decreases in the negative surface ζ potential and increases in the surface hydrophobicity of the fouled RO membrane can be explained by the adsorption of hydrophobic and hydrophilic DOM components onto the RO membrane surfaces [23, 30]. All desrobing agents were effective in recovering the negative surface ζ potential and the surface hydrophobicity of the RO membranes, however their recovery rates were strongly influenced by the type of cleaning agent used. The recovery rates of the negative surface ζ potential on the fouled RO membranes were in the order of cleaned RO-S (–24.6 mV) > cleaned RO-B (–21.8 mV) > cleaned RO-DI (–17.5 mV) > cleaned RO-A (–11.4 mV). Similar trends were observed for changes in the contact angle of the fouled RO membranes after the cleaning procedures. The hydrophobicity of the cleaned RO membrane surfaces decreased from cleaned RO-A (64.3 º) > cleaned RO-DI (56.7 º) > cleaned RO-B (51.7 º)> cleaned RO-S (51.3 º). These observations are intimately correlated to the amount of desorbed organic foulants from the RO membrane surfaces using DI, acid, base, and salt solutions (DOC of RO-DI = 25.39 mg C m^{-2}; DOC of RO-A = 15.95 mgC m^{-2}; DOC of RO-B = 46.14 mgC m^{-2}; DOC of RO-S = 65.12 mg C m^{-2}). The lower hydrophobicity of the RO membrane surfaces cleaned using base and salt solutions, and the higher hydrophobicity of the fouled RO membrane surfaces compared to the virgin RO membrane surfaces, are notable. This result illustrates that the reduced negative surface ζ potential (through formation of initial fouling layers by deposition of hydrophilic DOM components onto the RO membrane surfaces) may enhance subsequent fouling formation of the RO membranes by hydrophobic DOM components [140, 146].

Table 4-5. Physicochemical properties of the virgin, fouled, and cleaned RO membranes using DI water, acid, base, and salt solutions (n = 3).

	Surface ζ potential at pH 7 (mV)	Contact angel (°)
Virgin RO	–27.4 (±1.6)	58.3 (±3.8)
Fouled RO	1.7 (±3.1)	65.1 (±2.5)
Cleaned RO-DI	–17.5 (±1.9)	56.7 (±0.7)
Cleaned RO-A	–11.4 (±2.6)	64.3 (±5.9)
Cleaned RO-B	–21.8 (±3.6)	51.7 (±4.8)
Cleaned RO-S	–24.6 (±2.4)	51.3 (±1.2)

4.3.5 Effects of cleaning agent types on the recovery of salt rejection and permeate flux

The salt rejection (NaCl = 0.1 M) and permeate flux (feed: DI water) of the virgin, fouled, and cleaned RO membranes under controlled conditions (feed water pressure = 1,000 KPa; cross flow velocity = 0.5 L min^{-1}; effective surface area = 96 cm^2; channel height = 0.04 cm; temperature = 20 ± 0.7 ºC) are compared in Fig. 4-6. The fouled RO membranes exhibited a much lower permeate flux (1.2 L m^{-2} hr^{-1}) than the virgin RO membrane (6.5 L m^{-2} hr^{-1}) due to formation of membrane foulants.

Moreover, a significant decrease was observed for the salt rejection rate of the fouled RO membranes (88.2%) compared to the virgin RO membranes (97.5%). There may be two possible reasons; i) The interaction between concentration polarization and formed cake layer is highly depending on the intrinsic properties of the formed cake layer (e.g., porosity, thickness). The formed cake layer can cause cake-enhanced concentration polarized which cause increasement of salt passage through the RO membranes [148]. ii) the increased salt concentrations at the RO membrane surfaces (due to the hindered back diffusion of salts from the RO membrane surfaces by forming colloidal cake layers on those surfaces) can increase the passage of salts through the RO membranes [149].

All the applied desorbing agents were effective in recovering salt rejection and permeate flux. However, the recovery rates varied markedly according to the types of desorbing agents. The recovery rates of the salt rejection through the cleaning using DI water, acid, base,

and salt solutions were in the order of cleaned RO-DI (salt rejection = 90.1%) > cleaned RO-A (salt rejection = 92.1%) > cleaned RO-S (salt rejection = 94.8%) > cleaned RO-B (salt rejection = 95.0%). Although cleaned RO-B showed a slightly better salt rejection than cleaned RO-S, the differences were negligible (< 0.2%). Unlike recovery rates of salt rejection, recovery rates of permeate flux were strongly associated with the amount of desorbed organic foulants from the RO membrane surfaces (DOC of RO-DI = 25.39 mgC m^{-2}; DOC of RO-A = 15.95 mgC m^{-2}; DOC of RO-B = 46.14 mgC m^{-2}; DOC of RO-S = 65.12 mgC m^{-2}). The recovery rates of the permeate flux through the cleaning using DI water, acid, base, and salt solutions were in the order of cleaned RO-DI (permeate flux = 3.6 L m^{-2} hr^{-1}) < cleaned RO-A (permeate flux = 4.1 L m^{-2} hr^{-1}) < cleaned RO-B (permeate flux = 4.8 L m^{-2} hr^{-1}) < cleaned RO-S (permeate flux = 5.3 L m^{-2} hr^{-1}), which is consistent with the recovery rates of the negative surface ζ potential and the contact angle with the exception of RO-A. This is because that acid cleaning is more effective for desorbing inorganic foulants than organic foulants. The recovery rates of surface features more influenced by the amount of desorbed organic foulants on membranes surface [136,138,140,145]. Therefore, permeate flux recovery rate of RO-A can be higher than that of RO-DI, even though the surface features recovery of RO-A is lower than that of RO-DI. These observations suggest that salt cleaning can efficiently recover the salt rejection and the permeate flux of the RO membranes used for UPW production [141].

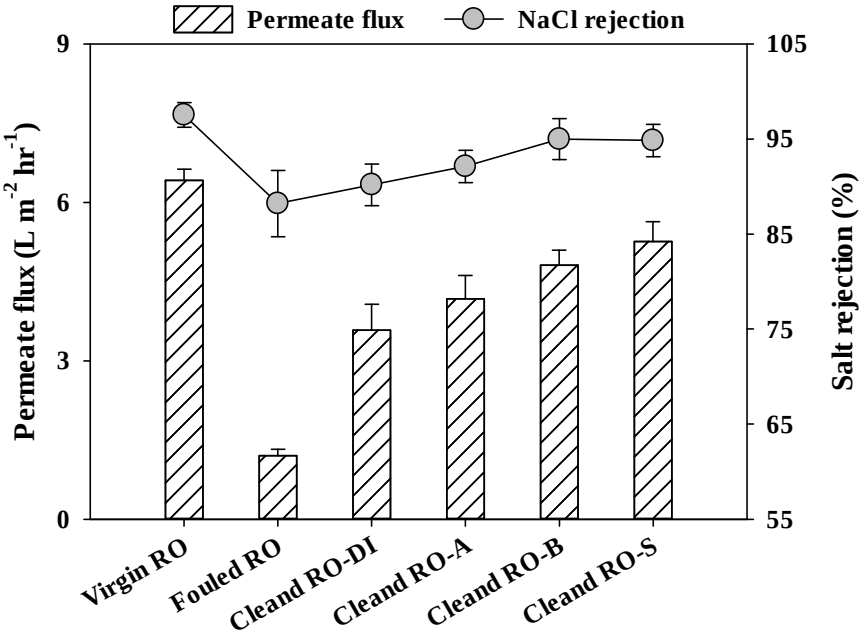

Figure 4-7. The permeate flux (feed water: DI water) and salt rejection (NaCl = 0.1 M) of the virgin, fouled, and cleaned RO membranes under controlled conditions (feed water pressure = 1,000 KPa; cross flow velocity = 0.5 L min^{-1}; effective surface area = 96 cm^2; channel height = 0.04 cm; temperature = 20 ± 0.7 ºC).

4.5 Summary

Fouling behaviors of the RO membranes and effects of desorbing agents (i.e., DI water, acid, base, and salt solutions) on the fouled RO membranes were identified through membrane autopsies and characterization of DOM and desorbed membrane foulants to provide deeper insights into the UPW production systems. The salt solution more effectively extracted organic foulants from the RO membrane surfaces (DOC = 65.12 mgC m^{-2}) compared to DI water (DOC = 25.39 mgC m^{-2}), acid (DOC = 15.95 mgC m^{-2}), and base (DOC = 46.14 mgC m^{-2}) solutions. This was attributed to the efficient desorption of hydrophilic organic foulants through structural changes in the cross-linked gel layers during exposure of the RO membrane surfaces to the salt solution. Consequently, the highest negative surface ζ potential (–24.6 mV) and the lowest contact angle (51.3 °) were observed for the cleaned RO-S. These results show that recovery of membrane surface features (i.e., surface ζ potential and contact angle) was directly correlated to the amount of desorbed organic foulants from the RO membrane surfaces. Although the salt rejection of cleaned RO-S (94.8%) was slightly lower than that of cleaned RO-B (95.0%), cleaned RO-S exhibited a much higher permeate flux (5.3 L m^{-2} hr^{-1}) compared to cleaned RO-B (4.8 L m^{-2} hr^{-1}). These observations show that salt cleaning is a promising option to recover the salt rejection and the permeate flux of the RO membranes fouled dominantly by hydrophilic DOM fractions and used for UPW production. Furthermore, the in-depth mechanism of salt cleaning for fouled membrane and its implication for water treatment process based on membrane technology can be further extended.

5.0 Conclusions

5.1 Surface charge characterization of nanofiltration membranes by potentiometric titrations and electrophoresis: Functionality vs. zeta potential

The surface charge properties (i.e., functionality and zeta (ζ) potential) of two nanofiltration (NF) membranes were characterized by potentiometric titrations and electrophoresis to predict how electrostatic transport at the membrane surfaces affect their salt rejection and fouling propensities. The ζ potential was not suitable for evaluating the rejection of Na+ (NE20 membrane = 21–25%; NE70 membrane = 65–70%) and Cl− ions (NE20 membrane = 19–22%; NE70 membrane = 60–63%) and the fouling propensities of organic materials in the NF membranes due to its inherent measurement inaccuracies (Δ ζ potential = −1.8 × (Δ amount of desorbed organic foulants) + 45.9, R^2 = 0.07). The functionality accurately predicted both the rejection of NaCl and the fouling propensities of the organic materials, as the charge densities of the membranes determined by the functionality measurements truly reflected the acid dissociation constants of the carboxylic and amine functional groups and the points of zero charge values, but only for the TFC membranes. These results indicate that potentiometric titrations may provide valuable insights into how electrostatic transport at the membrane surface influences the salt rejection and fouling mechanisms of the NF membranes.

5.2 Influence of organic matter polarity on the intrinsic electrical surface property (pKa) of the negatively-charged nanofiltration membrane

The electrical surface properties (pK_a and PZC) of virgin and fouled NF membranes were determined using the potentiometric titration method with regard to the reversibility of the membranes (i.e., salt rejection and permeate flux). The lower PZC value observed for membrane fouled with MPD compared to the virgin NF membrane can be explained by the adsorption of positively-charged foulants on the negatively-charged membrane surface. In addition, the higher PZC value was observed for the membrane fouled with CCA by the adsorption of negatively-charged foulants on the negatively-charged membrane surface. Moreover, no significant change in PZC values was observed for the membrane fouled with DG. This is because of the adsorption of neutral foulants on the negatively-charged membrane surface. These observations indicate that the PZC measurements may offer significant insights into differences in PZC values, in terms of the properties of membrane foulants, based on the

ionization degree of the surface functional groups. All the desorbing agents applied were effective at recovering salt rejection and permeate flux. However, the recovery rates varied markedly according to the types of desorbing agents used. The recovery rates of the salt rejection and permeate flux when the membrane fouled with MPD was cleaned with DI water and acidic (A), basic (B), and salt (S) solutions in were in the order cleaned with S (salt rejection = 85.1%; permeate flux 9.1 L m^{-2} hr^{-1}) > cleaned with DI (salt rejection = 84.7%; permeate flux 11.3 L m^{-2} hr^{-1}) > cleaned with B (salt rejection = 84.1%; permeate flux = 12.1 L m^{-2} hr^{-1}) > cleaned with A (salt rejection = 87.3%; permeate flux = 15.7 L m^{-2} hr^{-1}). In addition, the recovery rates of the salt rejection and permeate flux in the membrane fouled with CCA were in the order cleaned with A (salt rejection = 82.7%; permeate flux 13.4 L m^{-2} hr^{-1}) > cleaned with DI (salt rejection = 83.1%; permeate flux 13.5 L m^{-2} hr^{-1}) > cleaned with S (salt rejection = 84.1%; permeate flux = 13.7 L m^{-2} hr^{-1}) > cleaned with B (salt rejection = 88.3%; permeate flux = 16.3 L m^{-2} hr^{-1}). The recovery rates of the salt rejection and permeate flux in the membrane fouled with DG were in the order cleaned with DI (salt rejection = 81.1%; permeate flux 11.7 L m^{-2} hr^{-1}) > cleaned with A (salt rejection = 82.7%; permeate flux 12.3 L m^{-2} hr^{-1}) > cleaned with B (salt rejection = 84.1%; permeate flux = 14.1 L m^{-2} hr^{-1}) > cleaned with S (salt rejection = 88.3%; permeate flux = 15.1 L m^{-2} hr^{-1}). These observations suggest that the electrical surface property can be a promising tool for the effective selection of cleaning agents (acidic, basic, and salt solutions) to recover the performance of the fouled NF membranes.

5.3 Autopsy of a fouled reverse osmosis membrane used for ultrapure water production

This study investigated the fouling and cleaning behaviors of reverse osmosis (RO) membranes in a lab–scale ultrapure water (UPW) production system via membrane autopsies and characterization of dissolved organic matter (DOM) and membrane foulants. Most DOM was effectively removed by the MFC filter, with the exception of the peak at 150 Da. The RO membranes were effective in reducing conductivity, DOM, total nitrogen (TN), and ultraviolet A (UVA_{254nm}); polishing using an IER filter resulted in ultra-trace levels of all these parameters required for semiconductor manufacturing (> 18.2 ΩM). The quantity of the desorbed RO membrane foulants varied considerably in terms of dissolved organic carbon (DOC), depending on the desorbing agents used: 0.1 N NaCl (65.12 mgC m^{-2}) > 0.1 N NaOH (46.14 mgC m^{-2}) > deionized water (25.39 mgC m^{-2}) > 0.1 N HCl (15.95 mgC m^{-2}). The high cleaning efficiency of the salt solution (0.1 N NaCl) was attributed to the efficient desorption of

hydrophilic DOM foulants from the RO membrane surfaces. These results demonstrate that salt cleaning may be a promising option with which to recover the performance of the RO membranes fouled primarily by hydrophilic DOM fractions.

5.4 Conclusions and recommendations for future research

Based on the three main chapters, we report that the functionality measurements reflect the electrostatic transport properties of negatively- and positively-charged organic materials even at the negatively-charged membrane surfaces, where interaction occurs between the negative and positive surface charges of the amphoteric surfaces and the charged solutes. Thus, the electrical surface property, which can be determined by the functionality measurement, is a promising tool for understanding the mechanisms of fouling and rejection at the membrane surface in terms of NOM and membrane surface properties. In a previous study, three target foulants (MPD, CCA, and DG) were used to understand these mechanisms. Therefore, an understanding of combined influence of colloids, NOM, and various ions on the membrane surface is required to optimize the membrane processes and to select various cleaning agents in terms of various water characteristics.

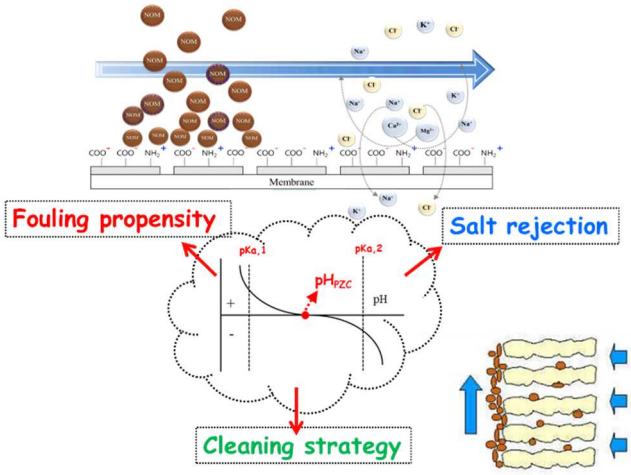

Figure 5.1 Schematic of the electrostatic transport characteristics of NOM and ions at the surface of membrane that interact with both negative and positive surface charges.

References

[1] C. Jucker, M.M. Clark Adsorption of aquatic humic substances on hydrophobic ultrafiltration membranes. *J. Membr. Sci.* 97 (1994) 37-52.

[2] J.A. Nilson, F.A. DiGiano Influence of NOM composition on nanofiltration. *AWWA 88* (1996) 53-66.

[3] J. Cho, G Amy, J Pellegrino Membrane filtration of natural organic matter: initial comparison of rejection and flux decline characteristics with ultrafiltration and nanofiltration membranes. *Water Res.* 33 (1999) 2517-2526.

[4] W.W. Wu, P.A. Chadik Effect of bromide ions on haloacetic acid formation during chlorination of Biscayne aquifer water. *J. Environ. Eng*. 124 (1998) 932-938

[5] P.C. Singer Occurrence of haloacetic acids in chlorinated drinking water. *Water Sci. Technol.: Water Supply* 2 (2002) 487-492

[6] C.M. Villanueva, M. Kogevinas, J.O. Grimals HAAs and THMs in finished drinking water from heterogeneous sources. *Water Res.* 37 (2003) 953-958

[7] P.M. Huck Measurement of biodegradable organic matter and bacterial regrowth in drinking water *J. Am. Water Works Assoc.* 82 (1990) 78-86.

[8] I.C. Escorbar, A.A. Randall, J.S. Taylor Bacterial growth in distribution systems: effect of assimilable organic carbon and biodegradable dissolved organic carbon *Environ. Sci. Technol.* 35 (2001) 3442-3447.

[9] J.A. Leenheer, J.-P. Croué, M. Benjamin, G.V. Korshin, C.J. Hwang, A. Bruchet, and G.R. Aiken Comprehensive isolation of natural organic matter from water for spectral characterizations and reactivity testing, *ACS Symposium Series* 76 (2004) 68-83.

[10] I.C. Escorbar, A.A. Randall Assimilable organic carbon (AOC) and biodegradable dissolved organic carbon (BDOC): complementary measurements. *Water Res.* 35 (2001) 4444-4454.

[11] D.M. Owen G.L. Amy, Z.K. Chowdhury Characterization of Natural Organic Matter and its relationship to treatability. *AWWA Research Foundation* (2007)

[12] J. Cho, G.L. Amy, J. Pellegrino Membrane filtration of natural organic matter: comparison of flux decline, NOM rejection, and foulants during filtration with three UF membranes. *Desalination* 127 (2000) 283-298.

[13] J.K. Edzwald, W.C. Becker, K.L. Wattier Surrogate parameters for monitoring organic matter and THM precursors. *J. Am. Water Works Assoc.* 77 (1985) 122-132.

[14] R.A. Van Steenderen, P.G. Von Rossum *Water SA 11* (1985) 57-60.

[15] A.C. Edwards, M.S. Cresser Relationships between ultraviolet absorbance and total organic carbon in two upland catchments. *Water Res.* 21 (1987) 49-56.

[16] G.L. Amy, M.R. Collins, C.J. Kuo, P.H. King Comparing gel permeation chromatography and ultrafiltration for the molecular weight characterization of aquatic organic matter *J. Am. Water Works Assoc.* 79 (1987) 43-49.

[17] S.K. Hong, M. Elimelech Chemical and physical aspects of natural organic matter (NOM) fouling of nanofiltration membranes *J. Membr. Sci.* 132 (1997) 159-181.

[18] Y. Wang, C. Combe, M.M. Clark The effects of pH and calcium on the diffusion coefficient of humic acid *J. Membr. Sci*. 183 (2001) 49-60.

[19] B.E. Logan, Q. Jiang Molecular size distribution of dissolved organic matter, *J. Environ. Eng.* 116 (1990) 1046-1062.

[20] Y. Chin, G. Aiken, E. O'Loughlin Molecular Weight, Polydispersity, and Spectroscopic Properties of Aquatic Humic Substances, *Environ. Sci. Technol.* 28 (1994) 1853-1858.

[21] N.G. Her Identification and characterization of foulants and scalants on NF membrane, *Ph.D. diss University of Colorado at Boulder* (2002)

[22] E.M. Thurman, R. Malcolm Preparative Isolation of Aquatic Humic Substances, *Environ. Sci. Technol.* 15 (1981) 463-466.

[23] J.A. Leenheer, T.I. Noyes A filtration and column-adsorption system for onsite concentration and fractionation of organic substances from large volumes of water, *U.S. Geological Survey Water-Supply Paper* (1984) 2230.

[24] G.R. Aiken, D.M. McKnight, K.A. Thorn, E.M. Thurman Isolation of hydrophilic organic acids from water using nonionic macroporous resins, *Org. Geochem* 18 (1992) 567-573.

[25] J. Cho, G.L. Amy, J. Pellegrino Characterization of clean and natural organic matter (NOM) fouled NF and UF membranes, and foulants characterization, *Desalination* 118 (1998) 101-108.

[26] G.L. Amy Interaction between natural organic matter (NOM) and membranes: rejection and fouling. *Water Sci. Tech.* 40 (1999) 131-139.

[27] M.R. Collins, G.L. Amy, C. Steelink Molecular weight distribution, carboxylic acidity, and humic substances content of aquatic organic matter: implication for removal during water treatment, *Environ. Sci. Technol*. 20 (1986) 1028-1032.

[28] M. Elimelech, W.H. Chen, J.J. Waypa Measuring the zeta (electrokinetic) potential of reverse osmosis membranes by a streaming potential analyzer *Desalination* 95 (1994) 269-286

[29] A.E. Childress, M. Elimelech Effect of solution chemistry on the surface charge of polymeric reverse osmosis and nanofiltration membranes *J. Membr. Sci.* 119 (1996) 253-268.

[30] B. Kwon, S. Lee, M.B. Gu, J. Cho. Minimization of membrane organic fouling and haloacetic acids formation by controlling amino sugars and/or polysaccharide-like substance included in colloidal NOM *Water Supply* 3 (2003) 223-228.

[31] S. Sourirajan, T. Matsuura Reverse Osmosis/Ultrafiltration Process Principles, National Research Council, *Ottawa Canada* (1981)

[32] M. Mulder Basic Principles of Membrane Technology, Kluwer Academic Publishers, Dordrecht/Boston/London (1991)

[33] A. Seidel, J.J. Waypa, M. Elimelech, Role of charge (Donnan) exclusion in removal of arsenic from water by a negatively charged porous nanofiltration membrane, *Environ. Eng. Sci.* 18 (2001) 105–113.

[34] C.M. Tam, A.Y. Tremblay Membrane pore size characterization: single and multicomponent solute probe techniques *J. Membr. Sci.* 57 (1991) 271-281.

[35] S.I. Nakao Review: determination of pore size and pore size distribution. 3. Filtration membranes, *J. Membr. Sci.* 96 (1994) 131-165.

[36] S. Singh, K.C. Khulbe T. Matsuura, P. Ramamurthy Membrane characterization by solute transport and AFM, *J. Membr. Sci.* 142 *(*1998) 117-127.

[37] A. Braghetta F.A. DiGiano, P.B. William Nanofiltration of Natural Organic Matter: pH and Ionic Strength Effects *J. Environ. Eng.* 123 *(*1997) 628-641.

[38] S. Lee, G. Park, G.L. Amy, S.K. Hong, S.H. Moon, D.H. Lee, J. Cho, Determination of membrane pore size distribution suing the fractional rejection of nonionic and charged macromolecules, *J. Membr. Sci.* 201 (2002) 191-201.

[39] J. Bear Hydraulics of Groundwater, *MacGraw-Hill*, NewYork, NY (1979).

[40] R.J. Hunter Foundation of Colloid Science Vol. 1, *Clarendon Press,* Oxford (1986).

[41] P.C. Hiemenz Principles of Colloid and Surface Chemistry, 2nd ed., *Marcel Dekker,* New York, NY (1986).

[42] A.W. Neumann, R.J. Good Surface and Colloid Science 11, *Plenum Press,* New York, NY (1979)

[43] C. Dahlgren, H. Elwing and K.-E. Magnusson Comparison of contact angles calculated from the diameter of sessile drops and submerged air bubbles in contact with a solid surface, *Colloids Surf.* 17 (1986) 295-311.

[44] M. Oldani, G. Schock Characterization of ultrafiltration membranes by infrared spectroscopy, ESCA, and contact angle measurements, *J. Membr. Sci.* 43 (1989) 243-255.

[45] V. Gekas, P. Aimar, J. Lafaille, V. Sanchez, A simulation study of the adsorption concentration polarization interplay in protein ultrafiltration *Chem. Eng. Sci.* 48 (1993) 2753-2765

[46] J.T.G. Overbeek "Colloid Science," Vol. 1, *Elsevier,* Amsterdam, (1952) p. 194.

[47] D.J. Shaw Electrophoresis, *Academic Press,* London (1969)

[48] R.J. Hunter Zeta potential in Colloid Science, *Academic Press,* London, (1981).

[49] J.N. Israelachvili Adhesion forces between surfaces in liquids and condensable vapors *Surf. Sci. Rep.* 14 (1992) 109-159.

[50] W. Stumm, Chemistry of Solid-Water Interface, *Wiley Interscience,* New York, 1992.

[51] M. Elimelech, J. Gregory, X. Jia, and R. A. Williams, Particle Deposition and Aggregation: Measurement, Modelling, and Simulation, Butterworth-Heinemann, Stoneham, MA, (1995)

[52] M. Elimelech, W.H. Chen, J.J. Waypa Measuring the zeta (electrokinetic) potential of reverse osmosis membranes by a streaming potential analyzer *Desalination* 95 (1994) 269-286

[53] C. Causserand, M. Nystrom, P. Aimar Study of streaming potentials of clean and fouled ultrafiltration membranes *J. Membr. Sci.* 88 (1994) 211-222.

[54] Y. Shim, S. Lee, J. Moon, J. Cho, Effect of natural organic matter and ionic species on membrane surface charge, *Environ. Sci. Technol.* 36 (2002) 3864–3871.

[55] K.J. Kim, A.G. Fane, M. Nystrom, A. Pihlajamaki, Chemical and electrical characterization of virgin and protein-fouled polycarbonate track-etched membranes by FTIR and streaming-potential measurements, *J. Membr. Sci.* 134 (1997) 199-208.

[56] S. Lee Evaluation of membrane filtration processes for drinking water treatment in terms of natural organic matter (NOM) and disinfection by-products (DBPs) M.S. Thesis, Gwanju institute of Science and Technology (2001)

[57] M. Hirose, H. Ito, Y. Kamiyama Effect of skin layer surface structures on the flux behavior of RO membranes, *J. Membr. Sci.* 121 (1996) 209-215.

[58] E.M. Vrijenhoek, S.K. Hong, M. Elimelech Influence of membrane surface properties on initial rate of colloidal fouling of reverse osmosis and nanofiltration membranes *J. Membr. Sci.* 188 (2001) 115-128.

[59] M. Elimelech, S. Bhattacharjee A novel approach for modeling concentration polarization in crossflow membrane filtration based on the equivalence of osmotic pressure model and filtration theory *J. Membr. Sci.* 145 (1998) 223-241.

[60] M.C. Porter Microfiltration in Synthetic Membranes: science, engineering, and applications, nato, *ASI Series*, Vol. 181. (1986)

[61] L. Mir, S.L. Michaels, V. Goel, R. Kaiser Crossflow microfiltration: application, design and cost, in Membrane Handbook, Van Nostrand Reinhold, New York. *(*1992).

[62] S. Lee, J. Cho, M. Elimelech Influence of colloidal fouling and feed water recovery on salt rejection of RO and NF membranes *Desalination* 160 (2003) 1-12.

[63] S.K. Hong, M. Elimelech Chemical and physical aspects of natural organic matter (NOM) fouling of nanofiltration membranes *J. Membr. Sci.* 132 (1997) 159-181.

[64] J. Laine, A. Calafat, M.Labady Preparation and characterization of activated carbons from coconut shell impregnated with phosphoric acid, *Carbon* 27 (1989) 191-195.

[65] S.C. Allgeier, R.S. Summers, J.G. Jacangel, V.A. Hatcher, D.M. Moll, S.M. Hooper, J.W. Swertfeger, R.B.A. Green, Simplified and rapid method for biodegradable dissolved organic carbon measurement. In Proceedings of 1996 AWWA Water Quality Technology Conference; *AWWA*, Denver, CO, (1996).

[66] M. Seidel, M. Elimelech Coupling between chemical and physical interaction and physical interactions in natural organic matter (NOM) fouling of nanofiltration membranes: implications for fouling control. *J. Membr. Sci.* 203 (2002) 245-255.

[67] G.L. Amy, M.R. Collins, C.J. Kuo, P.H. King Comparing gel permeation chromatography and ultrafiltration for the molecular weight characterization of aquatic organic matter *J. Am. Water Works Assoc.* 79 (1987) 43-49.

[68] R.D. Cohen, R.F. Probstein, Colloidal fouling of reverse osmosis membranes. *J. Colloid Interface Sci.* 114 (1986) 194–207.

[69] N.V. Churaev, I.P. Sergeeva, V.D. Sobolev, D.E. Ulberg, Electrokinetic study of polymer

surfaces, *J. Colloid Interface Sci.* 151 (1992) 490–497.

[70] H.J. Jacobasch, G. Bauböck, J. Schurz, Problems and results of zeta-potential measurements of fibers, Colloid Polymer Sci. 263 (1985) 3–24.

[71] M. Elimelech, W.H. Chen, J.J. Waypa, Measuring the zeta (electrokinetic) potential of reverse osmosis membranes by a streaming potential analyzer, *Desalination* 95 (1994) 269–286.

[72] H. Rho, K, Chon, J. Cho, Surface charge characterization of nanofiltration membranes by potentiometric titrations and electrophoresis: Functionality vs. zeta potential, Desalination 427 (2018) 19-26.

[73] A. Seidel, J.J. Waypa, M. Elimelech, Role of charge (Donnan) exclusion in removal of arsenic from water by a negatively charged porous nanofiltration membrane, *Environ. Eng. Sci.* 18 (2001) 105–113.

[74] W. Stumm, Chemistry of Solid-Water Interface, Wiley Interscience, New York, 1992.

[75] C. Causserand, M. Nystrom, P. Aimar, Study of streaming potentials of clean and fouled ultrafiltration membranes, *J. Membr. Sci.* 88 (1994) 211–222.

[76] M. Elimelech, Particle deposition on ideal collectors from dilute flowing suspensions – Mathematical formulation, numeric solution, and simulations, *Sep. Technol.* 4 (1994) 186–212.

[77] S. Mori, H. Okamoto, A unified theory of determining the electrophoretic velocity of mineral particles in the rectangular micro-electrophoresis cell, *Fusen* 27 (1980) 117–124.

[78] M. Elimelech, C.R. O'Melia, Effect of electrolyte type on the electrophoretic mobility of polystyrene latex colloids, *Colloids Surf.* 44 (1990) 165–178.

[79] Y. Shim, S. Lee, J. Moon, J. Cho, Effect of natural organic matter and ionic species on membrane surface charge, *Environ. Sci. Technol.* 36 (2002) 3864–3871.

[80] M.R. Collins; G. Amy, C. Steelink, Molecular weight distribution, carboxylic functionality, and humic substances content of aquatic organic matter: Implications for removal during water treatment, *Environ. Sci. Technol.* 20 (1986) 1028–1032.

[81] S. Lee, J. Cho, M. Elimelech, Combined influence of natural organic matter (NOM) and colloidal particles on nanofiltration membrane fouling, *J. Membr. Sci.* 262 (2005) 27–41.

[82] H. Seki, A. Suzuki, Adsorption of heavy metal ions onto insolubilized humic acid, *J. Colloid Interface Sci.* 171 (1995) 490–494.

[83] E. Illés, E. Tombácz, The role of variable surface charge and surface complexation in the adsorption of humic acid on magnetite, *Colloids Surf. A* 230 (2004) 99–109.

[84] M.A. Zazouli, S. Nasseri, M. Ulbricht, Fouling effects of humic acid and alginic acids in nanofiltration and influence of solution composition, Desalination 250 (2010) 688–692.

[85] M. D. Afonso, Surface charge on loose nanofiltration membranes, *Desalination* 191 (2006) 262-272.

[86] P. Le-Clech, V. Chen, T.A.G. Fane, Fouling in membrane bioreactors used in wastewater treatment, *J. Membr. Sci.* 284 (2006) 17–53.

[87] M.M. Pendergast, E.M.V. Hoek, A review of water treatment membrane nanotechnologies, *Energy Environ. Sci.* 4 (2011) 1946–1971.

[88] M. Elimelech, W.A. Phillip, The future of seawater desalination: Energy, technology, and

the environment, *Science* 333 (2011) 712–717.

[89] N.Y. Yip, A. Tiraderri, W.A. Phillip, J.D. Schiffrnan, L.A. Hoover, Y.C. Kim, M. Elimelech, Thin-film composite pressure retarded osmosis membranes for sustainable power generation from salinity gradients, *Environ. Sci. Technol.* 45 (2011) 4360–4369.

[90] J. Cho, G. Amy, J. Pellegrino, Membrane filtration of natural organic matter: Factors and mechanisms affecting rejection and flux decline with charged ultrafiltration (UF) membrane, *J. Membr. Sci.* 164 (2000) 89–110.

[91] A.E. Childress, M. Elimelech, Relating nanofiltration membrane performance to membrane charge (electrokinetic) characteristics, *Environ. Sci. Technol.* 34 (2000) 3710–3716.

[92] S. Bhattacharjee, J.C. Chen, M. Elimelech, Coupled model of concentration polarization and pore transport in crossflow nanofiltration, *AIChE J.* 47 (2001) 2733–2745.

[93] H.J. Jacobasch, J. Schurz, Characterization of polymer surfaces by means of electrokinetic measurement, *Prog. Colloid Polymer Sci.* 77 (1988) 40–48.

[94] M.R. Wiesner, S. Chellam, Mass transport consideration for pressure-driven membrane processes, *J. Am. Water Works Assoc.* 84 (1992) 88–95.

[95] L. Song, M. Elimelech, Particle deposition onto a permeable surface in laminar flow, *J. Colloid Interface Sci.* 173 (1995) 165–180.

[96] A.E. Childress, M. Elimelech, Effect of solution chemistry on the surface charge of polymeric reverse osmosis and nanofiltration membranes, *J. Membr. Sci.* 119 (1996), 253–268.

[97] R. Epsztein, E. Shaulsky, N. Dizge, D.M. Warsinger, M. Elimelech Role of ionic charge density in donnan exclusion of monovalent anions by nanofiltration. *Environ. Sci. Technol.* 52 (2018) 4108-4116.

[98] P. Xu, J.E. Drewes, T.-U. Kim, C. Bellona, G. Amy, Effect of membrane fouling on transport of organic contaminants in NF/RO membrane applications, *J. Membr. Sci*. 279 (2006), 165–175.

[99] G. Hurwitz, G.R. Guillen, E.M.V. Hoek, Probing polyamide membrane surface charge, zeta potential, wettability, and hydrophilicity with contact angle measurements, *J. Membr. Sci.* 349 (2010) 349–357.

[100] A. Tiraferri, M. Elimelech, Direct quantification of negatively charged functional groups on membrane surfaces, *J. Membr. Sci.* 389 (2012) 499–508.

[101] J. Cho, G. Amy, J. Pellegrino, Y. Yoon, Characterization of clean and natural organic matter (NOM) fouled NF and UF membranes, and foulants characterization, *Desalination* 118 (1998) 101–108.

[102] A. Kitahara, K. Furusawa, M. Ozaki, H. Ohshima, Zeta potential, Scientist Sha (1995) 57–61 Tokyo.

[103] A. Harada, K. Kataoka, Novel polyion complex micelles entrapping enzyme molecules in the core: Preparation of narrowly-distributed micelles from lysozyme and poly(ethyleneglycol)-poly(aspartic acid) block copolymer in aqueous medium, *Macromolecules* 31 (1998) 288–294.

[104] C. Appel, L.Q. Ma, R.D. Rhue, E. Kennelley, Point of zero charge determination in soils and minerals via traditional methods and detection of electroacoustic mobility, *Geoderma* 113 (2003) 77–93.

[105] W.S. Matthews, J.E. Bares, J.E. Bartmess, F.G. Bordwell, F.J. Cornforth, G.E. Drucker, Z. Margolin, R.J. McCallum, G.J. McCallum, N.R. Vanier, Equilibrium functionalities of carbon acids. VI. Establishment of an absolute scale of functionalities in dimethyl

sulfoxide solution, *J. Am. Chem. Soc.* 97 (1975) 7006–7014.

[106] E. Marcano-Martinez, M.B. McBride, Comparison of the titration and ion adsorption methods for surface charge measurements in oxisols, *Soil Sci. Soc. Am. J.* 53 (1989) 1040–1045.

[107] J.C. Parker, L.W. Zelazny, S. Samprath, W.G. Harris, A critical evaluation of the extension of zero point of charge (zpc) theory to soil systems, *Soil Sci. Soc. Am. J.* 43 (1979) 668–674.

[108] B. van Raij, M. Peech, Electrochemical properties of some oxisols and alfisols of the tropics, *Soil Sci. Soc. Am. Proc.* 36 (1972) 587– 593.

[109] J. Cho, G. Amy, J. Pellegrino, Membrane filtration of natural organic matter: Initial comparison of rejection and flux decline characteristics with ultrafiltration and nanofiltration membranes, *Water Res.* 33 (1999) 2517–2526.

[110] K. Chon, J, Cho, Fouling behavior of dissolved organic matter in nanofiltration membranes from a pilot-scale drinking water treatment plant: An autopsy study, *Chem. Eng. J.* 295 (2016) 268–277.

[111] E. Kang, Y. Lee, K. Chon, J. Cho, Effects of hydrodynamic conditions (diffusion vs. convection) and solution chemistry on effective molecular weight cut-off of negatively charged nanofiltration membranes, *Desalination* 352 (2014) 136–141.

[112] K. Chon, J. Cho, H.K. Shon, Advanced characterization of algogenic organic matter, bacterial organic matter, humic acids and fulvic acids, *Water Sci. Technol.* 67 (2013) 2228–2235.

[113] D.A. Skoog, J.J. Leafy, Principles of Instrumental Analysis, 4th ed., Saunders College Publishing, Philadelphia, (1992).

[114] L.J. Bellamy, The Infrared Spectra of Complex Molecules, 3rd ed., Chapman and Hall, New York, (1978).

[115] H. Lee, Y. Jin, Y.; S. Hong, Recent transitions in ultrapure water (UPW) technology: Rising role of reverse osmosis. *Desalination* 399 (2016), 185–197.

[116] G.C. Ganzi, A.D. Jha,; E. DiMascio,; J.H. Wood, Electrodeionization – theory and practice of continuous electrodeionization. *Ultrapure Water J.* 14 (1997) 64–69.

[117] J. Wood, J.Gifford, J. Arba,; M. Shaw, Production of ultrapure water by continuous electrodeionization. *Desalination* 250 (2010) 973–976.

[118] GWI, Global water market, 2014: meeting the word's water and wastewater need until 2018, Global Water Intelligence, (2013)

[119] P.R. Puckorius, Does cooling water treatment vary between industries? *Ind. Water Treat.* 32 (2015) 37–42.

[120] N. Cohen, S. Sackstein, How to bring your high-purity water pretreatment systems into the 21st century. *Ultrapure Water J.* 32 (2015) 21–25.

[121] M.S.L. Tai, I. Chua, K. Line, W.J. Ngh, W.K. Tea, Removal of dissolved oxygen in ultrapure water production using microporous membrane modules. *J. Membr. Sci.* 87 (1994) 99–105.

[122] K. Li, I. Chua, W.J. Ng, W.K. Teo, Removal of dissolved oxygen in ultrapure water production using a membrane reactor. *Chem. Eng. Sci.* 50 (1995) 3547–3556.

[123] B. Jean-luc, D. Bruno, Contamination monitoring and analysis in semiconductor manufacturing. *Semicond. Technol.* 1999, 57–78

[124] H. Ohya, State of the art ultrapure water production in Japan. *Desalination* 80 (1991) 80, 159–165

[125] T. Ohmi, Ultraclean Technology Handbook: *Ultrapure Water*, 1 (1993) CRC Press.

[126] J. Hutcheson, Ultrapure water: systems for microelectronics. *Filtr. Sep.* 43 (2006) 22–25

[127] A. Wang UPW's membrane technology application trend on semiconductor. *Semicon. Man. Tech. Workshop* 2002, 294–298

[128] R. Singh, Production of high-purity water by membrane processes. *Desalin. Water Treat.* 3 (2009) 99–110.

[129] S.R. Gagnon, J. Case history of a water treatment system using EDI in Puerto Rico. *Ultrapure Water J.* 27 (2010) 12–24

[130] S.A. Pororov, N. Kornilova, K. Platonov, Ultra-pure water: intensive water demineralisation through ion exchange. *Filtr. Sep.* 48 (2011) 36–39.

[131] J.H. Lee, J.H. Choi The production of ultrapure water by membrane capacitive deionization (MCDI) technology. *J. Membrane Sci.* 409–410 (2012) 251–256.

[132] K. Chon, J. Cho, H.K. Shon, K. Chon, Advanced characterization of organic foulants of ultrafiltration and reverse osmosis from water reclamation. *Desalination* 301 (2012) 301, 59–66

[133] K. Chon, J. Cho, H.K. Shon, Advanced characterization of algogenic organic matter,

bacterial organic matter, humic acids and fulvic acids. *Water Sci. Technol.* 67 (2013) 2228–2235.

[134] J. Cho, G. Amy, J. Pellegrino, J.; Yoon, Y. Characterization of clean and natural organic matter (NOM) fouled NF and UF membranes, and foulants characterization. *Desalination* 1998, 118

[135] K. Chon, J. Cho, H.K. Shon, Fouling characteristics of a membrane bioreactor and nanofiltration hybrid system for municipal wastewater reclamation. *Bioresour Technol.* 130 (2013) 239–247.

[136] K. Chon, J. Cho, H.K. Shon, Fouling characteristics of a membrane bioreactor and nanofiltration hybrid system for municipal wastewater reclamation. *Bioresour Technol.* 130 (2013) 239–247.

[137] S.A. Huber, A. Balz, M. Abert, W. Pronk, Characterization of aquatic humic and non-humic matter with size-exclusion chromatography-organic carbon detection-organic nitrogen detection (LC-OCD-OND). *Water Res.* 45 (2011) 879–885.

[138] K. Chon, K. Lee, I.S. Kim, A. Jang, Performance assessment of a submerged membrane bioreactor using a novel microbial consortium. *Bioresour. Technol.* 210 (2016) 2–10.

[139] J.A. Leenheer, J.P. Croué, Characterizing dissolved aquatic organic matter. *Environ. Sci. Technol.* 37 (2003) 18A–26A.

[140] K. Chon, J. Cho, Fouling behavior of dissolved organic matter in nanofiltration membranes from a pilot-scale drinking water treatment plant: An autopsy study. *Chem. Eng. J.* 295 (2016) 268–277.

[141] S. Lee, M. Elimelech, Salt cleaning of organic-fouled reverse osmosis membranes. *Water Res.* 41 (2007) 1134–1142.

[142] H. Lee, G. Amy, J. Cho, Y. Yoon, S.-H. Moon, I.S. Kim, Cleaning strategies for flux recovery of an ultrafiltration membrane fouled by natural organic matter. *Water Res.* 35 (2001) 3301–3308.

[143] W. Stumm, Chemistry of the Solid–Water Interface. Wiley, Inc. New York (1992).

[144] H. Rho, K. Chon, J. Cho, Surface charge characterization of nanofiltration membranes by potentiometric titrations and electrophoresis: Functionality vs. zeta potential. Desalination 427 (2018) 19–26

[145] K. Chon, K. Chon, J. Cho, Characterization of size fractionated dissolved organic matter from river water and wastewater effluent using preparative high-performance size exclusion chromatography. *Org. Geochem.* 103 (2017) 105–112.

[146] K. Chon, S.J. Kim, J. Moon, J. Cho, Combined coagulation-disk filtration process as a pretreatment of ultrafiltration and reverse osmosis membrane for wastewater reclamation: an autopsy study of a pilot plant. *Water Res.* 46 (2012) 1803–1806.

[147] V. Kanokkantapong, T.F. Marhaba, B. Panyapinyophol, P. Pavasant, FTIR evaluation of functional groups involved in the formation of haloacetic acids during the chlorination of raw water. *J. Hazard. Mater.* B136 (2006) 188–196.

[148] E.M.V. Hoek, M. Elimelech, Cake-enhanced concentration polarization: A new fouling mechanism for salt-rejecting membranes. *Environ. Sci. Technol.* 37 (2003) 37 5581–5588.

[149] S. Lee, J. Cho, M. Elimelech, Influence of colloidal fouling and feed water recovery

on salt rejection of RO and NF membranes. *Desalination* 160 (2004) 1–12.

Curriculum Vitae Hojung RHO

CONTACT INFORMATION

School of Urban and Environmental Engineering Urban and Environmental Engineering, Ulsan National Institute of Science and Technology (UNIST), UNIST-gil 50, Ulsan, Republic of Korea

E-mail: hjrho2014@gmail.com
Phone: +82-10-9808-9271

RESEARCH INTERESTS

Environmental surface chemistry
- Membrane surface chemistry
- Removal of organic pollutant using physicochemical treatments (Sorption and filtration)
- Characterization of Natural Organic Matters (NOM)
- Aquatic organic foulants analysis in membrane process

EDUCATION

Ulsan National Institute of Science and Technology (UNIST), Ulsan, Republic of Korea **Aug. 2019**
- **Combined MS-Ph.D**., Department of Urban and Environmental Engineering
- **Dissertation:** Electrostatic transport characteristic of NOM and ions at the surface of nanofiltration and reverse osmosis membrane

Yonsei University, Seoul, Republic of Korea **Feb. 2015**
- Master candidate, School of Civil and Environmental Engineering

Hankuk University of Foreign Studies, Republic of Korea **Feb. 2014**
- **Bachelor's degree**, Department of Environmental Science

LANGUAGE

Korean: Native
English: proficient

RESEARCH EXPERIENCES

Organic water interface engineering lab. **Mar. 2015 ~ Aug. 2019**
Ulsan National Institute of Science and Technology (UNIST), Republic of Korea
(Ph.D. student)

NOM water treatment lab. Yonsei University, Republic of Korea **Mar. 2014 ~ Feb. 2015**
(MS student)

Mar. 2012 ~ Feb. 2013

AWARDS

2014 International Desalination Workshop, the best oral presentation by Korea Minister of Land and Infrastructure

PUBLICATIONS

6. **Hojung Rho**, Kangmin Chon, Jaeweon Cho*, Influence of the organic matter polarity on the intrinsic electrical surface property (pKa) of negatively charged nanofiltration membrane, In preparation.

5. **Hojung Rho**, Kangmin Chon*, Jaeweon Cho*, An Autopsy Study of a Fouled Reverse Osmosis Membrane Used for Ultrapure Water Production, *Water*, 11 (6) 1116, **2019**

4. **Hojung Rho**, Jongkwan Park*, Jaeweon Cho*, Rapid and Effective Isolation of Dissolved Organic Matter Using Solid-Phase Extraction Cartridges Packed with Amberlite XAD 8/4 Resins, Water, 11 (1) 67, **2019**

3. Jinhee Park, Jin-Sung Ra, **Hojung Rho,** Jaeweon Cho, Sang Don Kim*, Validation of a biotic ligand model on site-specific copper toxicity to Daphnia magna in the Yeongsan River, Korea, *Ecotoxicology and Environmental Safety*, 149, 108–115, **2018**

2. Sung-Ju Im, **Hojung Rho,** Sanghyun Jeong, Am Jang, Organic fouling characterization of a CTA-based spiral-wound forward osmosis (SWFO) membrane used in wastewater reuse and seawater desalination, *Chemical Engineering Journal*, 336, 141-151, **2018**

1. **Hojung Rho**, Kangmin Chon*, Jaeweon Cho*, Surface charge characterization of nanofiltration membranes by potentiometric titrations and electrophoresis: Functionality vs. zeta potential, *Desalination*, 427, 19-26, **2018**

CONFERENCE PARTICIPATION (International)

Hojung Rho, Kangmin Chon, Jaeweon Cho, An autopsy study of fouled RO membrane involved in DI generator, focusing on the chemical cleaning strategy, the 10th international desalination workshop, 22th-25th , November, **2017**

Taewoo Nam, Huijin Heo, Jongkwan Park, **Hojung Rho**, Jaeweon Cho Identifying biodegradable portions of seawater organic matter (SOM) with desalination membranes, using a prep-LC with both aromatic and non-aromatic detections, the 3rd international Conference on desalination using membrane technology, 2nd-5th, April, **2017**

Hojung Rho, Kangmin Chon, Jaeweon Cho, Envisaging the electrostatic transport of oragnic foulants, based on the equilibrium constant, pKa, of membrane surface. the 3rd international Conference on desalination using membrane technology, 2nd-5th, April, **2017**

Hojung Rho, Huijin Heo, Taewoo Nam, Jaeweon Cho, Envisaging the electrostatic transport of natural organic matter and ions at the membrane surface, based on membrane surface charge, the 5th IWA Regional Conference on Membrane Technology, 21th-24th August, **2016**

Hojung Rho, Jongkwan Park, Jaewoen Cho, The Effect of Membrane Surface Charge on Natural Organic Matter Diffusivity in Nanofiltration Membrane

Process, International Desalination Workshop, 18th~21th November, **2015**

Jongkwan Park, **Hojung Rho**, Jaeweon Cho, Determining haloacetic acids formation potential of NOM fractionated based on molecular size, using IC-ESI-MS, 2015 International Environmental Engineering Conference & Annual Meeting of the Korean Society of Environmental Engineers, 28th~30th October, **2015**

Hojung Rho, Jongkwan Park, Jaeweon Cho, A study on electrostatic repulsion between Natural Organic Matter and membrane surface: implication for membrane fouling, International Environmental Engineering Conference, 28th~30th October, **2015**

Hojung Rho, Jongkwan Park, Jaeweon Cho, Diffusivity of Natural Organic Matter: Measurement, mechanism and implication in membrane process, Challenges in Environmental Science & Engineering, 28th September~2th October, **2015**

Hojung Rho, Jaeweon Cho Proposing a titration method to evaluate membrane charge density (surface potential), as opposed to zeta potential measurement, 4th IWA Regional Conference on Membrane Technology 3th~5th December, **2014**

Hojung Rho, Keumju Yoon, Jaeweon Cho Determination of natural organic matter diffusion coefficient using diffusion cell, IWA Regional Conference on Membrane Technology 3th~5th December, **2014**

Hojung Rho, Jaeweon Cho Direct measurement of surface charge density of the membranes surface using acidic titration, against zeta potential, International Desalination Workshop, Korea, 5th~8th November, **2014**
(The best oral presentation)

RESEARCH PROJECT PARTICIPATION

Science Walden
(funded by Korea Ministry of Science, ICT and Future Planning, 2015-2018)

The study of colloidal mass transport at membrane surface
(funded by Korea Ministry of Science, ICT and Future Planning, 2016-2018)

Ion characterization in RO membrane plant at Kijang, Korea
(funded by Dosan heavy industry, 2015)

MD-PRO combined desalination technology
(funded by Korea Ministry of Land and Infrastructure, 2014-2015)

Developing NOM fractionation technology in wastewater treatment effluent and rain water
(funded by Korea Ministry of Science, ICT and Future Planning, 2014-2015)